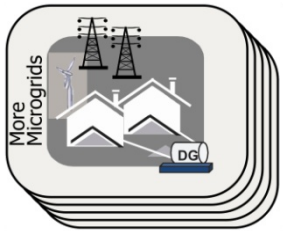

Advanced Architectures and Control Concepts for

MORE MICROGRIDS

Contract No: SES6-019864

WORK PACKAGE F

DF3. Field tests in the Ílhavo Municipal Swimming-Pool of transfer between connected and island operation modes

Final Version

December 2009

Document Information

Title: Field tests in the Ílhavo Municipal Swimming-Pool of transfer between connected and island operation modes

Date: 31-Dec-2009

Task(s): TF4. Field tests of the transfer from interconnected to isolated mode of microgrids operation & vice versa

Coordination:	António Amorim	antonio.amorim@edp.pt
	Francisco Mira	francisco.mira@edp.pt
	João Peças Lopes	jpl@fe.up.pt
Authors:	Nuno Melo	nuno.melo@edp.pt
	Fernanda Resende	fresende@inescporto.pt
	António Lebre	antoniojose.lebrecardoso@edp.pt
	André Madureira	agm@inescporto.pt
	Flávio Cação	flavio.cacao@edp.pt

Access:

__ Project Consortium
__ European Commission
X PUBLIC

Status:

__ For Information
__ Draft Version
__ Final Version (internal document)
__ Submission for Approval (deliverable)
X Final Version (deliverable, approved on.)

TABLE OF CONTENTS

Acknowledgments

The authors would like to express their thanks to the Ílhavo Town Council (Fernando Caçoilo and Augusto Nunes), António Pintor and EDP's AO Aveiro (Arnaldo Luís Carvalho and Hugo Costa) for their support and contributions to this work.

1 Introduction

The increasing penetration of microgeneration on Low Voltage (LV) distribution grids and the implementation of microgrids require a detailed analysis of the behaviour of micro-sources and loads in grid connected and islanding modes, as well as during transitions between both modes.

In the Portuguese field tests, EDP Distribuição (EDP) analysed the behaviour of a microturbine installed in the Ílhavo Municipal Swimming-Pool (MSP), supplying the local load in islanding mode and exporting power in grid connected mode. The interaction between this microturbine and a Diesel gen-set was also analysed in islanding mode.

This innovative project, of Combined Heat and Power (CHP) generation, of the Ílhavo Town Council, is the first swimming-pool micro-cogeneration application based on a microturbine in Portugal. A Capstone 60 MicroTurbine supports the main requirements of the swimming-pool water heating and combined electric power generation. Excluding daily peak demand periods, this system supplies the building power demand and exports the remaining power to the LV public distribution grid.

This document presents a brief characterization of the EDP's Medium Voltage (MV) and LV grids, where the microturbine is integrated and a detailed characterization of the Ílhavo MSP micro-cogeneration project, as well as the swimming-pool loads.

On the other hand, there are presented the results of Power Quality (PQ) monitoring campaigns in the MV and LV grids that supply this test site, actually voltage quality analysis performed in the MV busbar of the Ílhavo HV/MV substation (SE Ílhavo) and in the LV busbar of the ILH0074 MV/LV substation (PTD ILH0074), where the microturbine is directly connected.

This document also includes the results of the field tests defined to the More Microgrids Project, in close collaboration with INESC Porto, being achieved the following objectives:

- analysis of the microturbine behaviour in grid connected mode with the LV distribution grid, under several generation regimens, in order to identify its simulation parameters and to evaluate its impact on the PQ;
- analysis of the microturbine behaviour in islanding operation mode, without connection to the distribution grid, under several load regimens, in order to analyse its load following capability, as well as the voltage and frequency stability supplied to the Ílhavo MSP loads;
- validation of the possibility of transferring between grid connected and islanding operation modes;
- analysis of the system behaviour during critical operations such as: starting, black-starting and shutdown of the microturbine;
- parallel of the microturbine with a mobile Diesel gen-set, in islanding mode, in order to analyse the operation of the two micro-sources in a microgrid. This field test includes operation in several load and generation regimens.

Finally, the parameter identification of the theoretical models and their control systems used to represent the microturbine dynamic behaviour is presented.

2 Characterization of the Ílhavo MSP study case

2.1 Overview

In typical operating conditions, the microturbine is grid connected to the LV public distribution grid. During swimming-pool off-peak periods, the microturbine supplies the facilities' loads and exports the remaining power to the distribution grid. During swimming-pool peak periods, the power generated by the microturbine is not enough to supply all facilities demand and it is required to draw power from the public distribution grid.

The following photos show external and inside views of the Ílhavo MSP.

Figure 1 – External view of the Ílhavo MSP building

Figure 2 – Inside view of the Ílhavo MSP – Main tank

2.2 Description of the public distribution grid

The Ílhavo MSP is grid connected to the LV public distribution grid by a dedicated underground feeder from the PTD ILH0074. This MV/LV substation is integrated in the own building of the Ílhavo MSP.

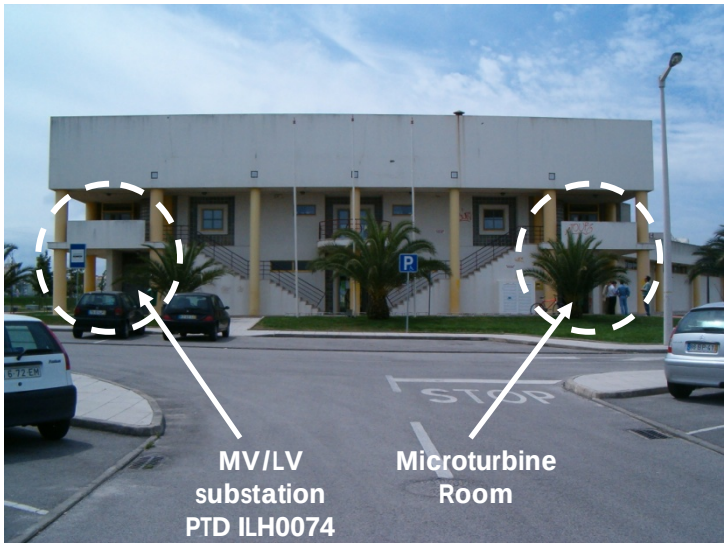

Figure 3 – Location of PTD ILH0074 and microturbine in the Ílhavo MSP building

The PTD ILH0074 is characterized by a 630 kVA dry power transformer, of 15 kV/400 V, which supplies 164 customers, through 5 LV feeders, and the local public lighting.

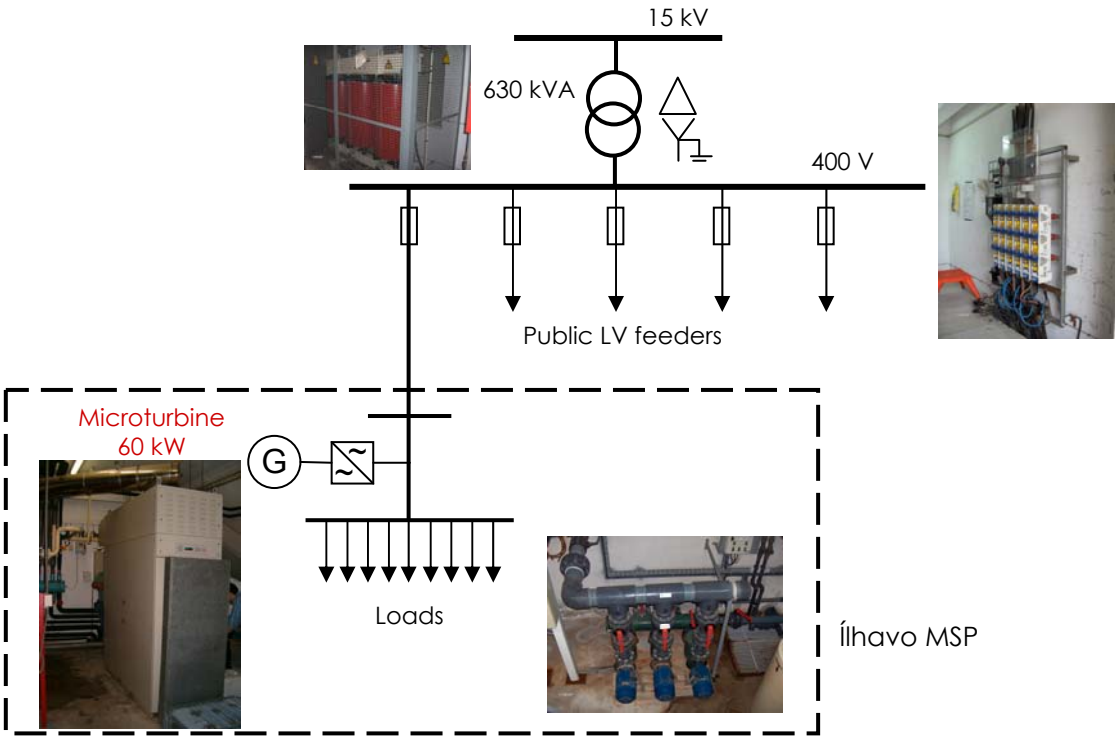

Figure 4 – Simplified single-line diagram of the PTD ILH0074 / Ílhavo MSP

The following figures present the four feeders that connect the remaining 163 LV customers supplied by this MV/LV substation. The Ílhavo MSP is supplied by the Feeder 3.

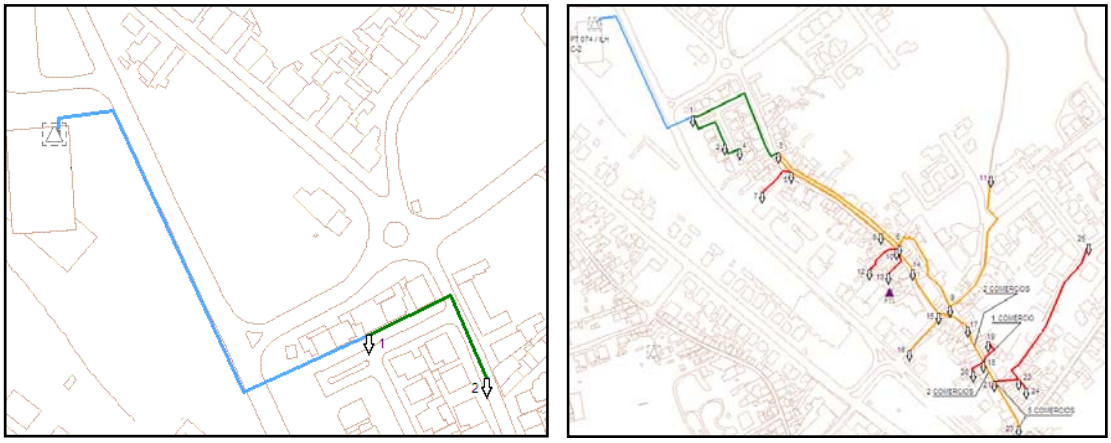

Figure 5 – LV public grid, Feeder 1 (left) and Feeder 2 (right)

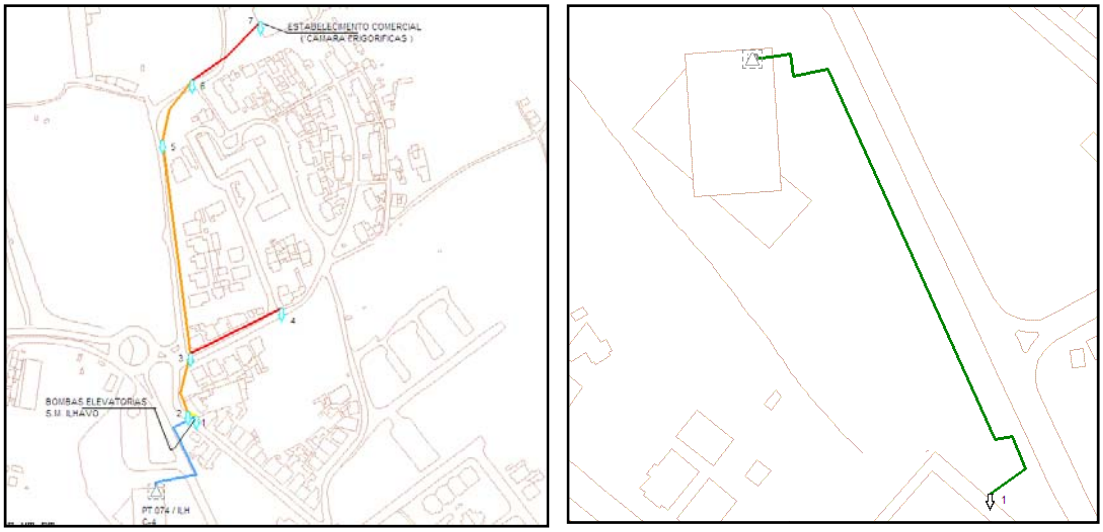

Figure 6 – LV public grid, Feeder 4 (left) and Feeder 5 (right)

The PTD ILH0074 is supplied by the SE Ílhavo, through a 15 kV overhead feeder (ÍLHAVO - Ílhavo I). Currently, this HV/MV substation is characterized by two 60/15kV power transformers, of 31,5 MVA each one, and supplies about 12 200 customers.

The following figure presents the diagram of the MV grid, which integrates the PTD ILH0074.

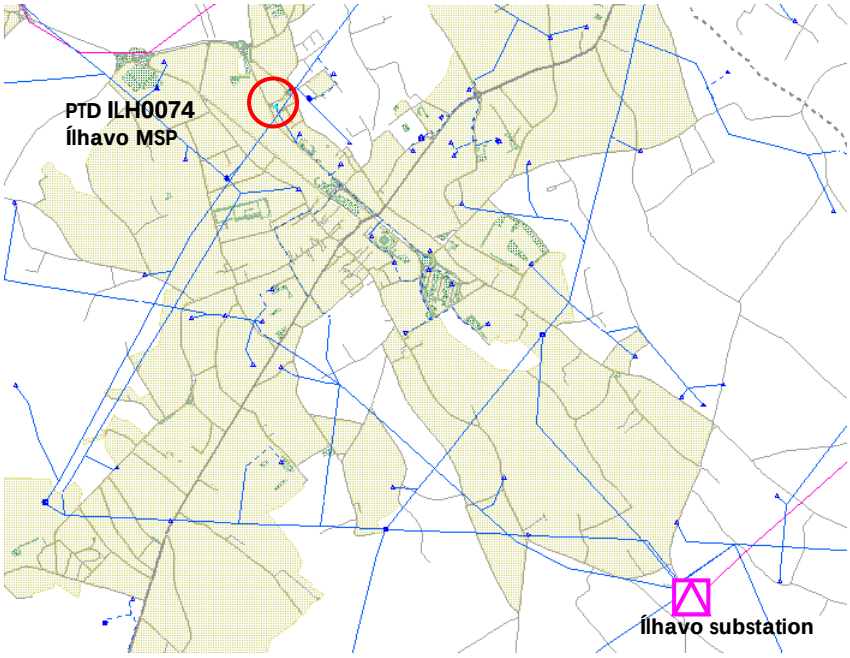

Figure 7 – Simplified diagram of the SE Ílhavo and its MV grid

2.3 Characterization of the Ílhavo MSP facilities

The Ílhavo MSP facilities are supplied in LV, directly from the PTD ILH0074 by an underground cable with about 25 m and it has a rated power of 87 kVA.

2.3.1 Main loads

Regarding the activity of this municipal building, main loads are characterized by:

- Air Treatment Units (ATU), that include basically 2 fans per unit;
- air conditioning systems (residential type);
- water pumps, that drive the swimming-pool hydraulic circuits;
- indoor and outdoor lighting.

The next figure shows the main switchboard of the facilities and their 8 main power circuits to the following sectors:

- sector 1;
- sector 2;
- sector 3;
- admission entrance;
- floor II;
- mechanical systems;
- building plugs;
- air treatment units.

Figure 8 – Main switchboard of the Ílhavo MSP

2.3.1.1 Sector 1

The load of the Sector 1 is mainly characterized by:

- general lighting (part I);
- plugs of the admission entrance;
- plugs of shower rooms, specially used by hand dryers.

2.3.1.2 Sector 2

The load of the Sector 2 is basically characterized by:

- general lighting (part II);
- other small loads.

2.3.1.3 Sector 3

The circuit of the Sector 3 supplies the following loads:

- swimming-pool spotlights – 26 lamps of 400 W (10,4 kW);
- other small loads (500 W).

2.3.1.4 Admission entrance

The admission entrance is mainly characterized by:

- lighting;
- 3 automatic selling machines.

2.3.1.5 Floor II

The second floor includes small loads as:

- general office lighting;
- administrative office lighting;
- personal computers.

2.3.1.6 Mechanical systems

In typical operating conditions, it can be measured about 27 A in the electric circuit that supplies the switchboard of the mechanical systems. This secondary panel supplies one of the main groups of loads, like:

- auxiliary water boiler:
  - 2 pumps of 1685 W;
  - 12 pumps of 245 W;
  - 1 pump of 50 W;
  - 4 circulation pumps of hot water to ATU.
- swimming-pool water circulation (typical current: 17 A)
  - main tank:
    - 3 circulation water pumps of 7,5 kW (starting in Y-D; operation of 2 simultaneous pumps in circular regimen – 1 backup pump);
    - 1 heat exchanger pump of 1685 W;
  - learning tank:
    - 2 circulation pumps of 5 kW (alternate operation);
    - 1 heat exchanger pump.
- hydro massage and splashing area:
  - hydro massage:
    - 2 circulation pumps of 3 kW (alternate operation):
    - 1 hydro massage compressor of 5 kW;
    - 1 heat exchanger pump;
  - splashing area:
    - 2 circulation pumps of 3 kW (alternate operation):
    - 1 heat exchanger pump.

Figure 9 – Auxiliary water boiler, supplied by natural gas, and respective circulation pumps


Figure 10 – Main tank and its 3 circulation pumps

2.3.1.7 Building plugs

This circuit is reserved to supply the most building plugs.

2.3.1.8 Air treatment units

The secondary switchboard dedicated to ATU supplies the following main loads:

- ATU 1 (typical current: 24 A) – Air treatment of the main swimming-pool room:
  - 1 blowing fan of 5 kW, with a soft-starter RSE 4025-C (11,2 A);
  - 1 extraction fan of 5 kW, with a soft-starter RSE 4025-C (12,5 A);
  - auxiliary systems.
- ATU 2 (typical current: 34 A) – Air treatment of the main swimming-pool room:
  - 1 blowing fan of 5 kW, with a soft-starter RSE 4025-C (12,2 A);
  - 1 extraction fan of 5 kW, with a soft-starter RSE 4025-C (10,5 A);
  - 1 dehumidification compressor of 5 kW, with a soft-starter RSE 4025-C (11 A);
  - auxiliary systems.
- ATU 3 (typical current: 23 A) – Air treatment of the main swimming-pool room:
  - 1 blowing fan of 7,5 kW, with a soft-starter RSE 4025-C (12,7 A);
  - 1 extraction fan of 7,5 kW, with a soft-starter RSE 4025-C (10 A);
  - auxiliary systems.
- ATU 4 – Air treatment of the shower rooms:
  - 1 blowing fan of 5 kW, with direct starting;
  - 1 extraction fan of 5 kW, with direct starting;
  - auxiliary systems.
- Air conditioning split 1 of 500 W;
- Air conditioning split 2 of 500 W.

Figure 11 – ATU 3 and its respective extraction and blowing fans

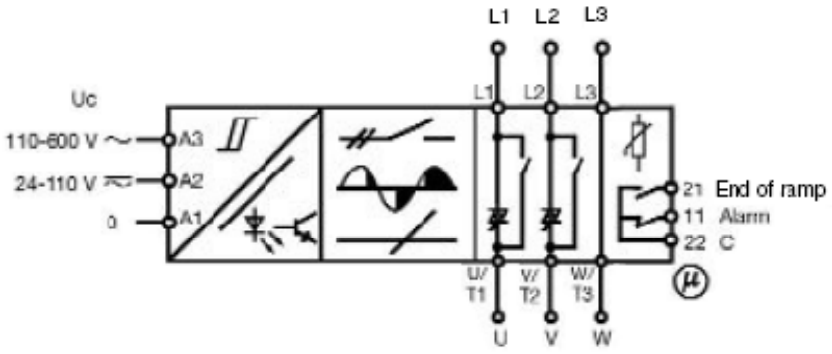

Figure 12 – Soft-starter RSE 4025-C functional diagram

2.3.2 Characterization of the micro-cogeneration system

The micro-cogeneration system is supported by a Capstone 60 MicroTurbine, of 60 kW, integrated in the private power grid of the Ílhavo MSP.

The generator group is composed by a natural gas turbine, an admission compressor and an electric generator, coupled by the same shaft and running at the same speed.

The output voltage is rectified to a DC bus, of 760 VDC, being later converted by a three-phase inverter, which injects power in the private power grid, supplying the local load, and exports the remaining power to the public distribution grid.

The following table shows the main electrical characteristics of the microturbine, operating in grid connected mode.

Net Power Output	60 (+0/-2) kW net 83 kVA max at 480 VAC 100A per phase max continuous 50/60 Hz (without gas compression)
Net Electrical Efficiency (LHV)	28 (±2) % (without gas compression)
Typical Heat Rate (LHV)	12,900 kJ (12,200 Btu) /kWh
Voltage Operating Range	360 to 528 VAC
Frequency Operating Range	50/60 Hz
Output Voltage Connection	3-phase, 3 or 4 wire wye (grid must be neutral grounded)
Output Current	100A RMS maximum steady state
Output Current THD	IEEE 519 compliant, 5%

Figure 13 – Microturbine electrical characteristics in grid connected mode

In islanding mode, during starting, shutdown and heavy load variations, as well as in transition events, the microturbine uses backup power, from a 288 V rated voltage battery, in order to have enough power to its starting up, ventilation during shutdown and to answer smoothly to some heavy load variations.

During the starting up phase, the electric machine operates as motor, accelerating progressively the set until the ignition speed of the gas turbine. From the ignition event, the acceleration is promoted by the gas turbine and the electric machine switches to operate as generator. This phase demands about 14 Wh, with a peak power of 6,8 kW, and takes about 42 seconds.

The normal shutdown cycle of the microturbine can delay up to 10 minutes, depending on its internal temperature. The shutdown phase starts with the gas supplying cut-off, however the gas turbine is kept turning in order to decrease its internal temperature. The rotation is maintained by the electric machine that comes back to operate as motor in this stage. This phase demands about 2 kW.

Figure 14 – Natural gas compressor (left) and Capstone 60 MicroTurbine (right)

This CHP project allows 60 kW electrical power and 120 kW thermal power. The heat contained in the exhaustion gases, of the turbine, is recovered for heating of the swimming-pool water, through a heat exchanger integrated in the micro-cogeneration system itself. After installation of this microturbine, the boiler is just used to support some peak temperature variations. Currently, it operates only as an auxiliary water boiler.

In order to assure the water circulation, it was installed a pump, of 200 W, in the hydraulic circuit of the heat exchanger.

According to the requirements of the gas turbine, the supplied natural gas from the distribution grid must be pressurized to 517 – 572 kPa. In order to guarantee these pressure values it was installed an auxiliary compressor, of 4 kW, in the inlet gas circuit.

The system integrates a dual mode controller, with a set of protections, which guarantees the switching to islanding mode in case of voltage interruption in the public grid, during the normal operation in grid connected mode. When voltage returns, the system switches, automatically, again to grid connected mode.

In undervoltage events, the protection systems switch the microturbine from grid connected mode to islanding mode, remaining the Ílhavo MSP load without supplying during about 4 minutes. After voltage recovery the undervoltage relay detects the voltage in about 0,5 seconds, switching the system from islanding to grid connected mode, being the loads liable to an interruption up to 5 seconds. These situations were realized in the field tests presented in the Chapter 5.

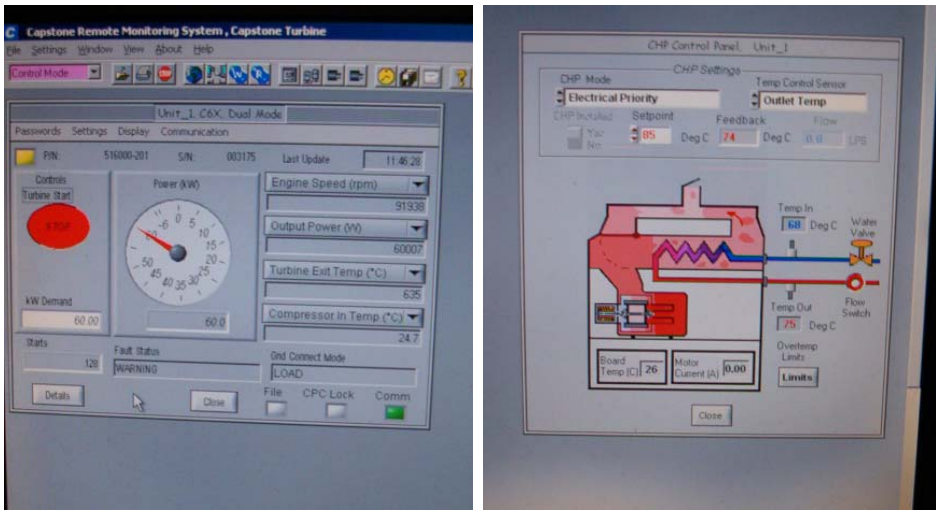

Figure 15 – Microturbine control and monitoring software

According to forecasting studies developed during the beginning of the project, the microturbine has not been operating in August due to no swimming-pool activity and by maintenance purposes. During a great part of the year, the heat generated by the microturbine has been enough to support the facilities demand, except in peak temperature variations. During the Autumn and Winter months it has been required a significant operation of the water heating boiler.

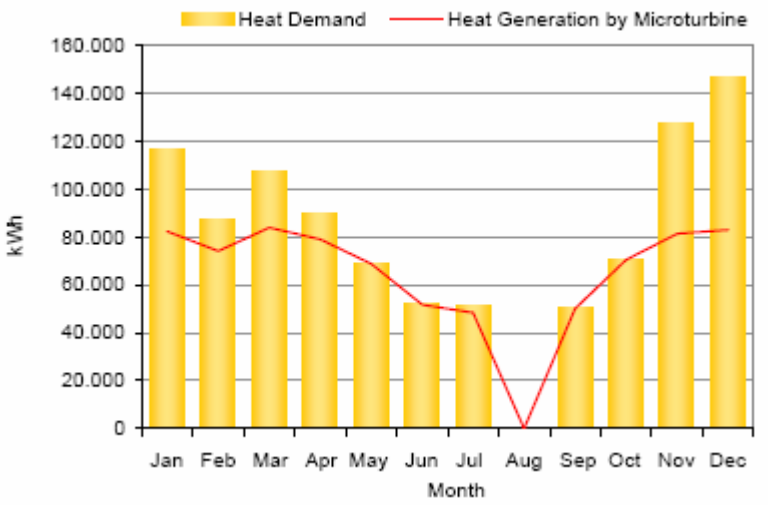

Figure 16 – Energy balance (estimated) / Heat demand and generation

Mainly from March to August, the electricity generated by the microturbine has been enough to support the facilities demand, exporting the remaining power to the public grid. From September to November some power has been demanded from the public grid.

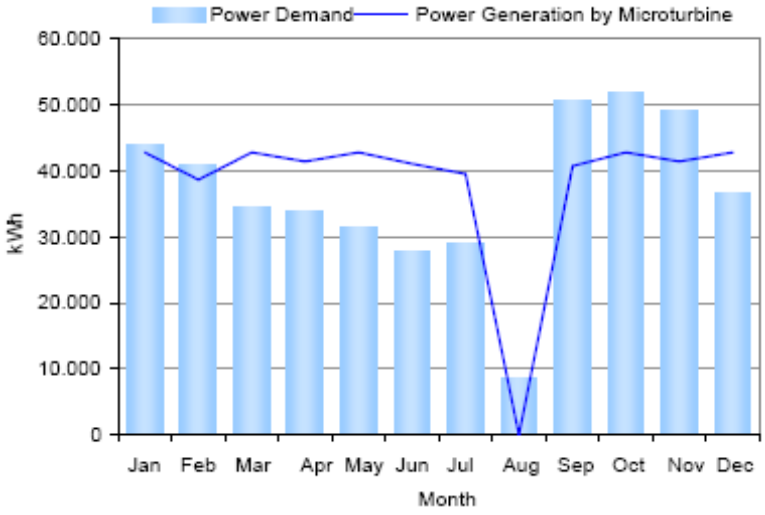

Figure 17 – Energy balance (estimated) / Power demand and generation

3 Power quality in the MV grid

From 13 July to 4 October of 2006, it was installed a PQA, Topas 1000, for voltage monitoring of the MV busbar (15 kV) of the SE Ílhavo, which supplies the PTD ILH0074.

Based on these PQ data and incident management recordings, it is possible to analyse the steady state voltage quality.

SE Ílhavo is geographically integrated in the Ílhavo municipality area, district of Aveiro – Portugal. The substation places in the HV grid as shown in the following simplified single-line diagram.

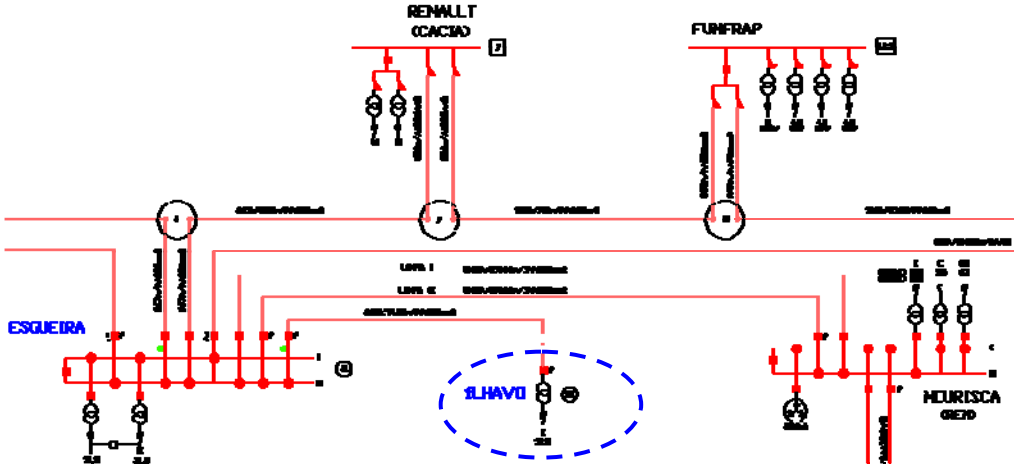

Figure 18 – Simplified single-line diagram of the HV grid (2006)

3.1 Steady state voltage quality analysis

In order to assess the voltage quality, the PQA was configured to analyse the voltage characteristics in the MV busbar, in accordance to the NP EN 50160 standard. The following figure shows the configuration of the PQA.

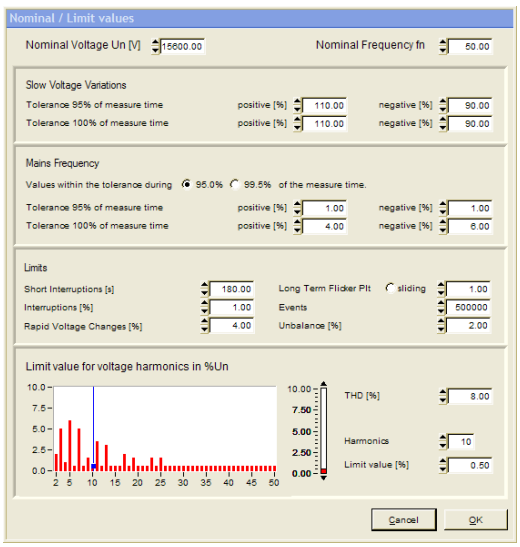

Figure 19 – Voltage quality analysis set-up based on the NP EN 50160 standard

According to this configuration, it was possible to draw the profile of voltage characteristics, mainly to the following parameters:

- voltage variations;
- harmonics;
- unbalance;
- flicker;
- fundamental frequency.

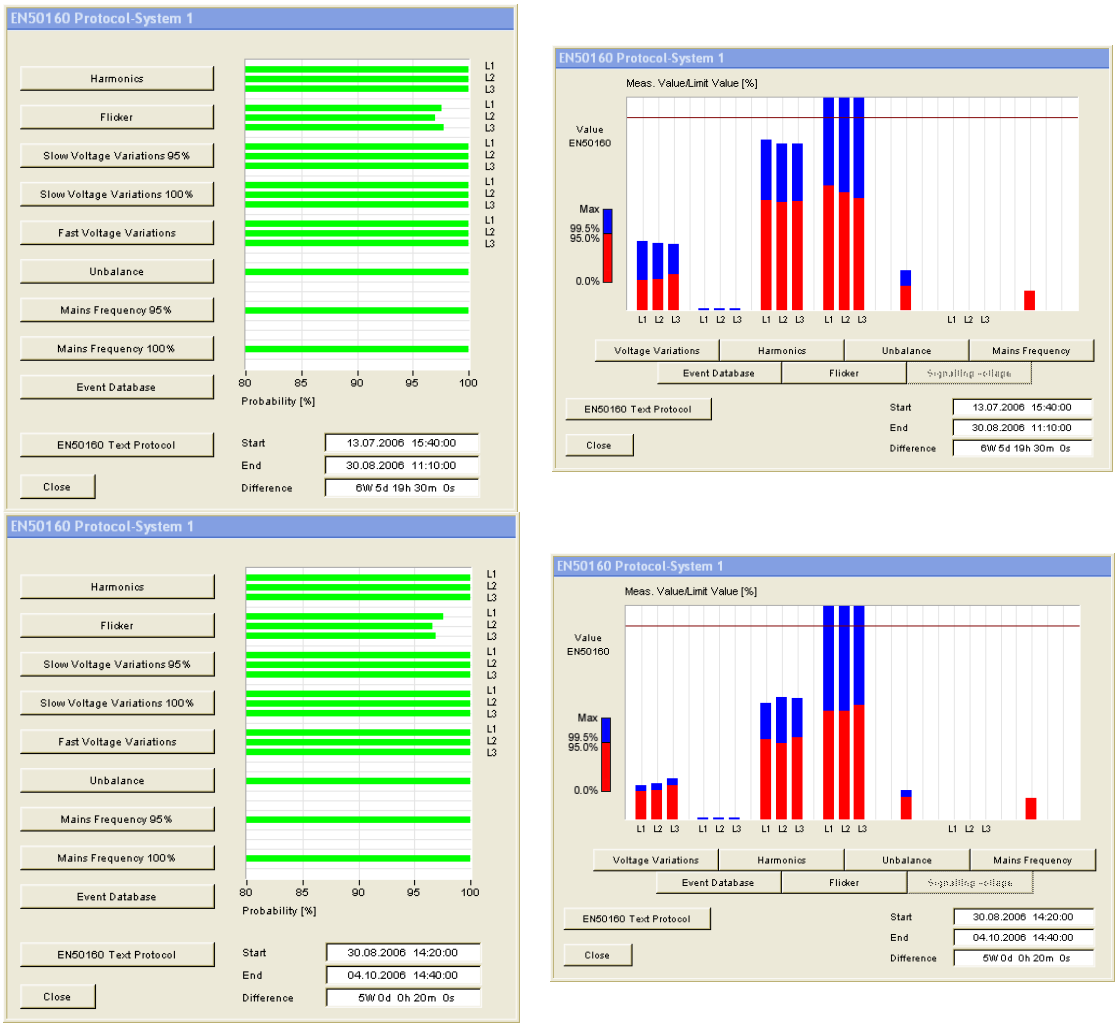

Figure 20 – Voltage compliance analysis with NP EN 50160 standard (MV busbar)

According to the results showed in this figure, it can be concluded that voltage measured in the MV busbar of the SE Ílhavo, during the monitoring period, was in compliance with NP EN 50160 standard, based on a reference voltage of 15,6 kV.

The long term flicker was the single parameter that exceeded the thresholds in some events. This situation was related to the occurrence of some voltage dips, which were not excluded from the flicker analysis. Anyway, the 95 percentil, required by the standard, was fulfilled.

3.1.1 Voltage variations

According to the analysis of the voltage RMS mean values, recorded in 10 minutes intervals, during the monitoring period there were not recorded significant variations, being the analysed voltage values inside of the voltage thresholds ($U_c \pm 10\%$).

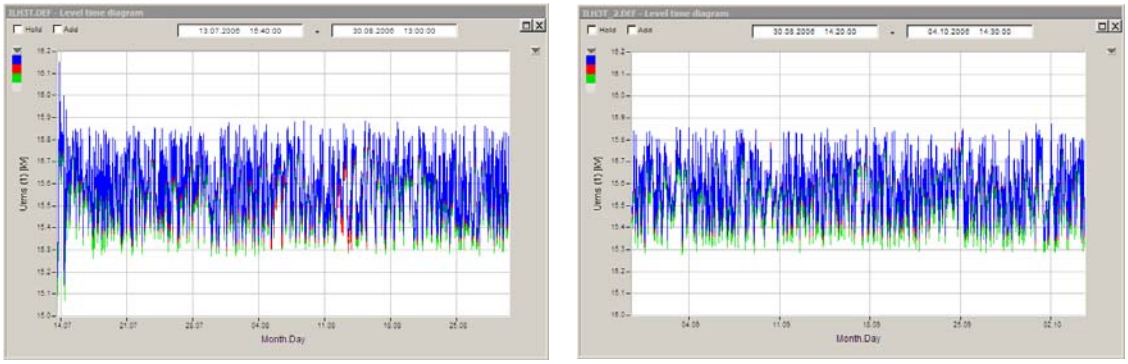

Figure 21 – Voltage RMS mean values, recorded in 10 minutes intervals (MV busbar)

3.1.2 Harmonic distortion

The Total Harmonic Distortion of voltage (THD_V), as well as individual harmonic voltages were inside of the standard tolerance limits. The following figure shows the THD_V relatively to fundamental, during the monitoring period. The admissible limit to THD_V is 8%.

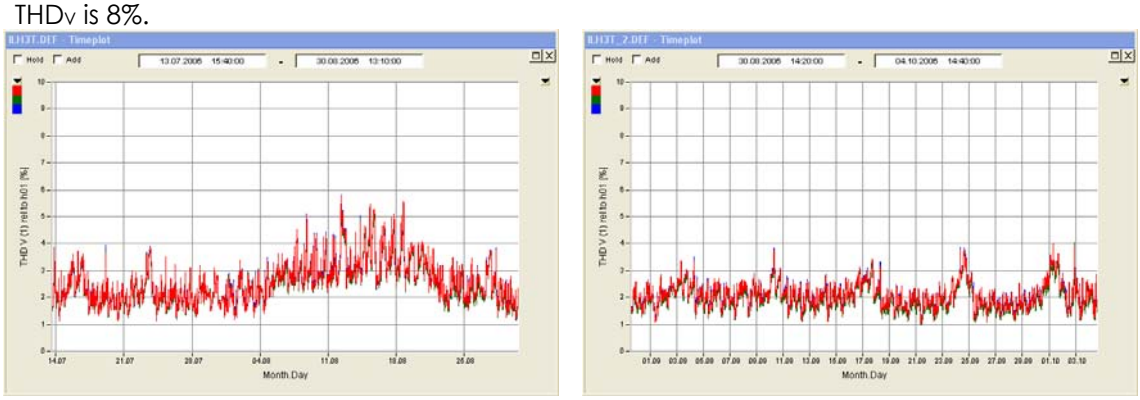

Figure 22 – Voltage THDv, recorded in 10 minutes intervals (MV busbar)

3.1.3 Voltage unbalance

During the monitoring period, the voltage unbalance values were considerably below to the standard limit (2%). The voltage unbalance typically did not exceed 0,3%.

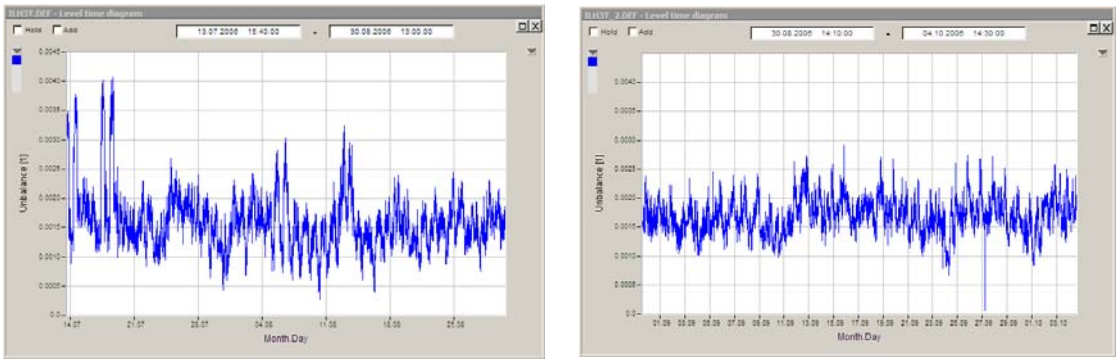

Figure 23 – Voltage unbalance, recorded in 10 minutes intervals (MV busbar)

3.1.4 Long term flicker

The long term flicker, caused by voltage fluctuations, was $P_{lt} > 1$ in some events, like voltage dips, but the standard compliance was guaranteed (95% of the time should be $P_{lt} \leq 1$). If these events were excluded from the flicker assessment, the long term flicker would be below to the limit of the NP EN 50160 standard during all the time.

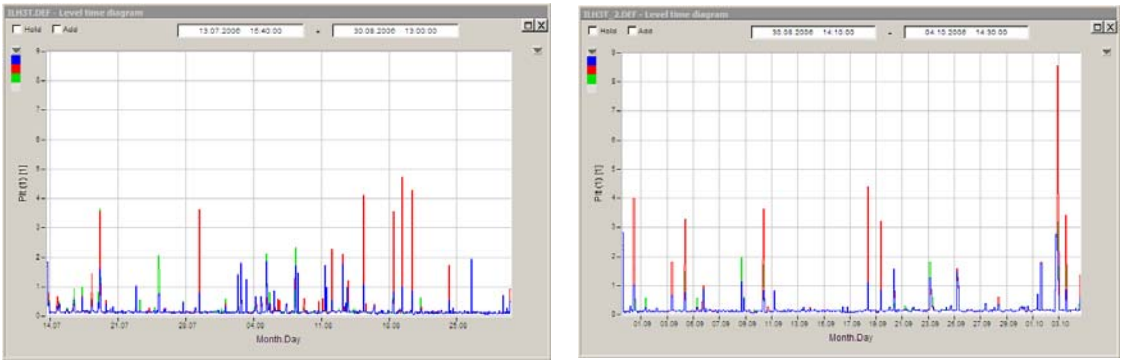

Figure 24 – Long term flicker (MV busbar)

3.1.5 Fundamental frequency

In terms of fundamental frequency, as expected all recorded values were in compliance with the standard limits.

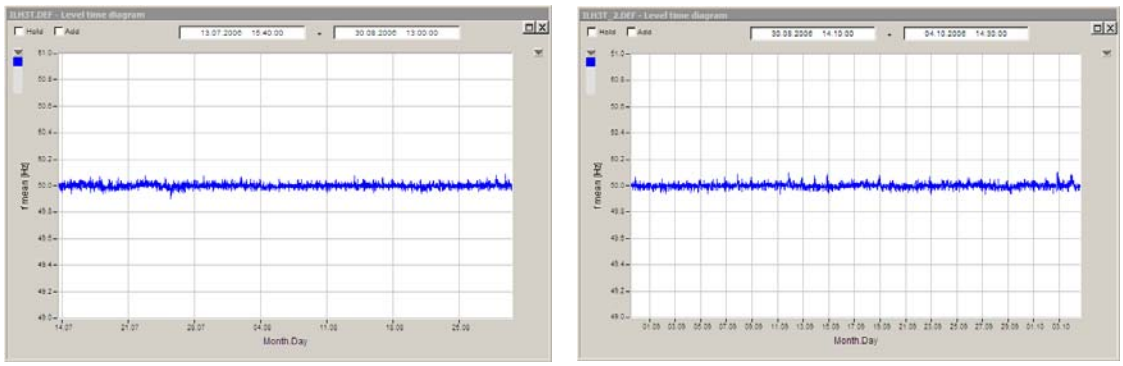

Figure 25 – Fundamental frequency (MV busbar)

4 Power quality in the LV grid

During the period from 5 January to 30 March of 2007, it was installed a PQA, QWave Power, to measure the voltage of the LV busbar of the PTD ILH0074. In this PQ monitoring campaign, the microturbine was still not operating.

During the period from 18 September to 26 October of 2009, it was installed another PQA, FLUKE 1760, to measure the voltage at the same LV busbar, in order to characterise the potential impact of the microturbine operation. In this new PQ monitoring campaign, the microturbine was already operating.

According to the PQ recording data and based on the incidents management information, it is possible to develop the following analysis:

- voltage continuity;
- steady state voltage quality;
- voltage dips.

4.1 PTD ILH0074 overview

The following figure shows the power transformer and the LV panel during the first monitoring campaign.

Figure 26 – Monitoring campaign in the PTD ILH0074

4.2 Voltage continuity analysis

The following table shows the number of voltage interruptions recorded in LV busbar of the PTD ILH0074 during both monitoring periods.

Table 1 – Voltage continuity in PTD ILH0074

VOLTAGE INTERRUPTIONS PTD ILH0074					
Campaign	ZQS RQS	Long term interruptions		Short term interruptions	Total duration
		N.º	Duration	N.º	
1st Campaign: 05.01.2007 – 30.032007	B	0	-	6	2 min 42 s
2nd Campaign: 18.09.2009 – 26.10.2009	B	0	-	0	-
ZQS – Quality of Service Zone; RQS – Portuguese Quality of Service Code					

4.3 Steady state voltage quality analysis

As shown to the SE Ílhavo, PQA were configured to analyse the voltage characteristics in the LV busbar in accordance to the NP EN 50160 standard.

With the PQ monitoring data it is possible to draw the profile of voltage characteristics, mainly to the following parameters:

- voltage variations;
- harmonics;
- unbalance;
- flicker;
- fundamental frequency.

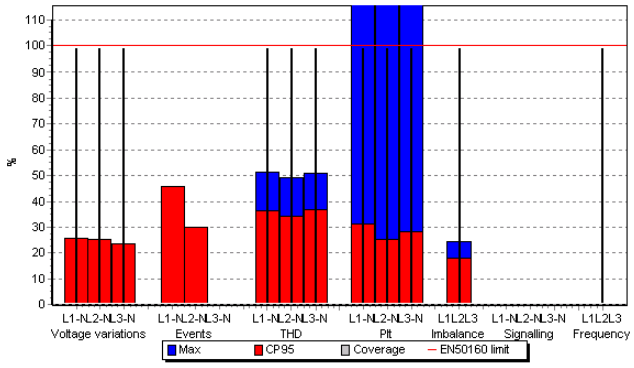

	Time step	EN 50160 limit	Average	CP95	Maximum
THD	10 min	8 %Un	1.92/1.78/1.99	2.90/2.75/2.93	4.11/3.95/4.07
Flicker Pst	10 min	1	0.15/0.14/0.14	0.22/0.22/0.22	2.86/3.49/2.97
Imbalance	10 min	2 %Un	0.22	0.36	0.49

Figure 27 – Voltage compliance analysis with NP EN 50160 standard – 1st campaign

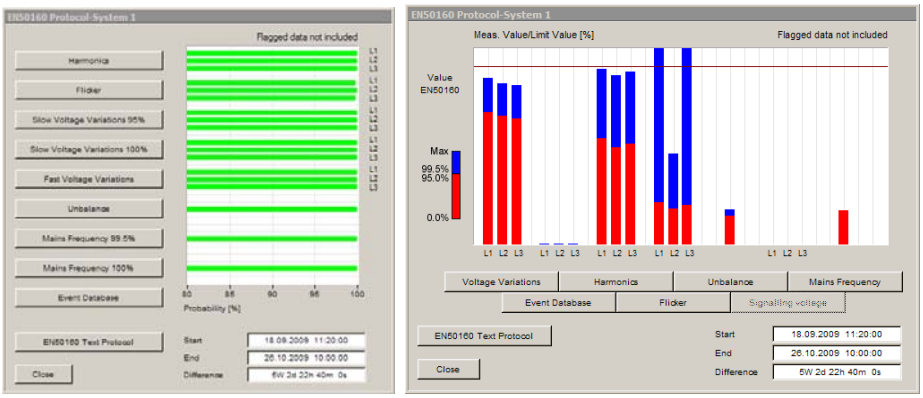

Figure 28 – Voltage compliance analysis with NP EN 50160 standard – 2nd campaign

According to the results showed in these figures, it can be concluded that voltage measured in the LV busbar of PTD ILH0074, during the monitoring periods, was in compliance with NP EN 50160 standard.

In terms of compliance to the NP EN 50160, the microturbine operation is not contributing to decrease the level of power quality. In fact, regarding the good short-circuit power of the distribution grid, only a slightly voltage increasing was recorded at the LV busbar. Anyway, the maximum voltage values remains quite below to the admissible value.

4.3.1 Voltage variations

Based on the analysis of the voltage RMS mean values, recorded in 10 minutes intervals, during the both monitoring periods, there were not recorded significant variations, being the analysed voltage values inside of the tolerance limits ($U_C \pm 10\%$).

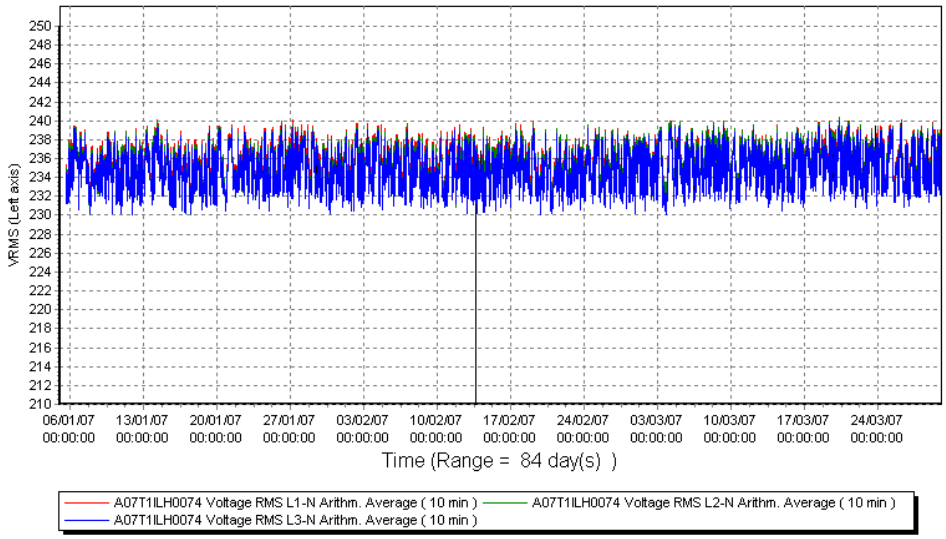

Figure 29 – Voltage RMS values, recorded in 10 minutes intervals – 1st campaign

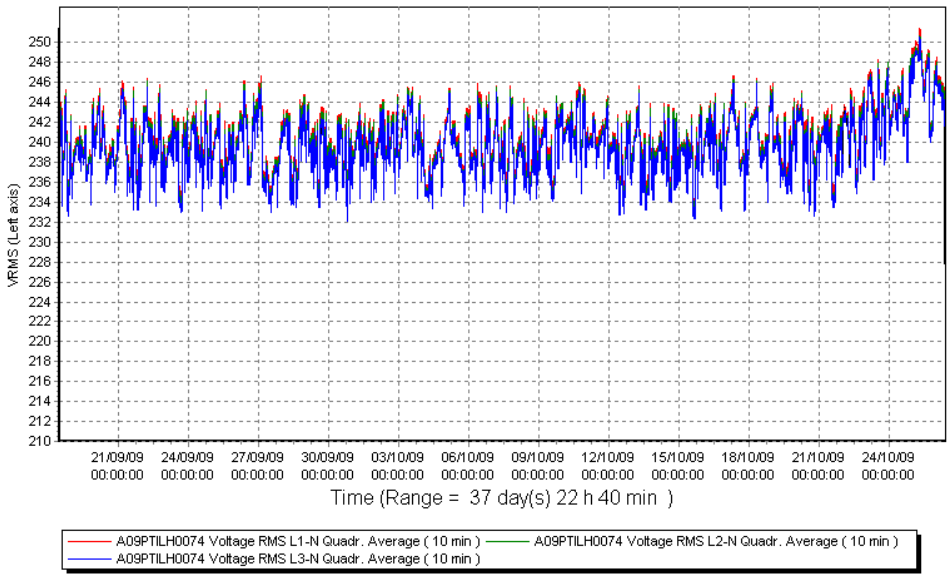

Figure 30 – Voltage RMS values, recorded in 10 minutes intervals – 2nd campaign

It is realized a slightly shift of the voltage RMS mean values. During the first campaign, without microturbine operation, voltage was typically below to 240 V and above of 230 V. During the second monitoring campaign, with microturbine operation, voltage was typically below to 244 V and above 234 V. In fact, it is realized an average increase of 4 V.

4.3.2 Harmonic distortion

The THD_V and individual harmonic voltages were bellow to the defined standard tolerance limits.

The following figures show the THD_V relatively to fundamental, during the both monitoring periods. It is realized a slightly increasing of the THDv during the 2nd campaign.

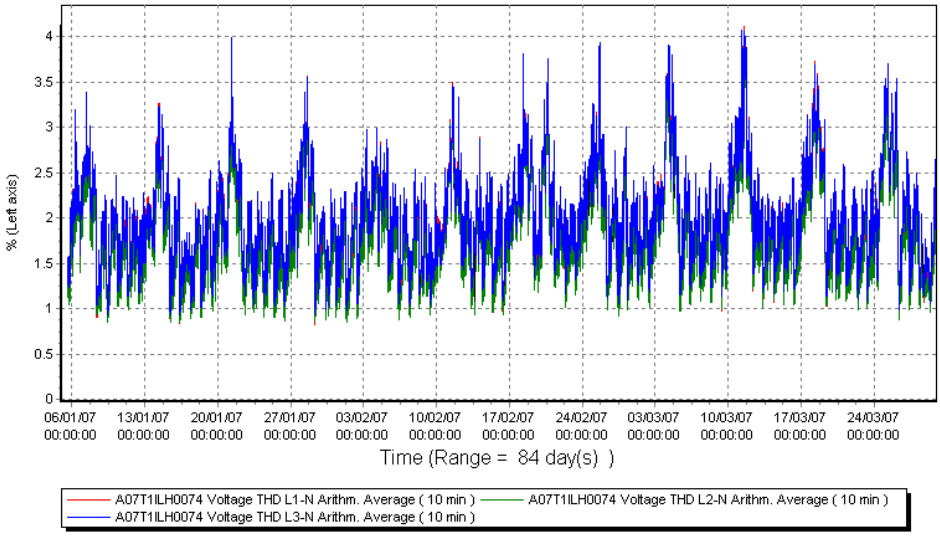

Figure 31 – Voltage THDv, recorded in 10 minutes intervals – 1st campaign

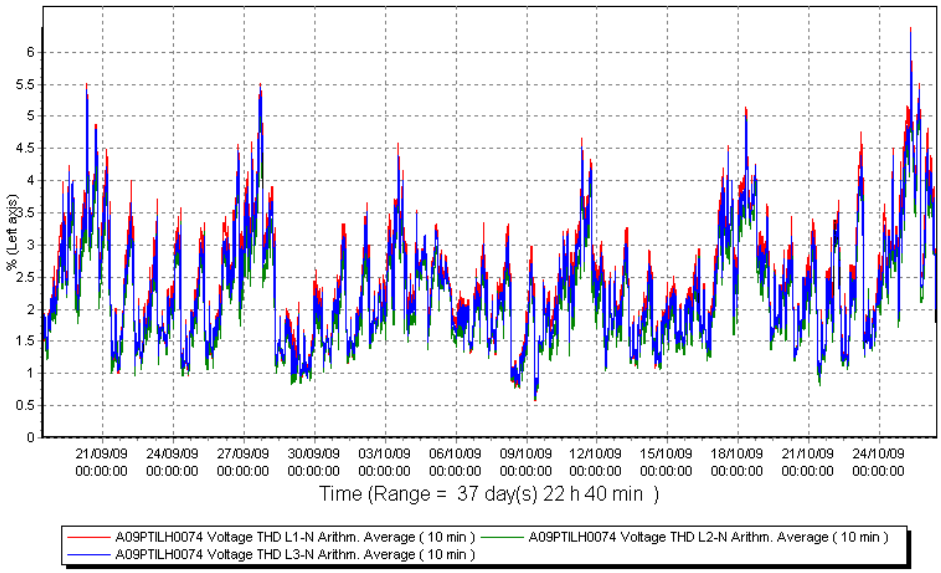

Figure 32 – Voltage THDv, recorded in 10 minutes intervals – 2nd campaign

4.3.3 Voltage unbalance

During the monitoring periods, the voltage unbalance values were considerably below to the standard limit (2%). The voltage unbalance normally did not exceed 0,36%.

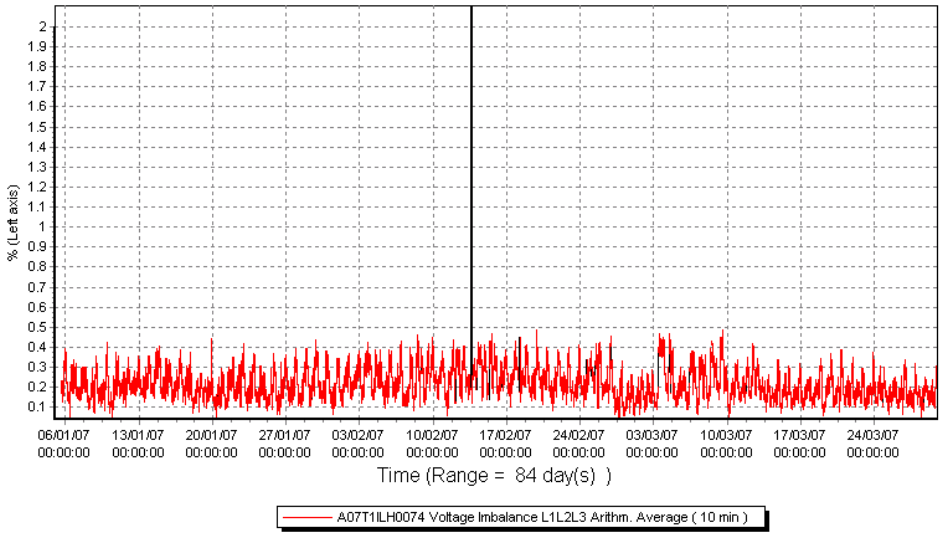

Figure 33 – Voltage unbalance recorded in 10 minutes intervals – 1st campaign

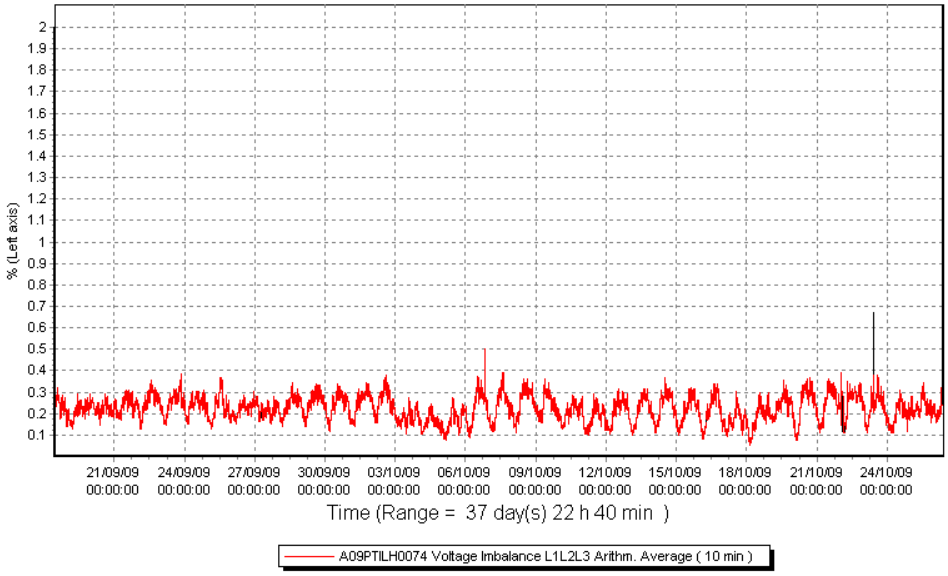

Figure 34 – Voltage unbalance recorded in 10 minutes intervals – 2nd campaign

4.3.4 Long term flicker

The long term flicker, caused by voltage fluctuations, was $P_{lt} > 1$ at some events, but the standard compliance was guaranteed (95% of the time should be $P_{lt} \leq 1$). As explained before to the SE Ílhavo, this situation was related to the occurrence of some voltage dips during the monitoring periods.

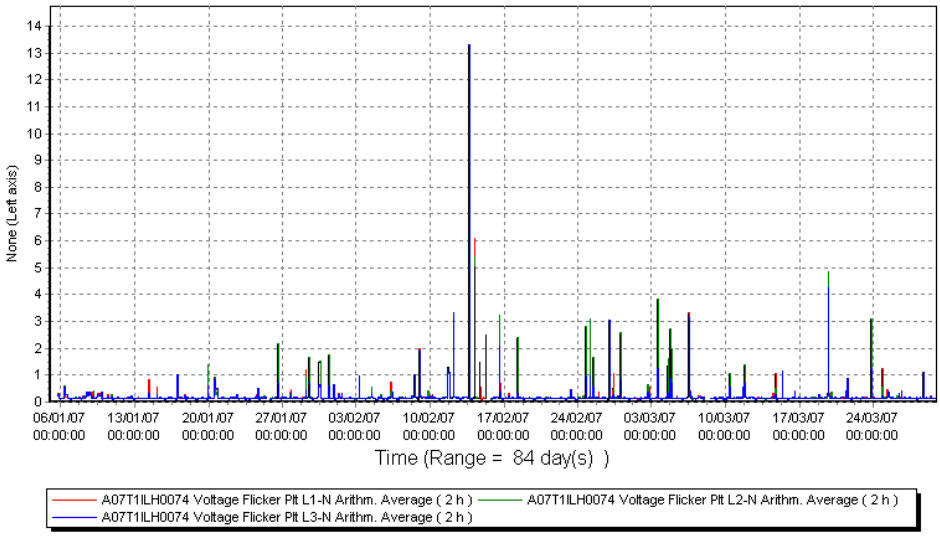

Figure 35 – Long term flicker – 1st campaign

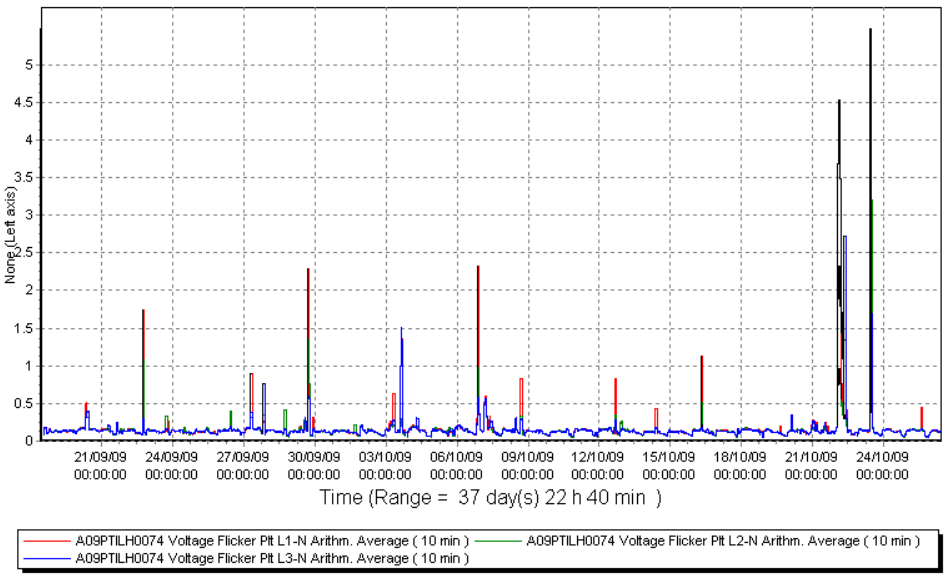

Figure 36 – Long term flicker – 2nd campaign

4.3.5 Fundamental frequency

In terms of fundamental frequency, all recorded values were in compliance with the standard limits in both monitoring campaigns.

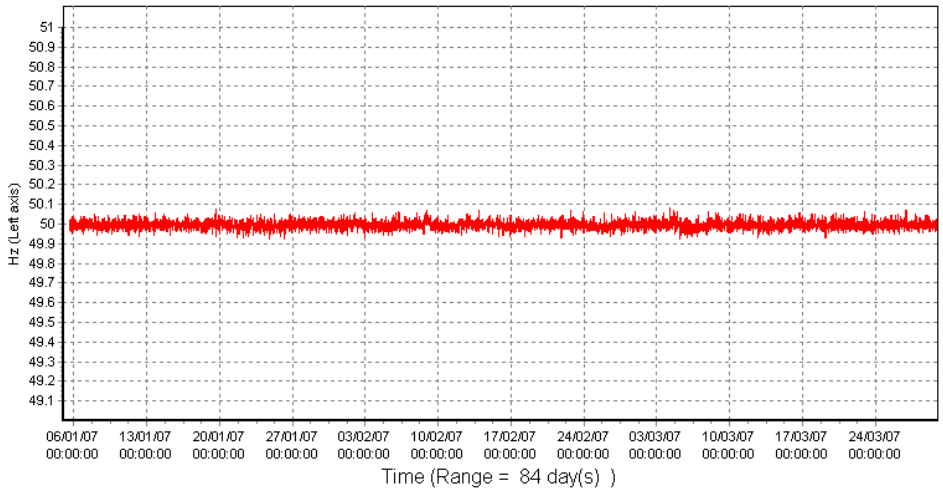

Figure 37 – Fundamental frequency – 1st campaign

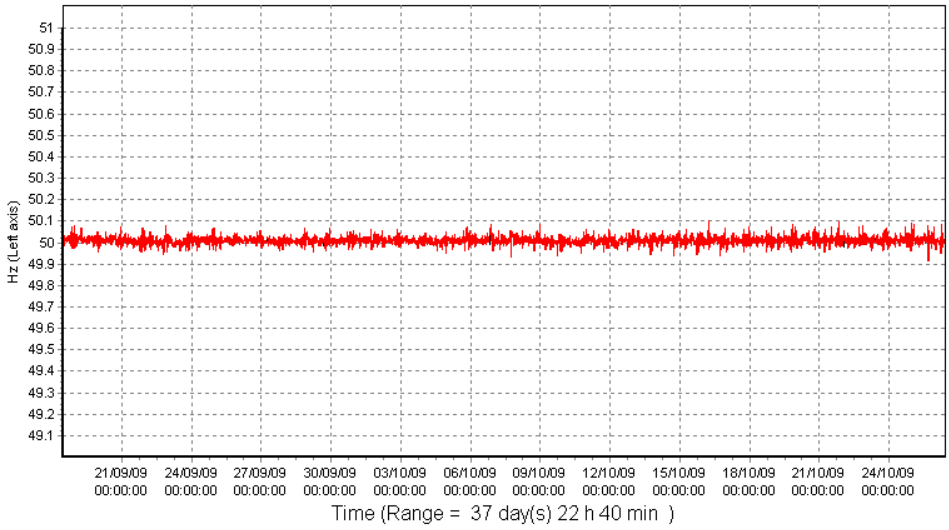

Figure 38 – Fundamental frequency – 2nd campaign

4.4 Voltage dips analysis

The following tables show a characterization of the events (voltage dips) recorded in the LV busbar of the PTD ILH0074 during the monitoring periods, being the number of events and the respectively severity determined only by measurements aggregation (equivalent event with amplitude of the deepest voltage dip and duration of the longest voltage dip), without any temporal aggregation.

Table 2 – LV Busbar events characterization - 1st campaign

LV Busbar EVENTS (From 05/01/2007 to 30/03/2007)								
t[s] Amplitude U (% of Uref)	0,01 < t <= 0,1	0,1 < t <= 0,25	0,25 < t <= 0,5	0,5 < t <= 1	1 < t <= 3	3 < t <= 20	20 < t <= 60	60 < t <= 180
90 > U >= 80	8	10			3			
80 > U >= 70	1	26	2	6	2			
70 > U >= 60		1						
60 > U >= 50		1	1					
50 > U >= 40			1		2			
40 > U >= 30		1						
30 > U >= 20								
20 > U >= 10								
10 > U >= 1								

According to this analysis methodology, during the 1st monitoring period, there were recorded 65 events (voltage dips) in the LV busbar, with amplitudes (ΔU) and durations typical below to 30% and 250 ms, respectively.

Table 3 – LV Busbar events characterization – 2nd campaign

LV Busbar EVENTS (From 18/09/2009 to 26/10/2009)								
t[s] Amplitude U (% of Uref)	0,01 < t <= 0,1	0,1 < t <= 0,25	0,25 < t <= 0,5	0,5 < t <= 1	1 < t <= 3	3 < t <= 20	20 < t <= 60	60 < t <= 180
90 > U >= 80		2						
80 > U >= 70		3						
70 > U >= 60		6	1					
60 > U >= 50								
50 > U >= 40								
40 > U >= 30								
30 > U >= 20		1						
20 > U >= 10								
10 > U >= 1								

According to this analysis methodology, during the 2nd monitoring period, were recorded 13 events (voltage dips) in the LV busbar, with amplitudes (ΔU) and durations typical below to 40% and 250 ms, respectively.

4.5 Load profile of PTD ILH0074 and Ílhavo MSP facilities

The following figures show the current RMS mean values, recorded in 10 minutes intervals. The first graph shows the total current measured in the secondary of the MV/LV transformer and the second graph shows the current of the feeder where is connected the microturbine. Both graphs are not comparable, however they are presented to show typical load profile of the PTD ILH0074 and the Ílhavo MSP facilities with microturbine operation.

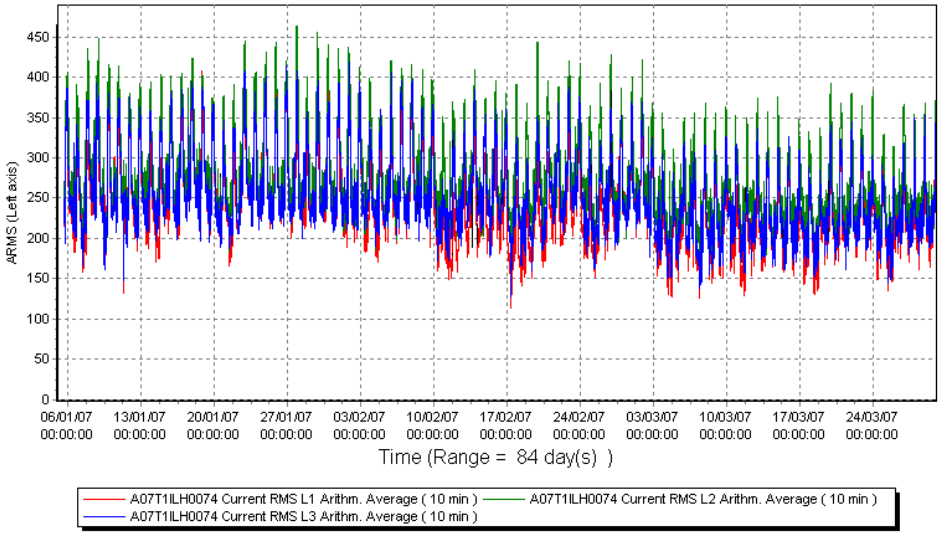

Figure 39 – Current RMS mean values of the MV/LV transformer, recorded in 10 minutes intervals – 1st campaign

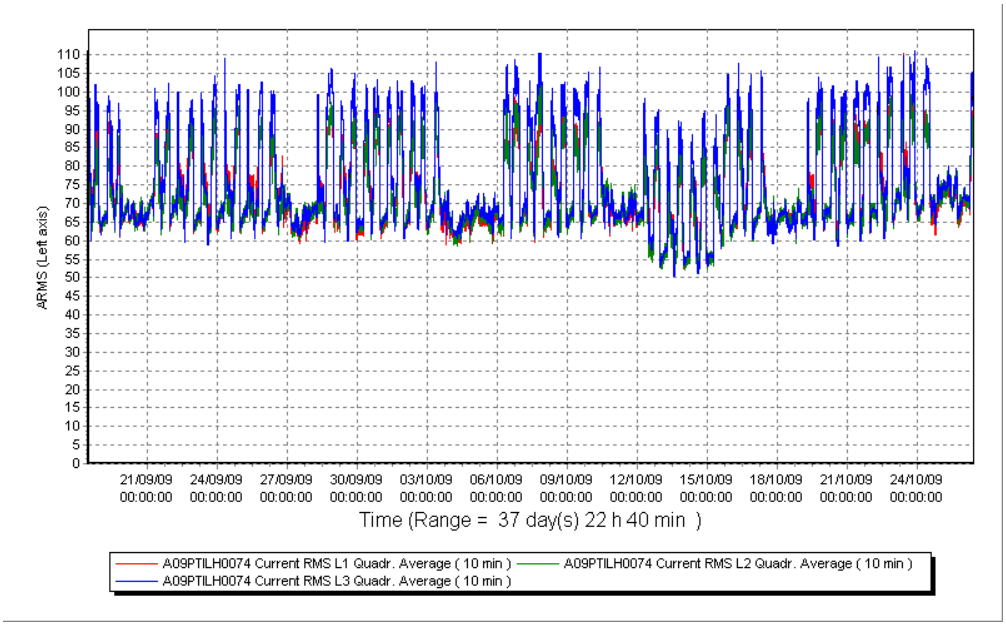

Figure 40 – Current RMS mean values of the Ílhavo MSP, recorded in 10 minutes intervals, with microturbine operation – 2nd campaign

5 Field tests in grid connected and islanding modes

Based on the characteristics of the test site, the first phase of field tests was developed in order to analyse the microturbine behaviour in the following scenarios:

- starting and shutdown of the microturbine;
- operation of the microturbine in grid connected mode with the public LV distribution grid, performing an extensive analysis of the microturbine response in order to identify its simulation parameters;
- operation of the microturbine in islanding mode to analyse the microturbine behaviour in several load regimens;
- black-starting of the microturbine;
- analysis of transitions and switching between grid connected and islanding modes in several load regimens.

In order to perform the above tests, it was installed a PQA, FLUKE 1760, in the circuit which connects the microturbine output to the switchboard of the Ílhavo MSP.

The following figure shows the monitoring device in the panel of the microturbine and the analysis laptop.

Figure 41 – Field tests measurement in the Ílhavo MSP

5.1 Microturbine operation in grid connected mode

This field test was developed in order to identify the simulation parameters of the microturbine and to analyse its behaviour during the starting phase, operating as motor and as generator.

Microturbine was operated in several generation regimens, decreasing and increasing gradually the generation set-point in steps of 5 kW.

The following time-line shows the development of this field test.

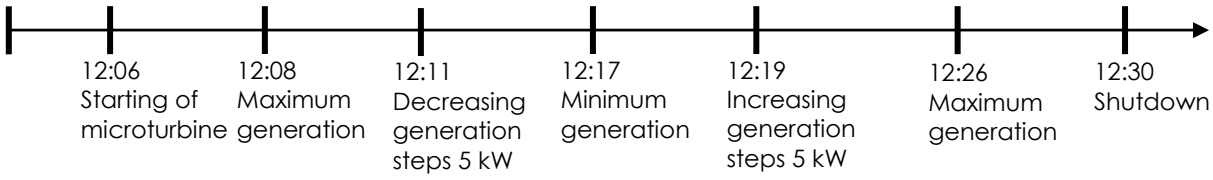

Figure 42 – Field tests time-line

5.1.1 Starting of the microturbine

These graphs show the starting phase of the microturbine, operating as motor, the switching to generation mode and the generation ramp up to the maximum power.

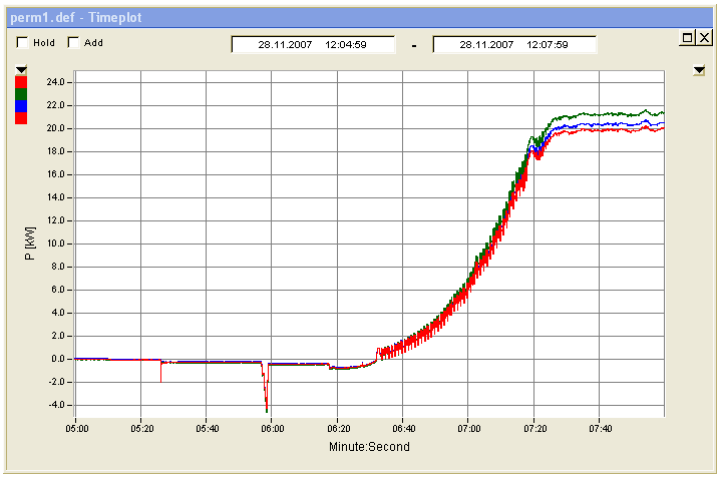

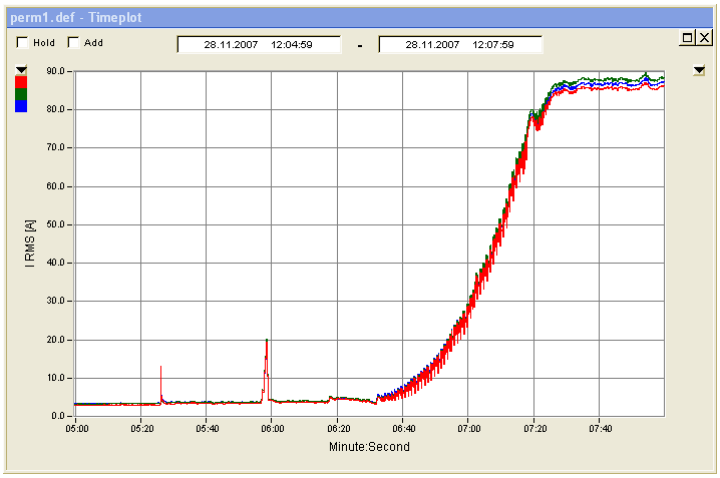

Figure 43 – Power and current during the starting of the microturbine

The rated power was not achieved due to the environmental conditions in the microturbine's room.

From the starting point to the maximum generation power it is realized a voltage increasing of about 2 V.

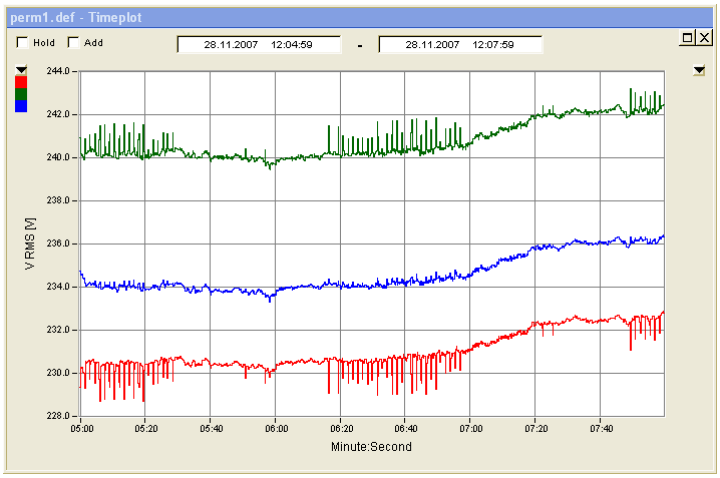

Figure 44 – Voltage RMS values during the starting of the microturbine

5.1.2 Microturbine operation in several generation regimens

This test shows the impact of the generation regimen on the voltage of the distribution grid. In fact, as consequence of the good short-circuit power and due to the reduced length of the circuit from the PTD ILH0074 to the microturbine, the impact of the generation on the voltage is quite reduced. It is realized a slight voltage increasing when microturbine operates at the maximum power.

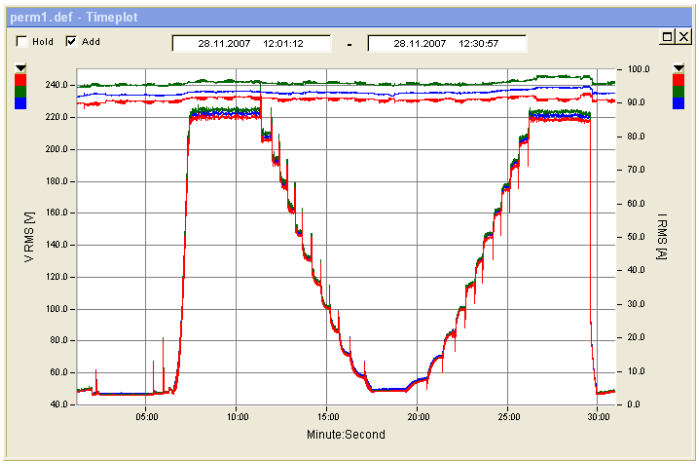

Figure 45 – Voltage and current RMS values during the Field Test 1

5.2 Microturbine operation in islanding mode

The field test in islanding operation mode was conducted to analyse the voltage and frequency response of the microturbine and to assess its capacity to follow heavy load variations.

The following time-line shows the evolution of this test.

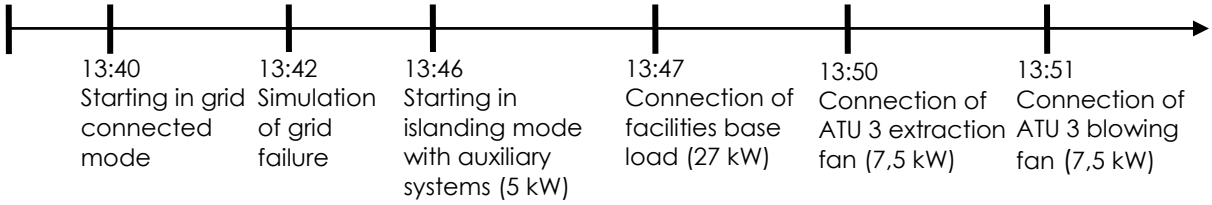

Figure 46 – Field tests time-line

5.2.1 Starting in grid connected mode

To conduct this test, the microturbine started in grid connected mode.

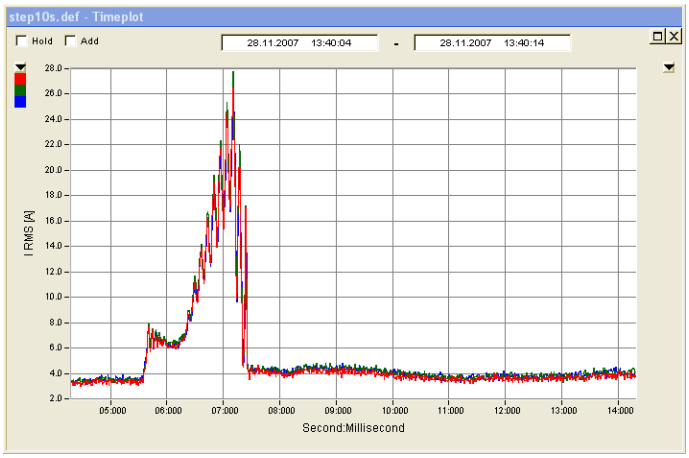

Figure 47– Current during the starting of the microturbine

This graph shows the peak of current achieved during the starting phase.

5.2.2 Simulation of grid failure

In this phase, it was simulated a voltage interruption in order to force the dual-mode controller to switch the microturbine to islanding operation mode. In these situations the microturbine is submitted to a forced shutdown.

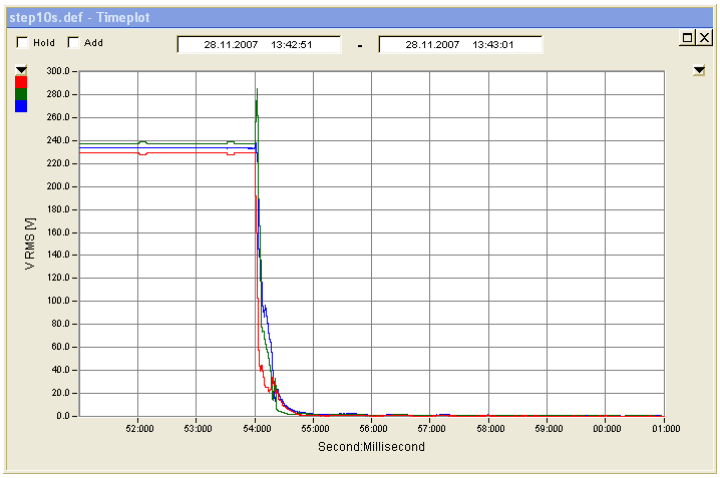

Figure 48 – Voltage RMS values in the grid failure

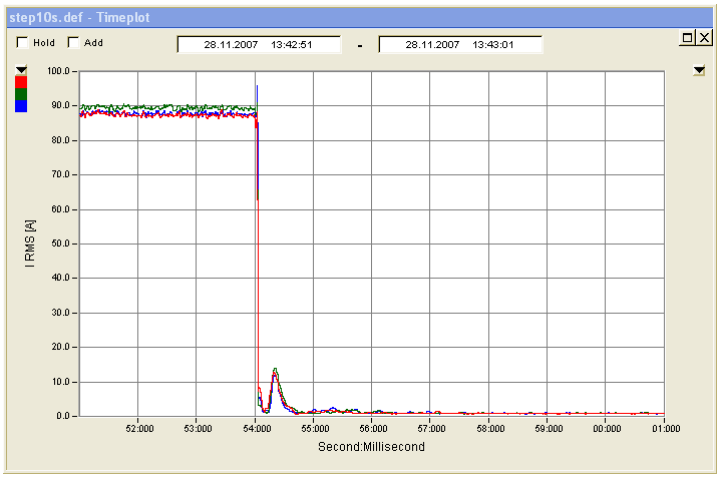

Figure 49 – Current RMS values in the grid failure

5.2.3 Starting in islanding mode with auxiliary systems

After the voltage interruption, the microturbine restarts in islanding mode, being the following auxiliary systems supplied by the battery backup:

- Gas compressor of 4 kW, that supplies the microturbine;
- Water pump for water circulation;
- Microturbine admission fan.

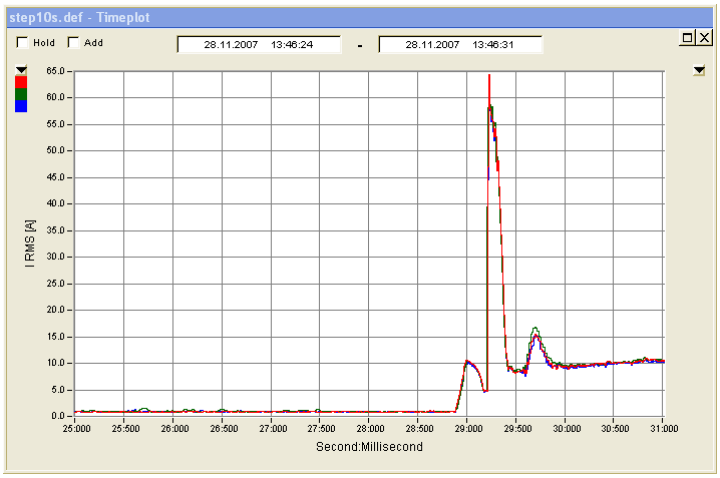

Figure 50 – Current during the starting in islanding mode

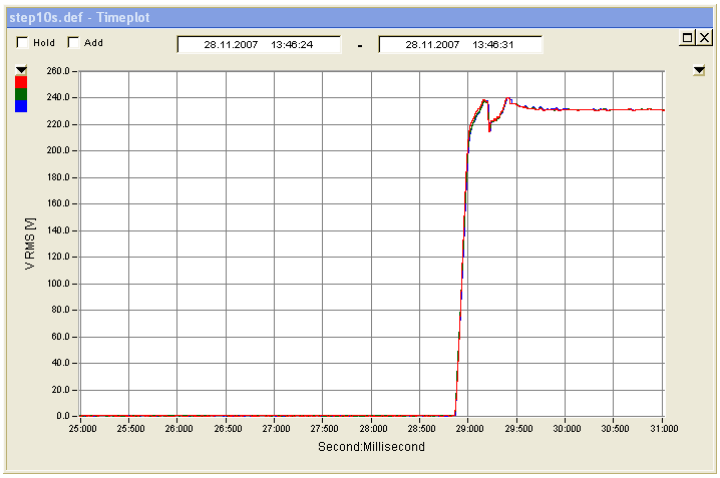

Figure 51 – Voltage RMS values during the starting in islanding mode

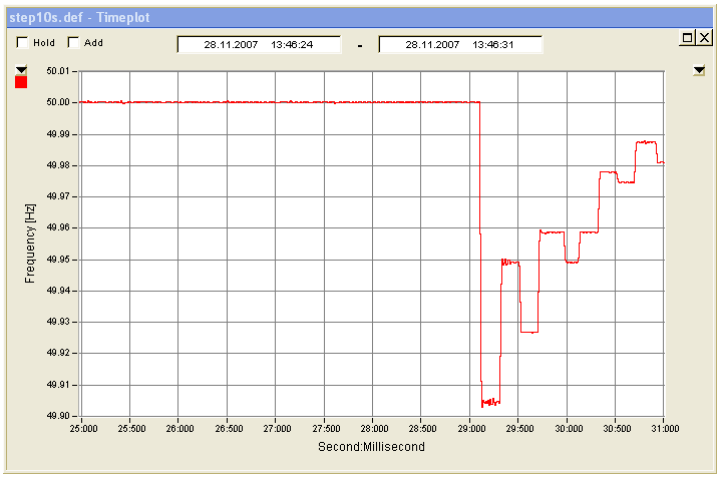

Figure 52 – Frequency during the starting in islanding mode

5.2.4 Connection of the facilities base load

The facilities base load includes the general services of the swimming-pool building, like pumps, lighting, computers, etc. In this step, it was connected, in islanding mode, about 27 kW. The larger loads of the swimming-pool, ATU, were maintained disconnected.

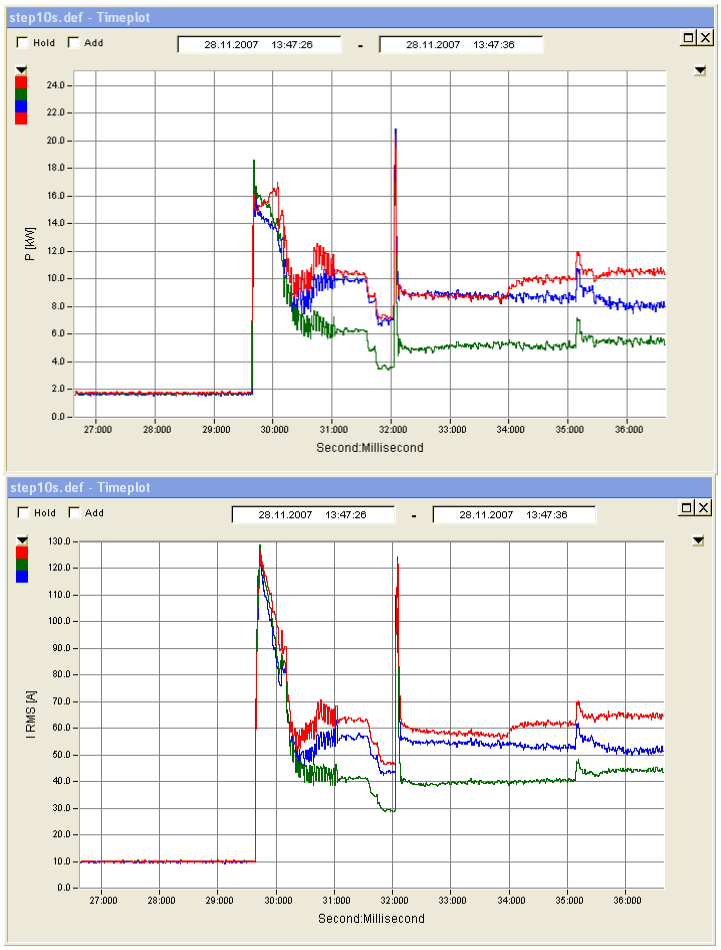

Figure 53 – Power and current during the connection of facilities base load

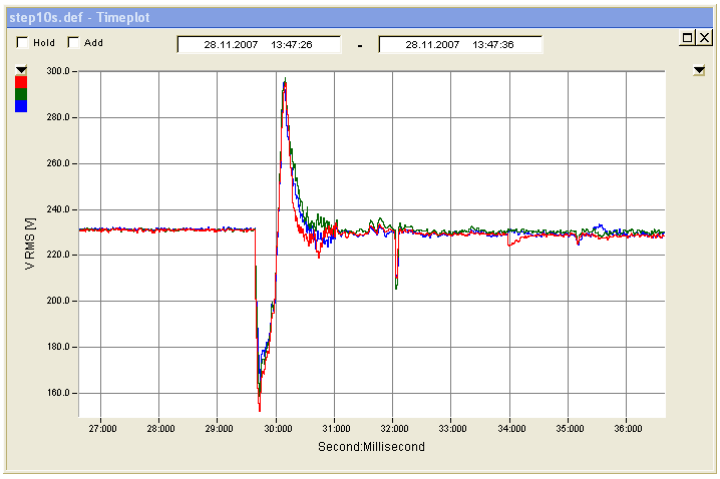

Figure 54 – Voltage RMS values during the connection of facilities base load

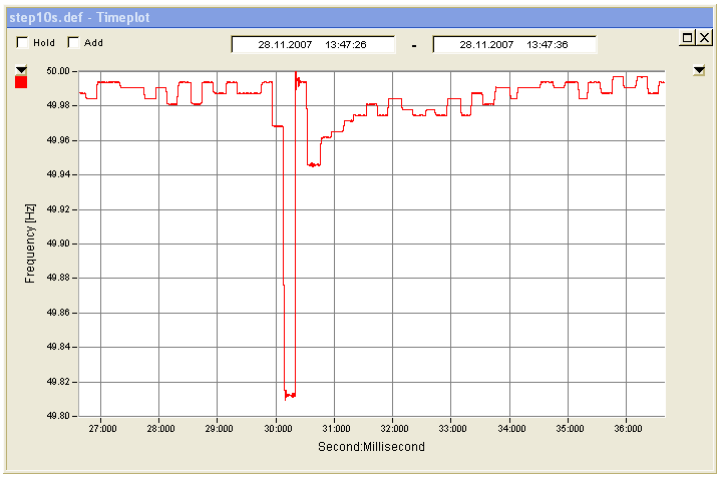

Figure 55 – Frequency during the connection of facilities base load

Based on these measurements, it was possible to confirm the expected impact of the load variation on the island voltage. The connection of 27 kVA caused a variation of 30% on the voltage RMS values and 0,3% on the fundamental frequency.

5.2.5 Connection of the ATU 3 extraction fan

The extraction fan connected in this step is characterized by an induction motor of 7,5 kW, started by a soft-starter.

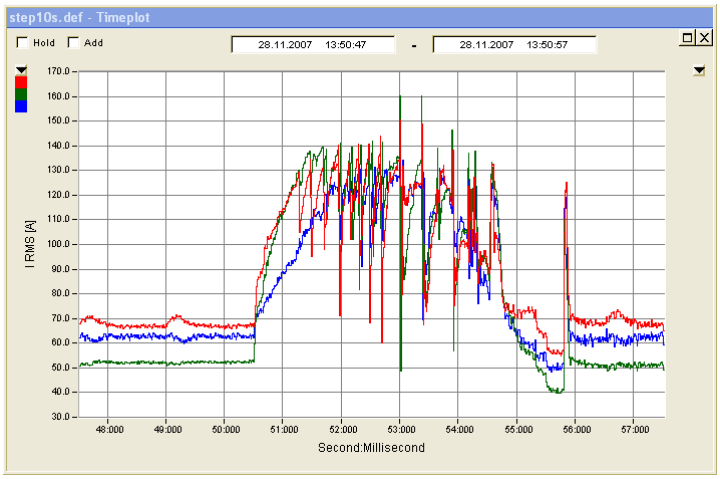

Figure 56 – Current during the starting of the extraction fan of the ATU 3

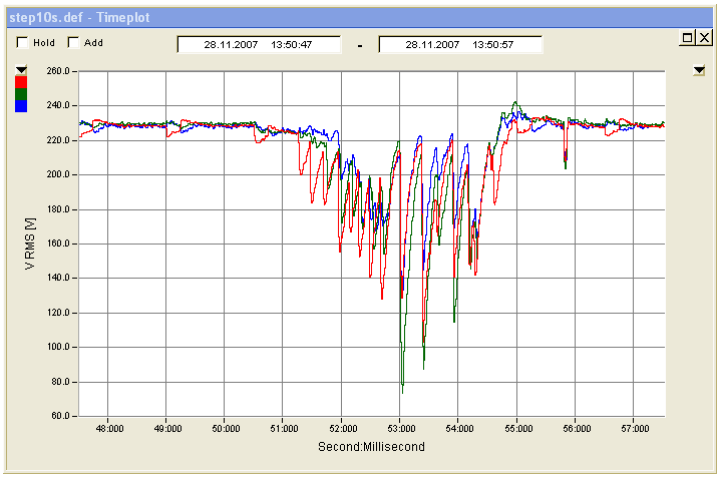

Figure 57 – Voltage RMS values during the starting of the extraction fan of the ATU 3

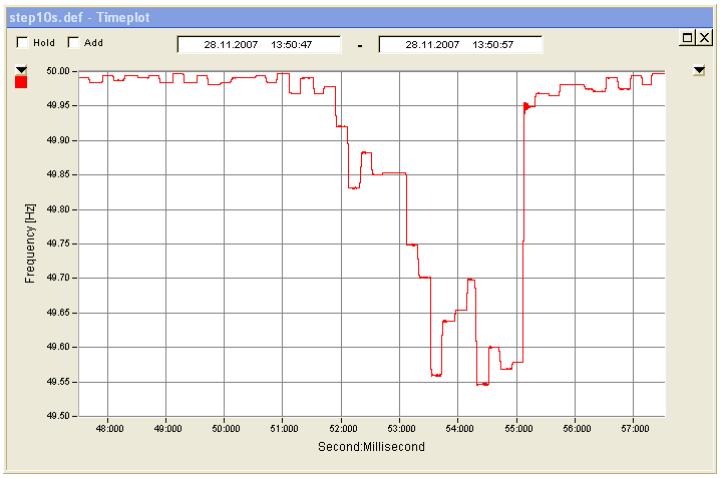

Figure 58 – Frequency during the starting of the extraction fan of the ATU 3

In this step, there were recorded a voltage dip of 65% amplitude and a frequency variation of 0,9%.

5.2.6 Connection of the ATU 3 blowing fan

The blowing fan connected in this step is also characterized by an induction motor of 7,5 kW, started by a soft-starter.

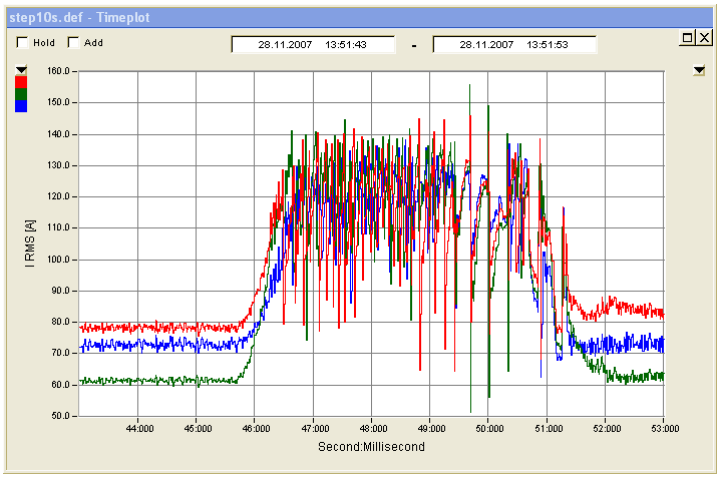

Figure 59 – Current during the starting of the blowing fan of the ATU 3

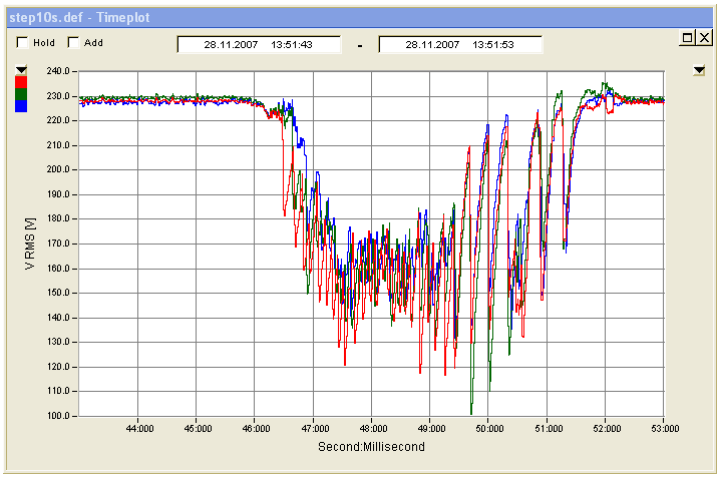

Figure 60 – Voltage RMS values during the starting of the blowing fan of the ATU 3

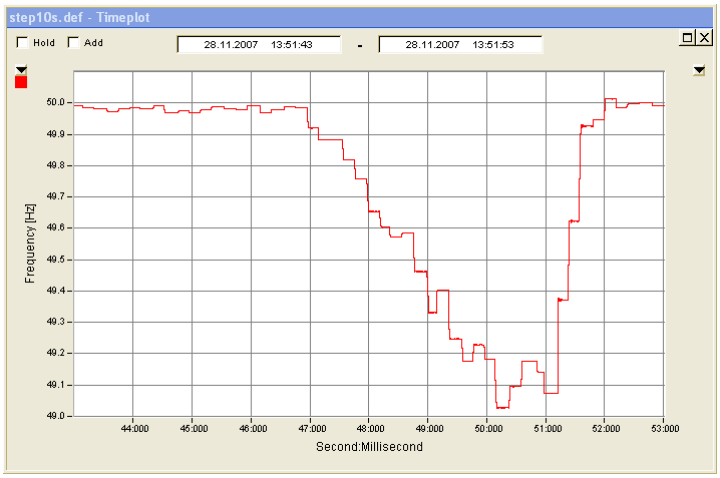

Figure 61 – Frequency during the starting of the blowing fan of the ATU 3

As realized in the previous step, there were recorded a severe voltage dip and a significant frequency variation with the connection of this motor.

5.3 Switching between grid connected and islanding modes

This field test was specially focused on the validation of the possibility to transfer between grid connected and islanding modes.

The following time-line shows the evolution of this test.

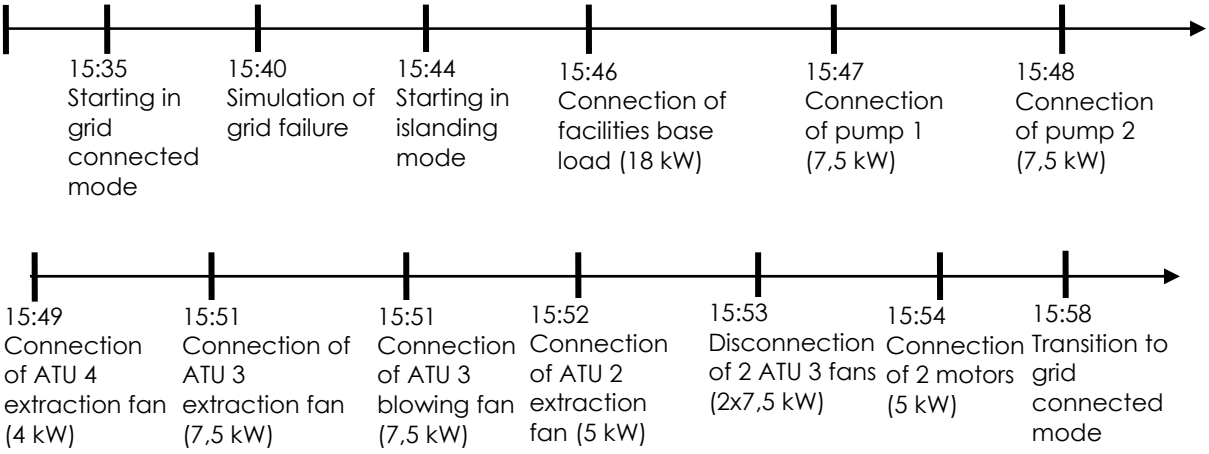

Figure 62 – Field tests time-line

5.3.1 Starting in grid connected mode

As performed to the previous tests, this phase also started with starting of the microturbine in grid connected mode.

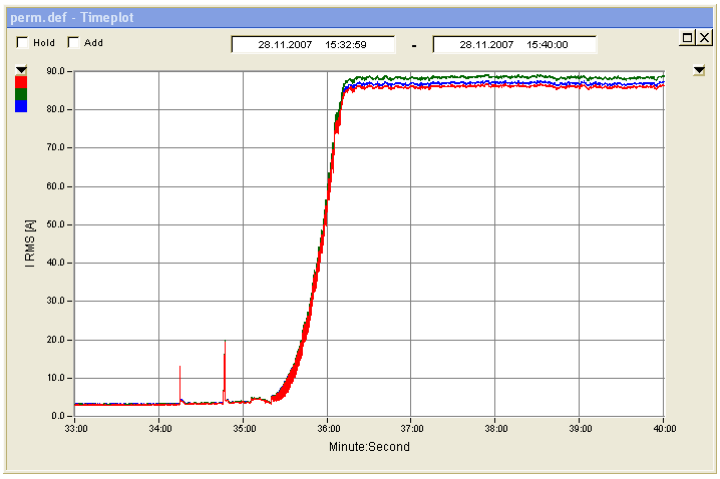

Figure 63 – Current during the starting of the microturbine

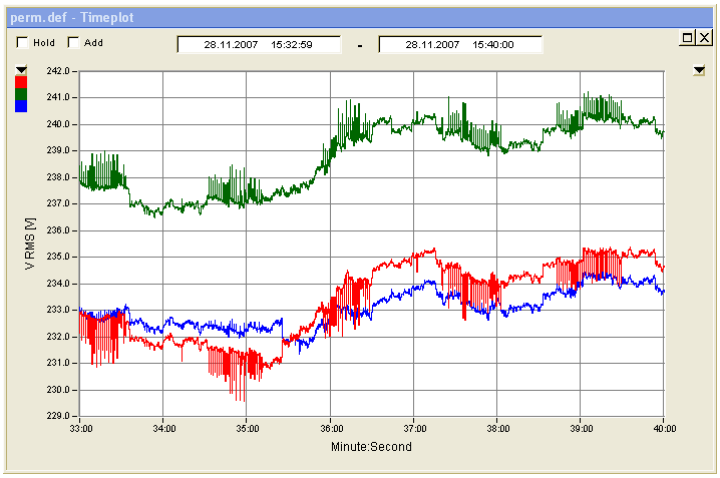

Figure 64 – Voltage RMS values during the starting of the microturbine

5.3.2 Simulation of grid failure and starting in islanding mode

The following 3 figures show the behaviour of the system during the transition from grid connected to islanding mode. After a grid failure, the microturbine shutdowns and restarts in islanding mode after about 3,5 minutes.

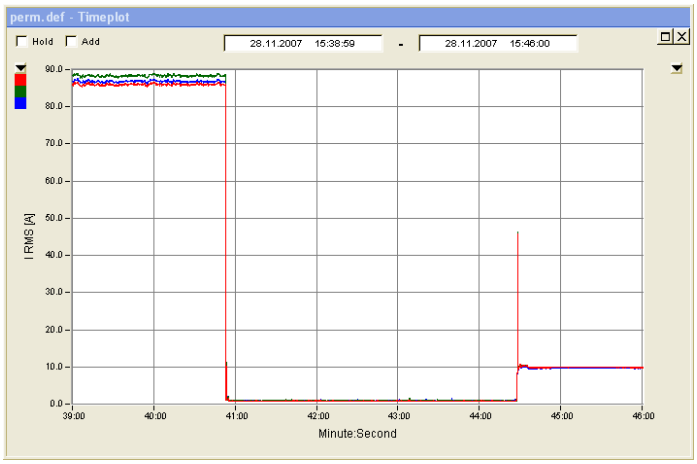

Figure 65 – Current RMS values of the microturbine

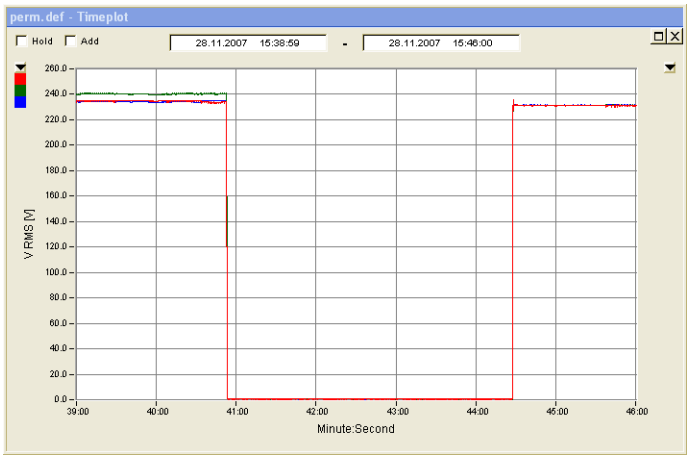

Figure 66 – Voltage RMS values of the microturbine

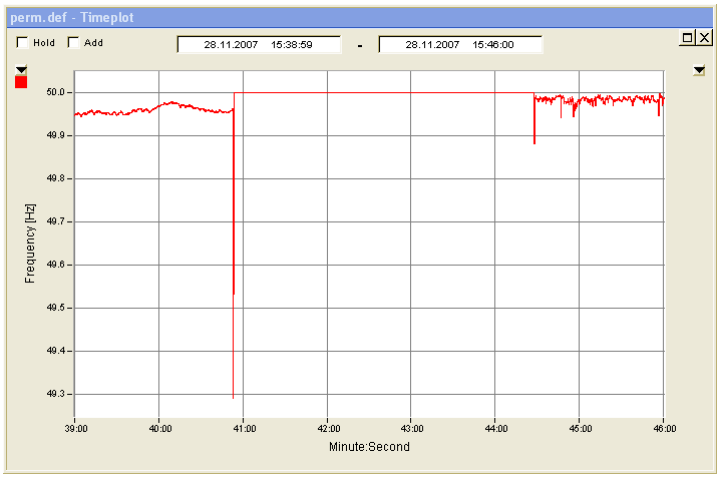

Figure 67 – Frequency in grid connected, switching and islanding modes

5.3.3 Connection of the facilities base load

The facilities base load corresponds to the general services of the swimming-pool building, like pumps, lighting, computers, etc, excluding ATUs. In this situation the load step was about 18 kW.

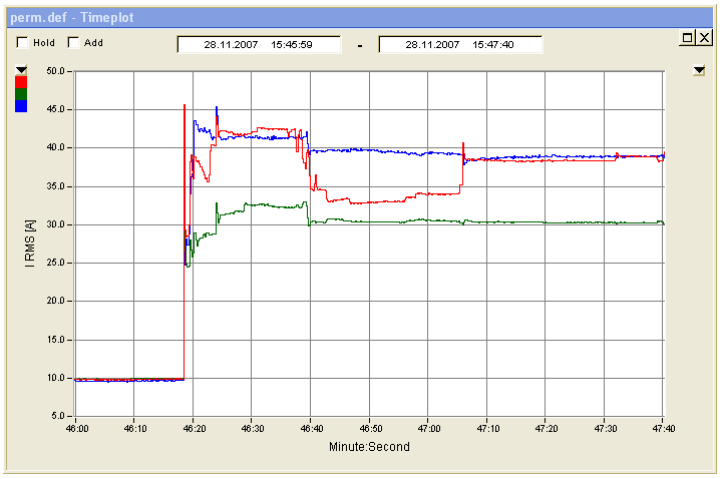

Figure 68 – Current during the connection of the facilities base load

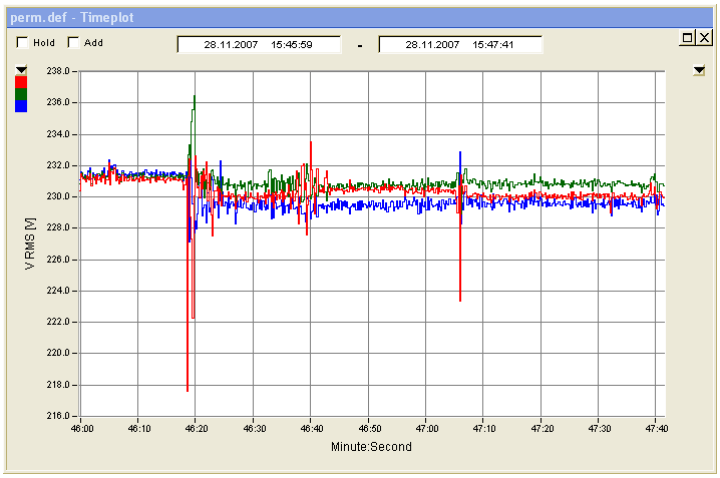

Figure 69 – Voltage RMS values during the connection of the facilities base load

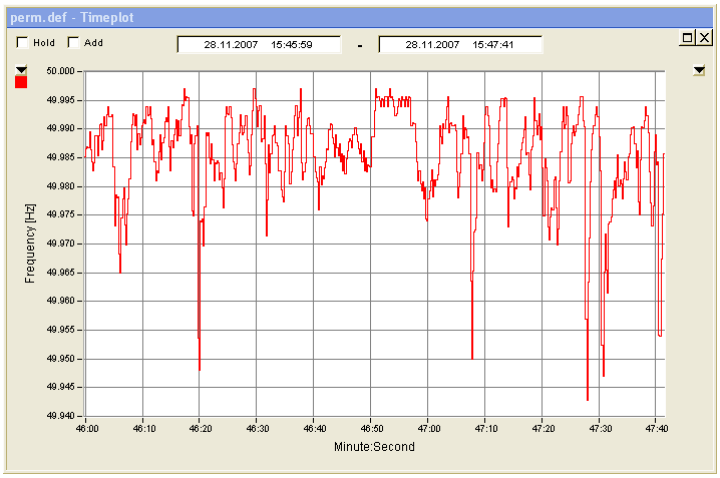

Figure 70 – Frequency during the connection of the facilities base load

5.3.4 Connection of pumps 1 and 2

Each pump connected in this step is characterized by an induction motor of 7,5 kW.

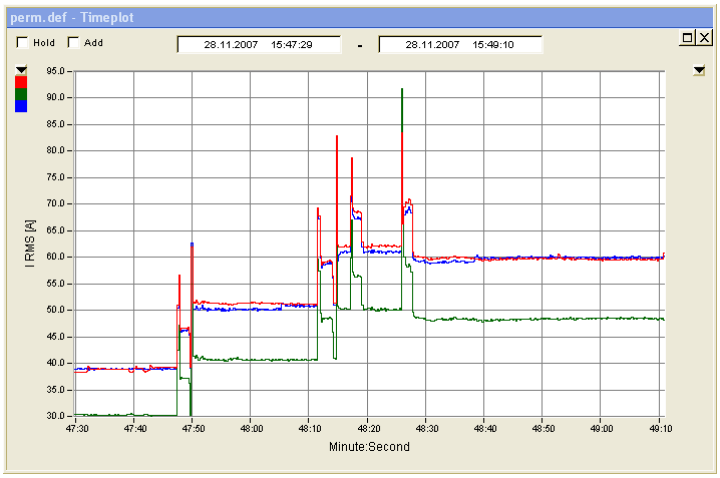

Figure 71 – Current during the connection of the pumps 1 and 2

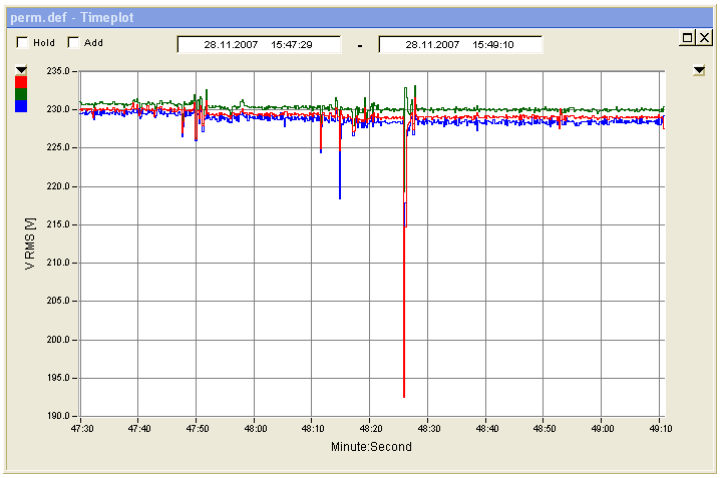

Figure 72 – Voltage RMS values during the connection of the pumps 1 and 2

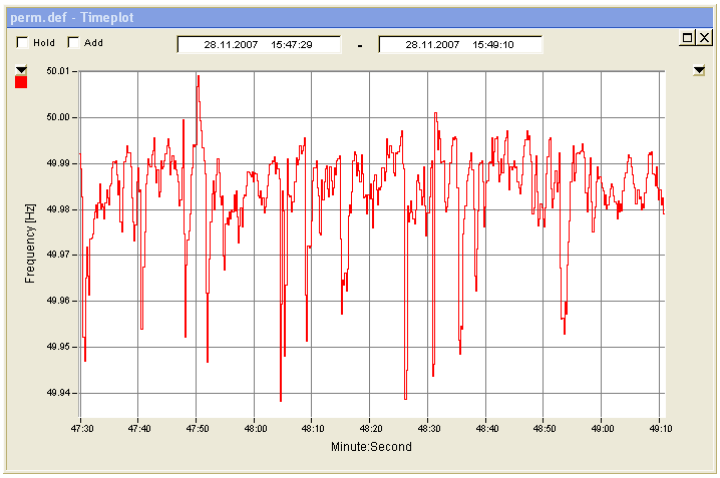

Figure 73 – Frequency during the connection of the pumps 1 and 2

In this test was recorded a voltage dip as consequence of connection of the pumps.

5.3.5 Connection of the ATU 4 extraction fan

The extraction fan connected in this step is characterized by an induction motor of 4 kW.

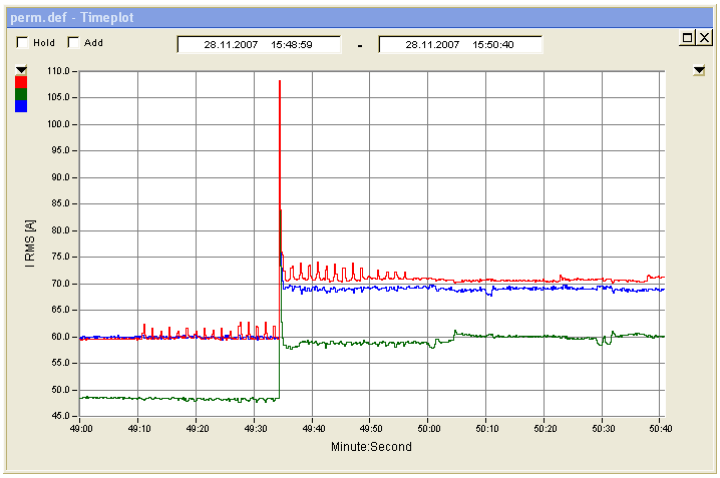

Figure 74 – Current during the connection of the extraction fan of the ATU 4

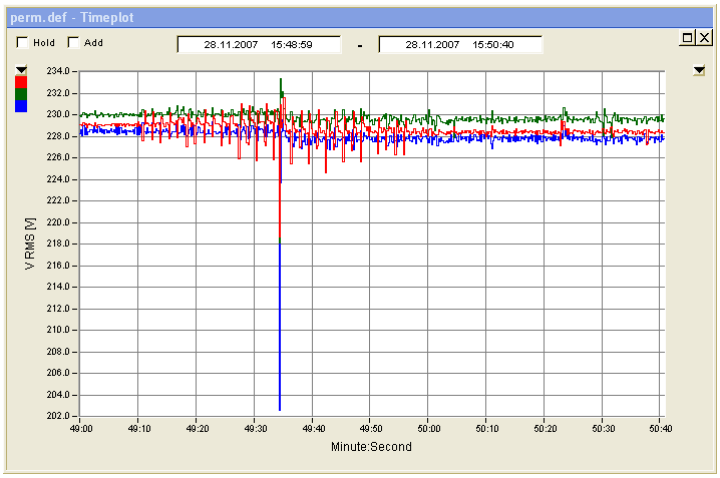

Figure 75 – Voltage RMS values during the connection of the extraction fan of the ATU 4

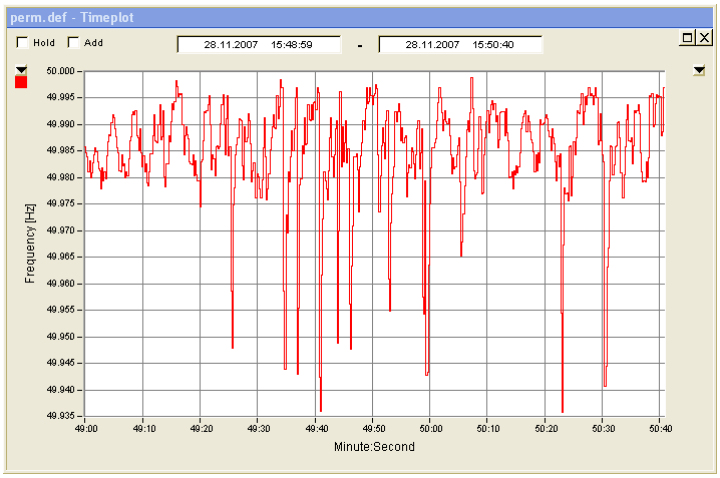

Figure 76 – Frequency during the connection of the extraction fan of the ATU 4

5.3.6 Connection of the ATU 3 extraction and blowing fans

Each extraction and blowing fan connected in this step is characterized by an induction motor of 7,5 kW.

Figure 77 – Current during the connection of the extraction and blowing fans of the ATU 3

Figure 78 – Voltage RMS values during the connection of the extraction and blowing fans of the ATU 3

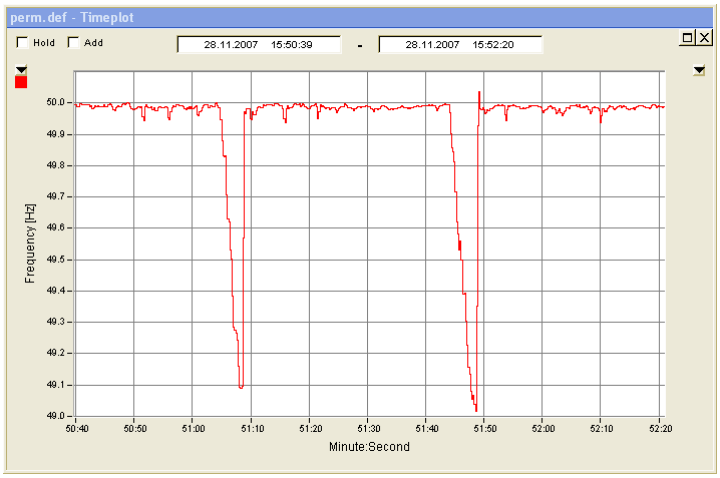

Figure 79 – Frequency during the connection of the extraction and blowing fans of the ATU 3

This test shows strong voltage dips and frequency variations with connection of heavy loads. It was recorded voltage dips of 40% amplitude and frequency variations of 2% (1 Hz). Due to the impact of this kind of loads on the voltage, it is recommended to implement a load control system to prevent the connection of the ATU.

5.3.7 Connection of the ATU 2 extraction fan

The extraction fan connected in this step is characterized by an induction motor of 5 kW.

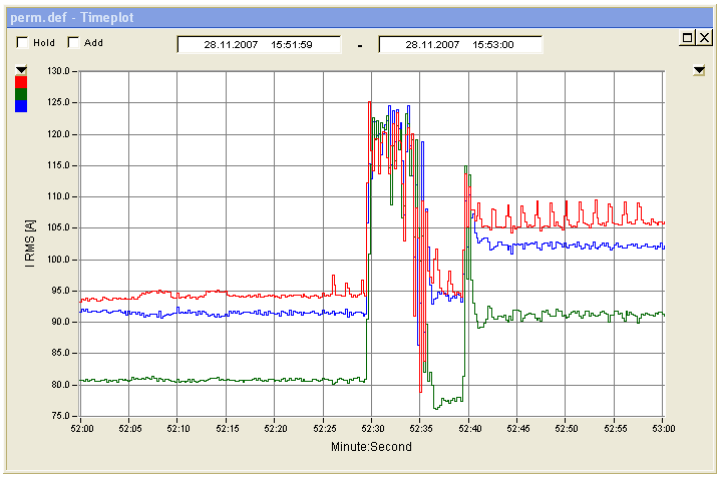

Figure 80 – Current during the connection of the extraction fan of the ATU 2

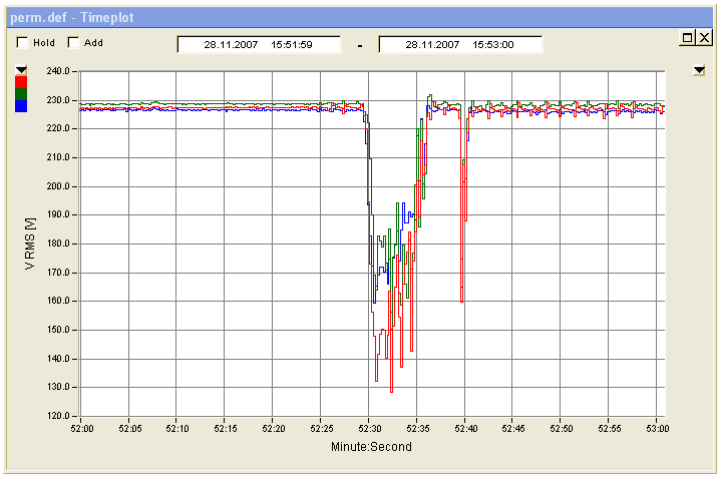

Figure 81 – Voltage RMS values during the connection of the extraction fan of the ATU 2

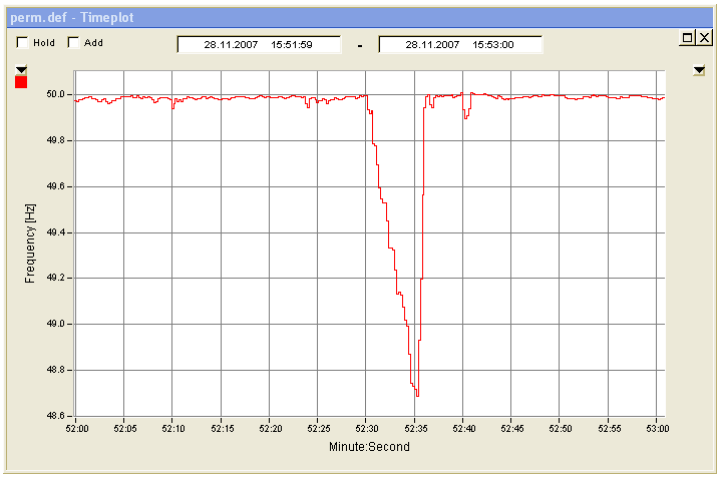

Figure 82 – Frequency during the connection of the extraction fan of the ATU 2

As expected, the behaviour of the system in this test was similar to the previous situation – Strong voltage dip and frequency variations.

5.3.8 Disconnection of the 2 fans of the ATU 3

In this case, it was analysed the behaviour of the system with disconnection of 2 fans (2 industion motors of 7,5 kW) of the ATU 3.

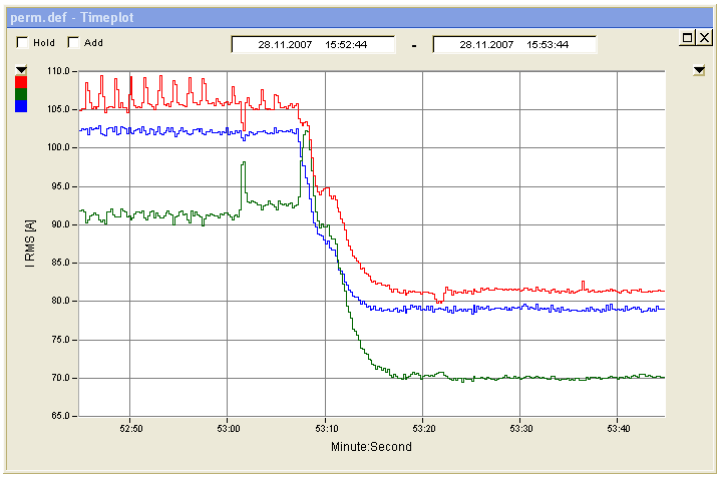

Figure 83 – Current during the disconnection of the 2 fans of the ATU 3

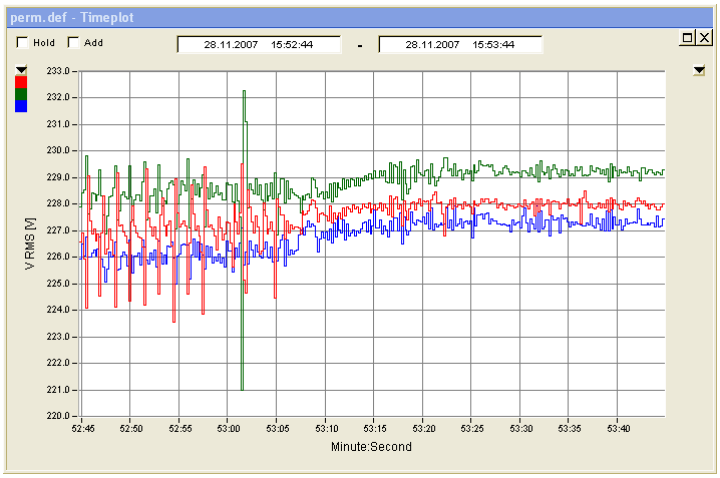

Figure 84 – Voltage RMS values during the disconnection of the 2 fans of the ATU 3

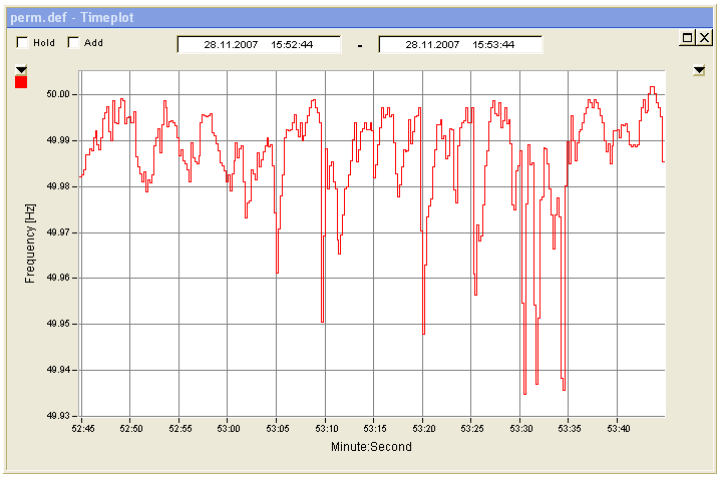

Figure 85 – Frequency during the disconnection of the 2 fans of the ATU 3

As expected, in this test the voltage and frequency variations were reduced.

5.3.9 Connection of 2 pumps of 5 kW

As performed in some previous tests, it was connected more 2 motors of 5 kW, in order to analyse the impact on the island voltage. As already realized, the connection of heavy loads in islanding mode causes strong voltage and frequency variations.

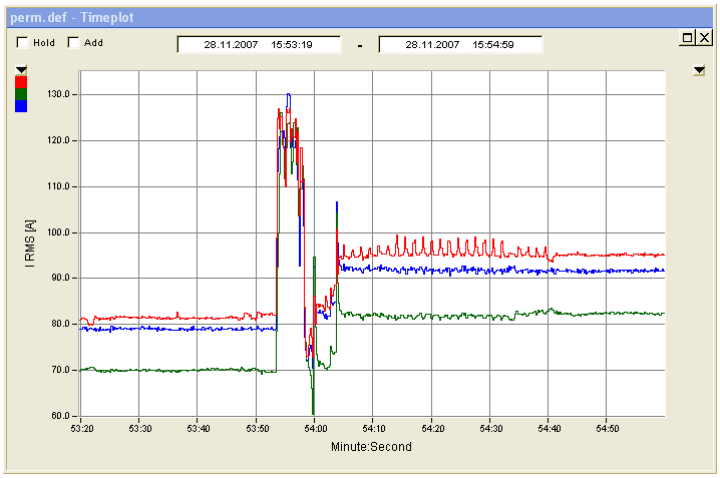

Figure 86 – Current during the connection of the 2 motors of 5 kW

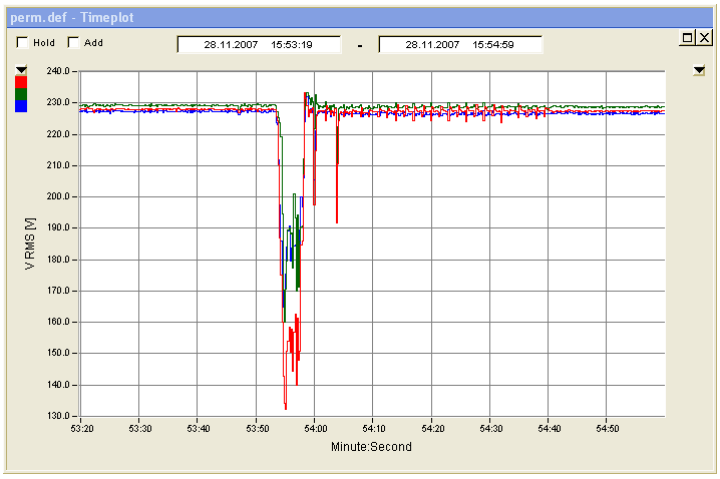

Figure 87 – Voltage RMS values during the connection of the 2 motors of 5 kW

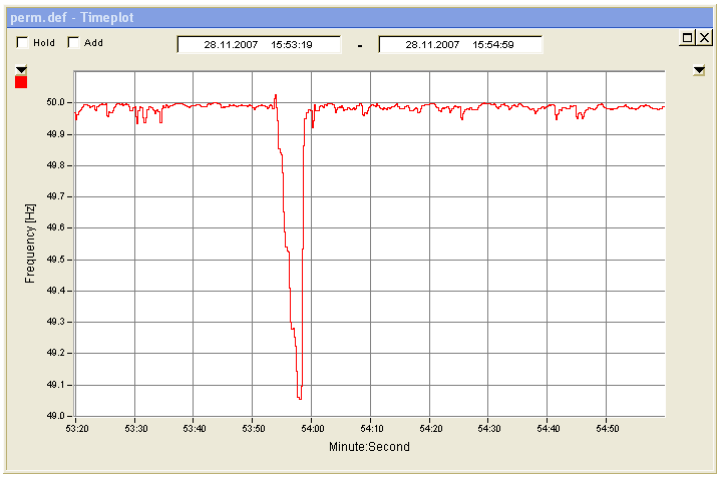

Figure 88 – Frequency during the connection of the 2 motors of 5 kW

The following 4 graphs show the behaviour of the system during all load connections in islanding operation mode.

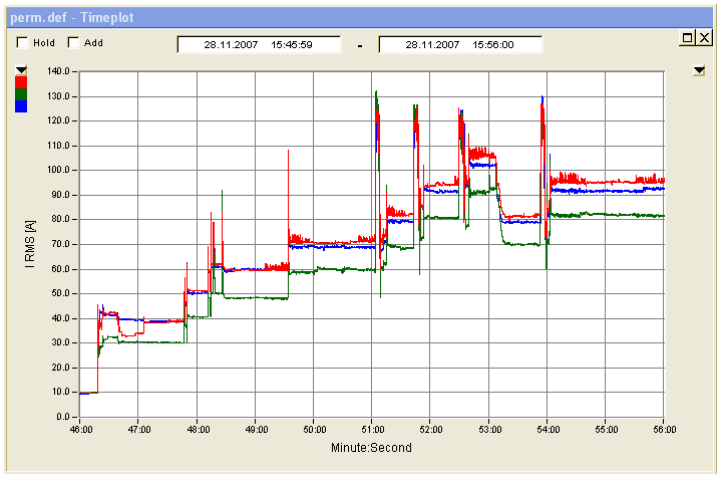

Figure 89 – Current RMS values in the microturbine output

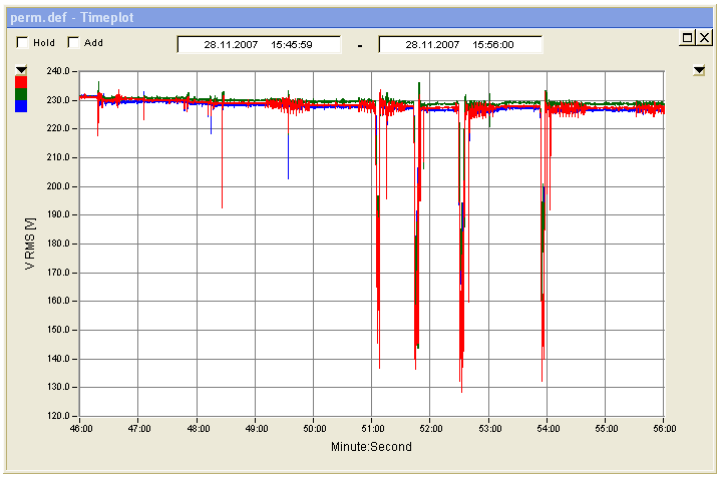

Figure 90 – Voltage RMS values in the microturbine output

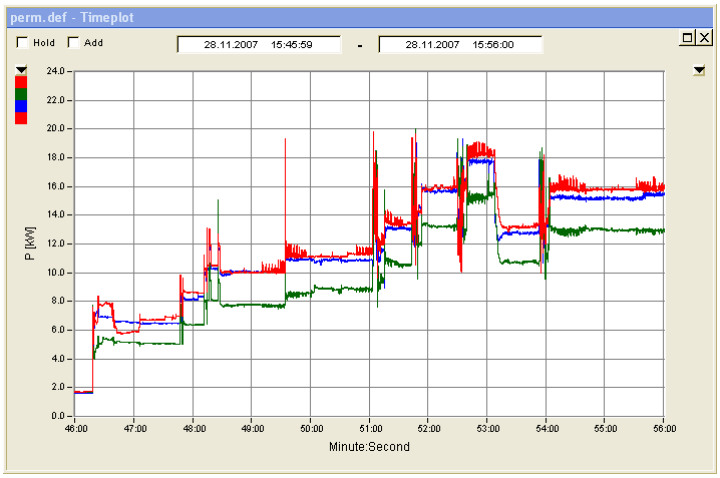

Figure 91 – Active power values in the microturbine output

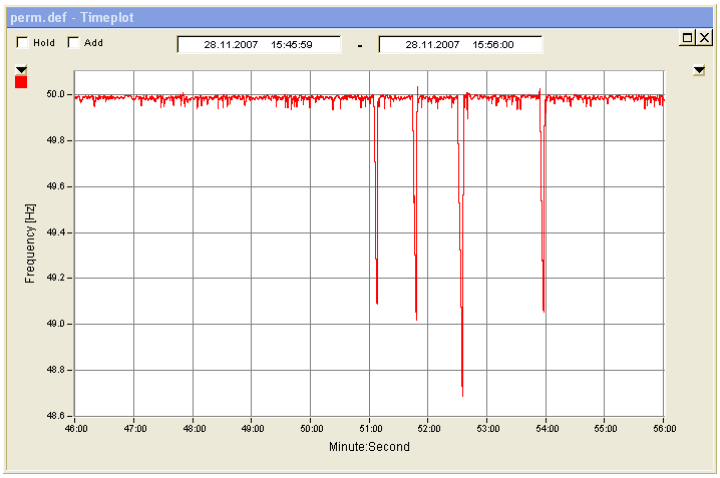

Figure 92 – Frequency values in the microturbine output

5.3.10 Transition from island to grid connected mode

The following 3 figures show the behaviour of the system during transition from islanding to grid connected mode.

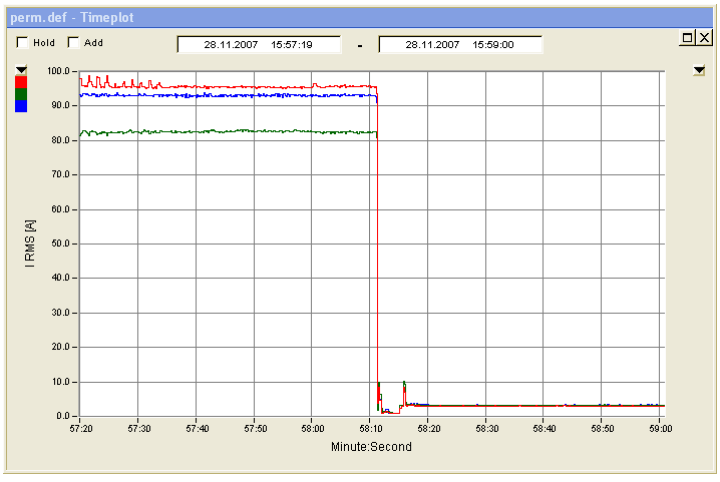

Figure 93 – Current RMS values during the transition to grid connected mode

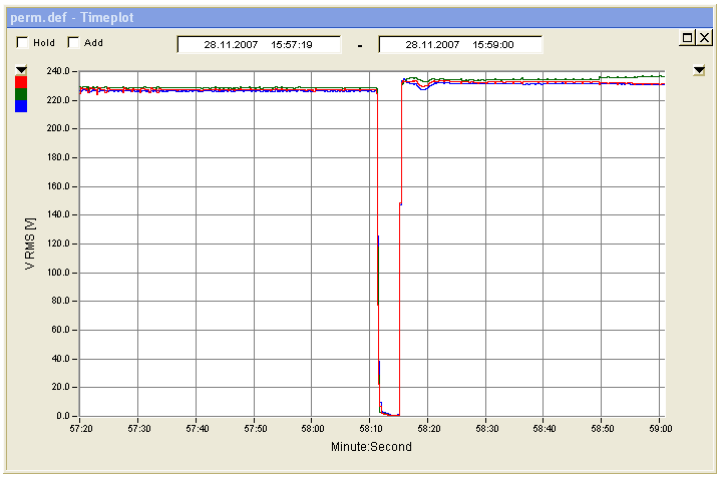

Figure 94 – Voltage RMS values during the transition to grid connected mode

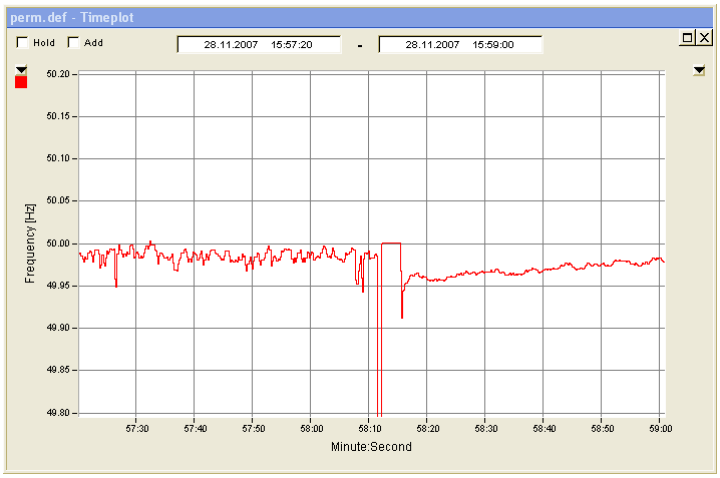

Figure 95 – Frequency during the transition to grid connected mode

6 Field Tests with Microturbine/Gen-set Operation

A second phase of tests was developed in order to analyse the interoperation of the microturbine with a Diesel gen-set, in islanding mode, in several load and generation regimens. These field tests allowed to study the following scenarios:

- Gen-set black-starting;
- Parallel of the microturbine to the gen-set;
- Operation of the microturbine in parallel with the gen-set in islanding mode – Analysis of the system behaviour in several load and generation regimens.

The following figure shows a simplified diagram of the microturbine and Diesel gen-set, used in these field tests, connected to the LV grid.

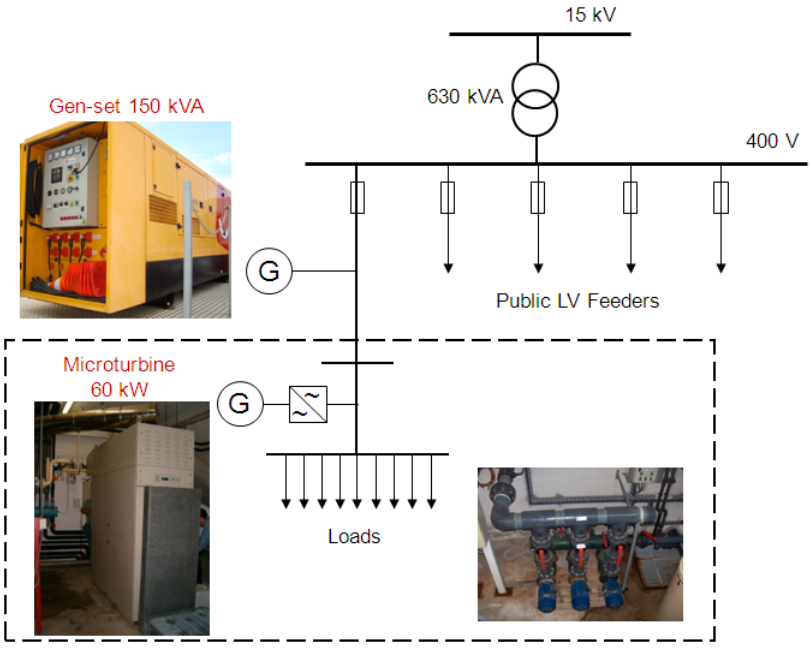

Figure 96 – Simplified single-line diagram of the PTD ILH0074 / Ílhavo MSP with a Diesel gen-set

Figure 97 – Overview of the Ílhavo MSP during the field tests

In order to conduct the required tests, 3 PQA Fluke 1760 were installed according to the following single-line diagram, recording voltage and currents in the measuring points.

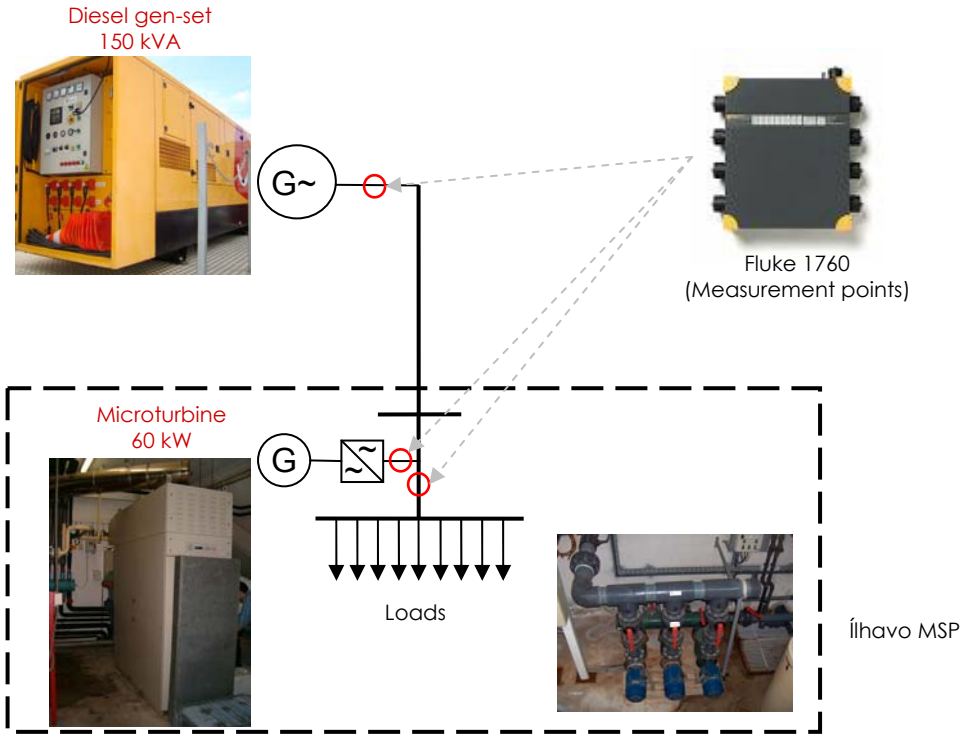

Figure 98 – Simplified single-line diagram and measurement points

The generator has a rated power of 150 kVA (121,6 kW) and its protective relays were configured to:

- Over voltage: 253 V;
- Under voltage: 207 V;
- Over frequency: 55 Hz;
- Under frequency: 45 Hz;
- Over current in steady-state: 210 A;
- Starting current limit: 70 A.

On the other hand, protections of the microturbine were configured to:

- Over voltage: 450 V (1900 ms);
- Under voltage: 360 V (1900 ms);
- Fast over voltage: 600 V (32 ms);
- Fast under voltage: 264 V (95 ms);
- Over frequency: 50,5 Hz (90 ms);
- Under frequency: 49,3 Hz (90 ms).

The next photos show monitoring devices monitoring the distribution board, where the gen-set was connected to the Ílhavo MSP feeder, the output of the microturbine and the load panel of the Ílhavo MSP.

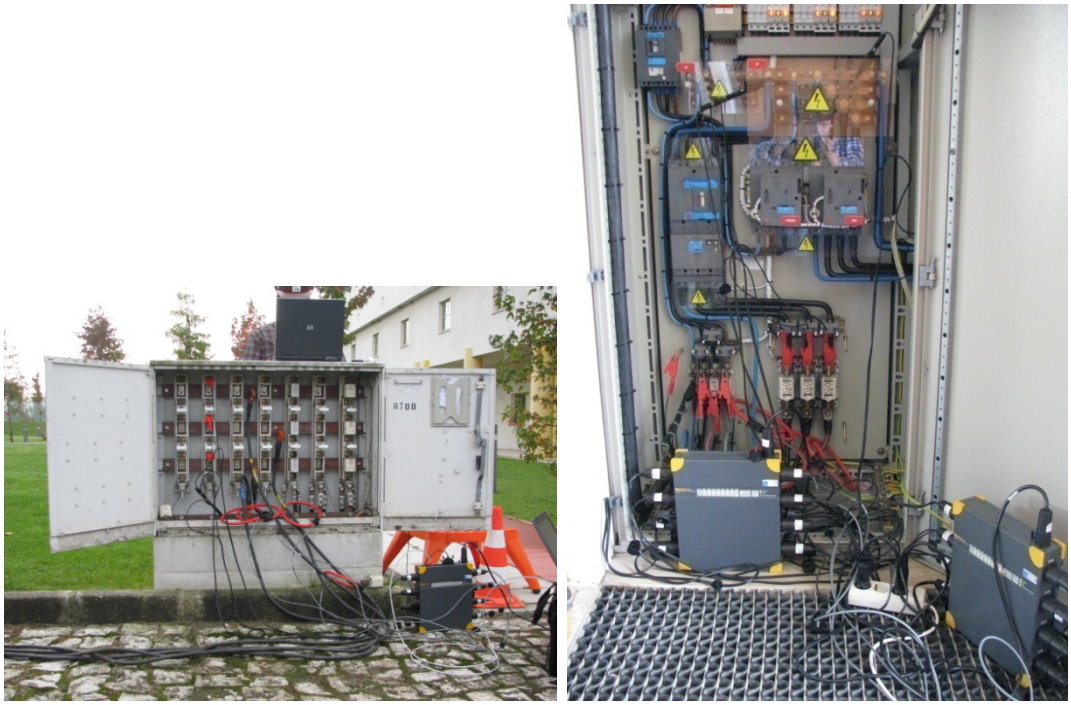

Figure 99 – Monitoring devices at the distribution board (left photo) and at the microturbine output and load panel (right photo)

6.1 Microturbine parallel after gen-set black-starting

This field test was developed in order to analyse the behaviour of the system during the microturbine parallel after the gen-set black-starting.

The following time-line shows the evolution of this field test.

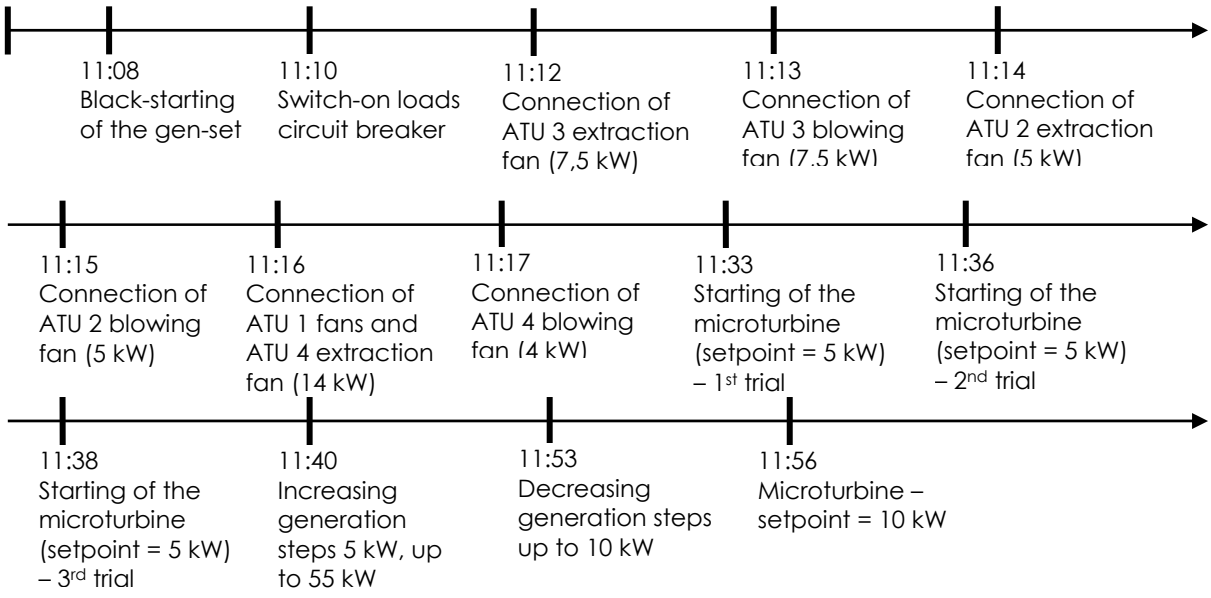

Figure 100 – Field tests time-line

6.1.1 Gen-set black-starting and connection of the MSP base load

This test phase started with the shut-down of the microturbine and disconnection of all Ílhavo MSP loads. The feeder from the PTD ILH0074 which supply the distribution board was also opened.

The following graphs show the black-starting of the Diesel gen-set and connection of micorturbine's ancillary systems (5kW) and MSP base load (25kW). After this action, the gen-set started to supply the MSP load and the microturbine's ancillary systems in LV islanding mode, without any connection to the distribution grid.

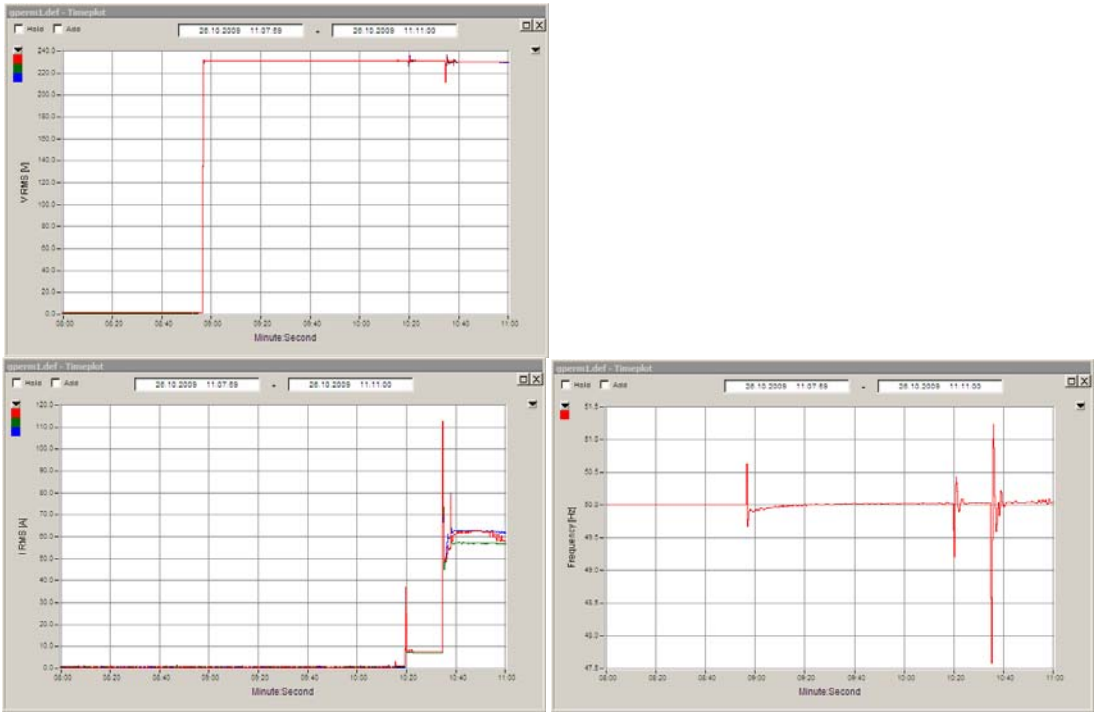

Figure 101 – Voltage, current and frequency at the generator output

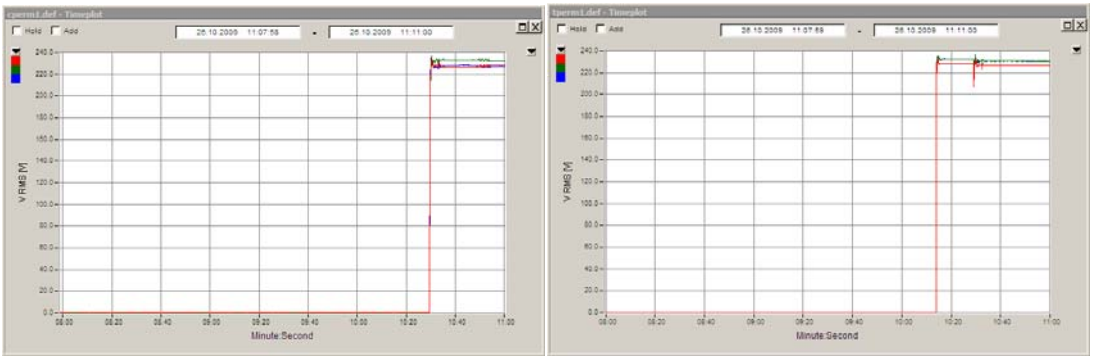

Figure 102 – Voltage and current at the load panel

Figure 103 – Voltage and current at the microturbine in/output

As expected, the connection of the MSP base load caused significant voltage and frequency variations. The voltage dipped to 212 V (8% variation) and frequency reached 47,5 Hz (5% variation).

6.1.2 Gen-set operation in several load regimens

After the switch-on of the base load circuit, during 5 minutes several loads were connected, step-by-step. In this phase were connected several fans, in 6 steps, of different power. In some steps was connected only 1 fan and in other steps were connected 2 fans simultaneously. These fans have rated powers of 4 kW, 5 kW or 7,5 kW.

The microturbine remained in standby, only drawing some power to supply its ancillary systems.

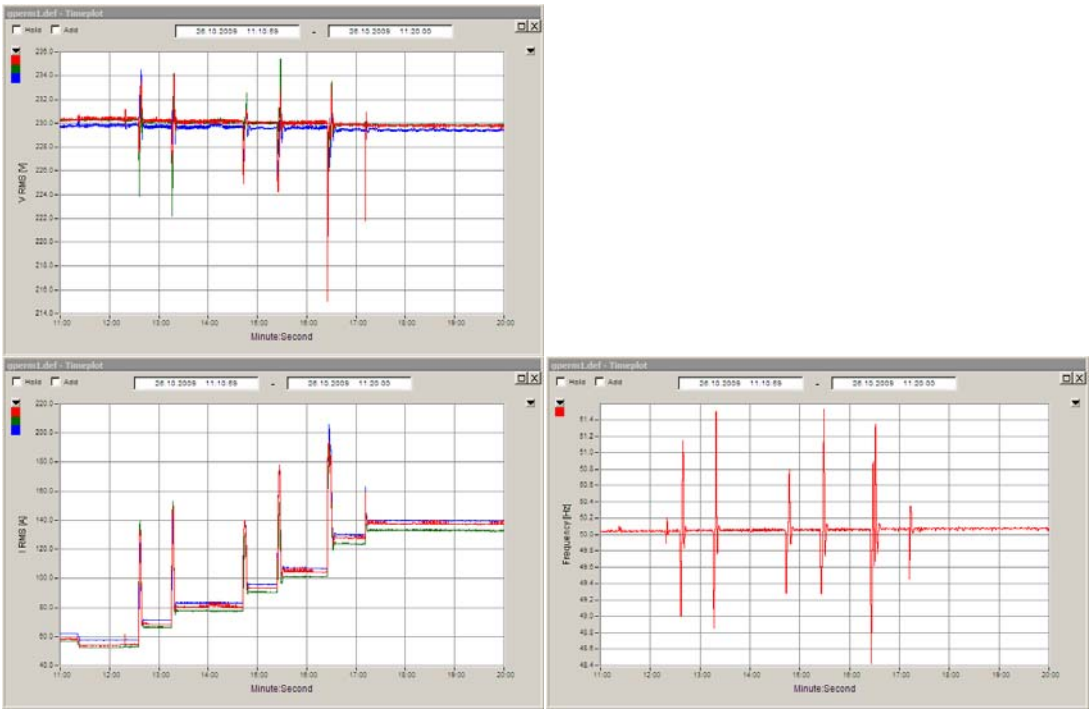

Figure 104 – Voltage, current and frequency at the generator output

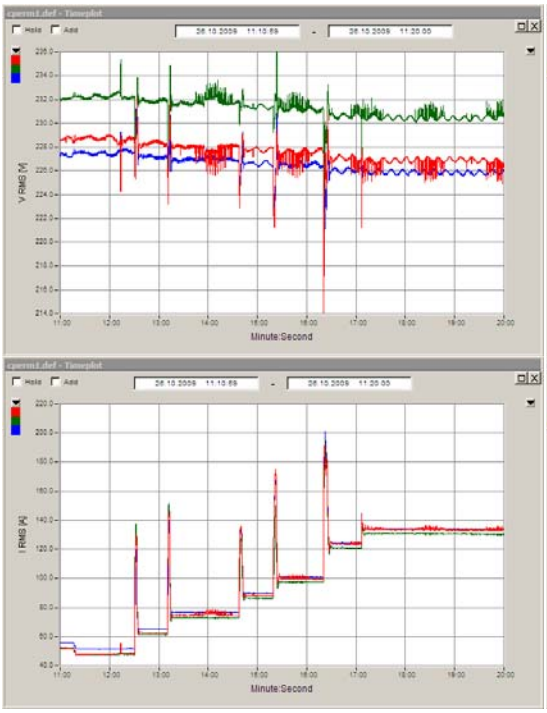

Figure 105 – Voltage and current at the load panel

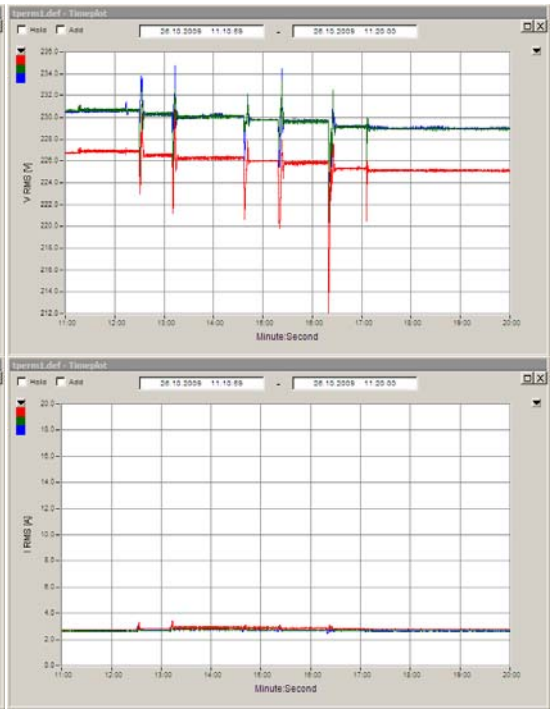

Figure 106 – Voltage and current at the microturbine in/output

As verified during the connection of the initial MSP base load, the connection of these fans over the generator caused some voltage and frequency variations. As the rated power of the connected fans is quite lower than the initial MSP base load, the impact on the voltage and frequency was also reduced.

6.1.3 Microturbine starting and parallel with the gen-set

With the previous actions, the gen-set achieved the steady-state generating about 70kW to supply connected loads.

At this moment, the parallel of the microturbine with the gen-set was attempted.

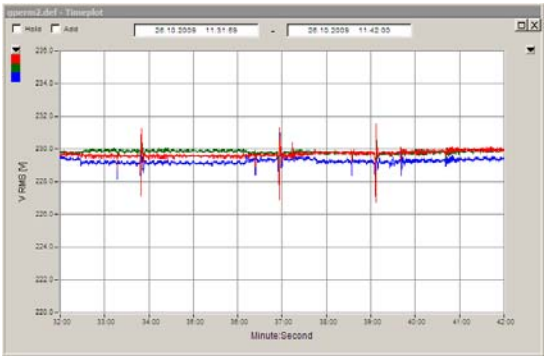

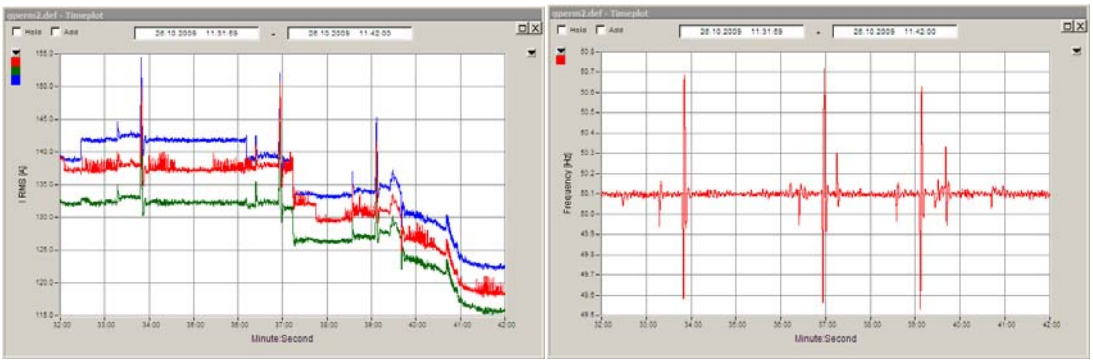

Figure 107 – Voltage, current and frequency at the generator output

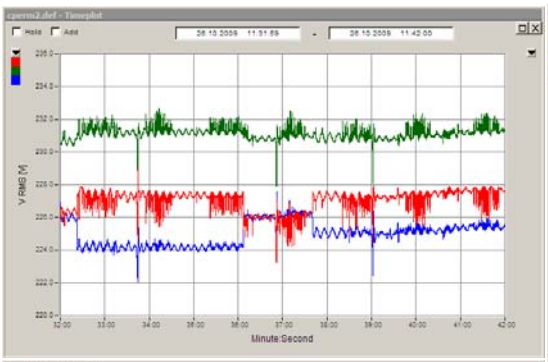

Figure 108 – Voltage and current at the load panel

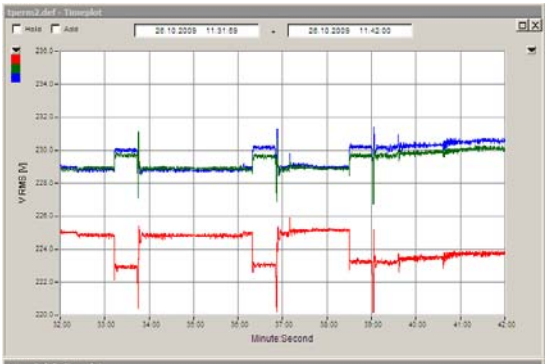

Figure 109 – Voltage and current at the microturbine in/output

As realized in the previous graphs, the parallel of the microturbine with the gen-set caused slightly frequency variations. At these events, there were recorded frequency variations of about +/-1%, which prevented the first 2 attempts, by tripping of the over frequency protective relay (it was configured to 50,5 Hz, 90 ms).

Based on the results of the first 2 attempts, the over frequency protection of the microturbine was changed from 50,5 Hz to 51,5 Hz, which allowed the parallel with the Diesel gen-set. For this step, the generation set-point of the microturbine was defined to 10 kW.

The following measurement shows the active power behaviour of the microturbine during the starting and attempts to parallel with the gen-set. In a first stage the system draws power to achieve the burning speed and then switches to generation mode.

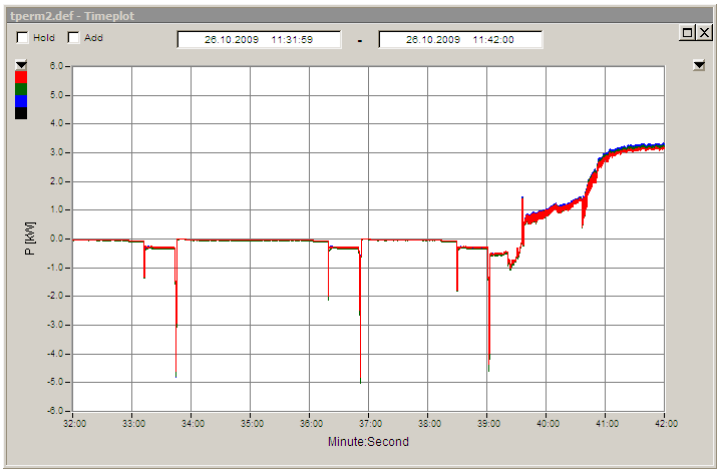

Figure 110 – Active power at the microturbine in/output

6.1.4 Microturbine operation in several generation regimens

During this test phase, the MSP load was maintained constant (about 68 kW) and the microturbine generation set-point was increased gradually in steps of 5 kW up to the maximum power (about 55 kW). After achieved the maximum power, the inverse sequence was conducted up to stabilize finally in a set-point of 10 kW.

The aim of this test was to analyse the response of the Diesel gen-set to variations of the microturbine generation.

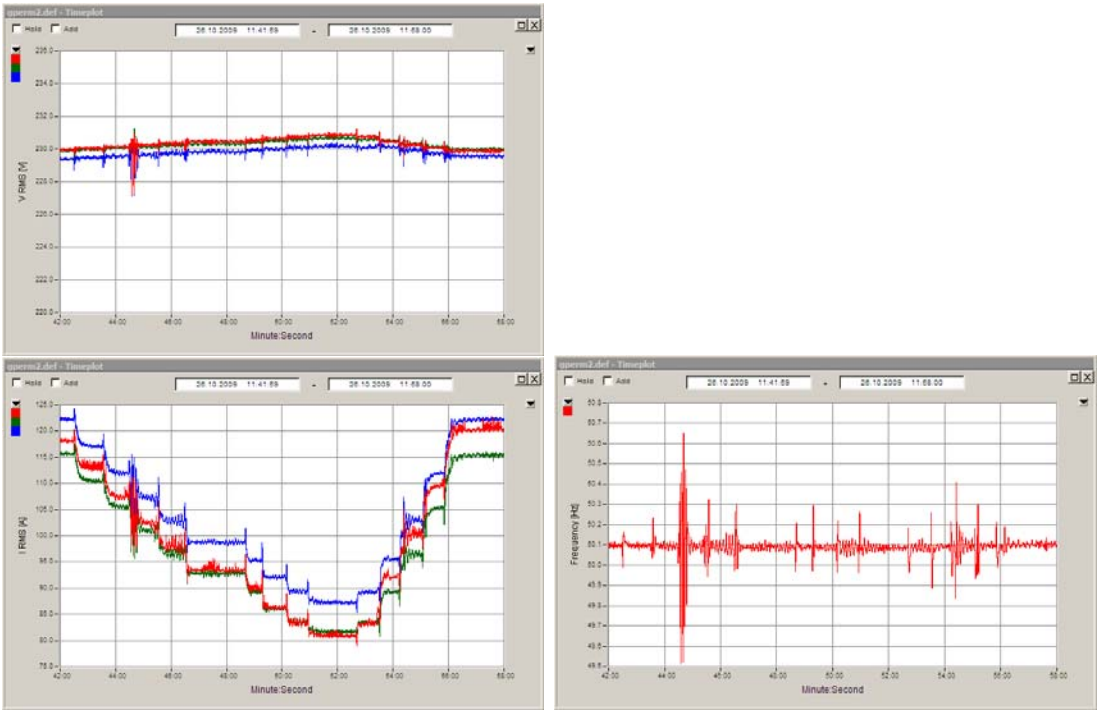

Figure 111 – Voltage, current and frequency at the generator output

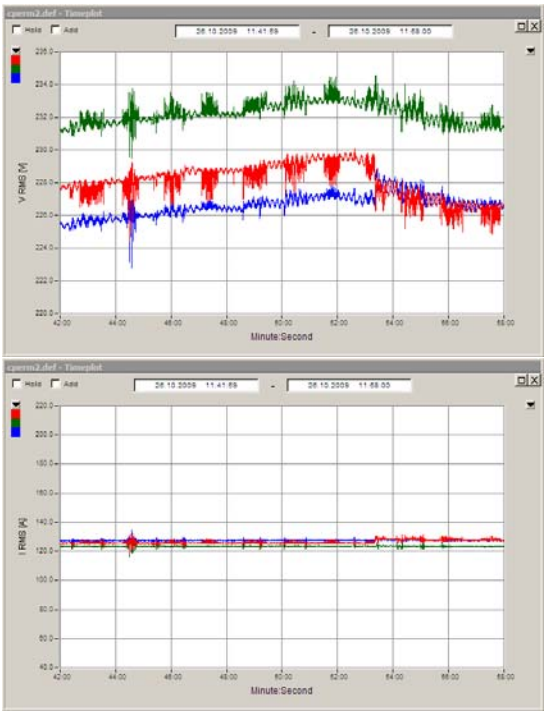

Figure 112 – Voltage and current at the load panel

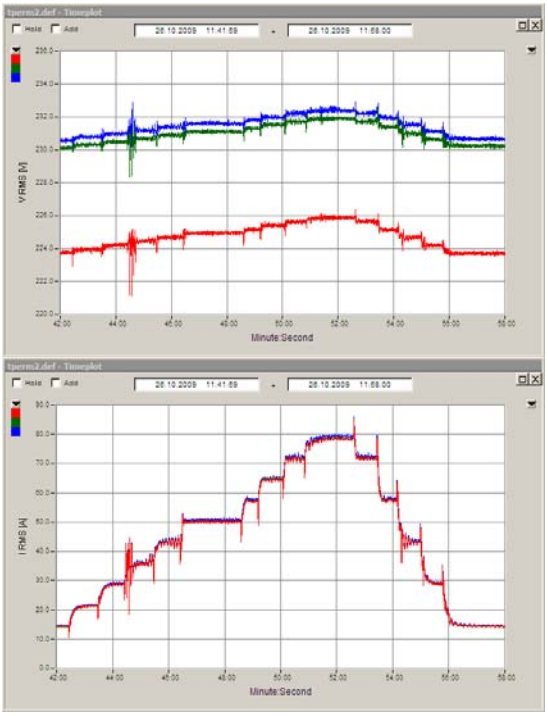

Figure 113 – Voltage and current at the microturbine in/output

As the Diesel gen-set operates as voltage source, it supported the voltage and frequency stability and answered to the different generation profile of the microturbine as load variation.

6.2 Operation in several load regimens

This field test was developed in order to analyse the behaviour of the system in several load regimens, during the operation of the microturbine in parallel with the Diesel gen-set, in islanding mode.

This test started with a MSP load of about 70 kW and generation of 60 kW by the Diesel gen-set. The generation set-point of the microturbine was maintained constant on about 10 kW during this test phase.

The following time-line shows the development of this field test.

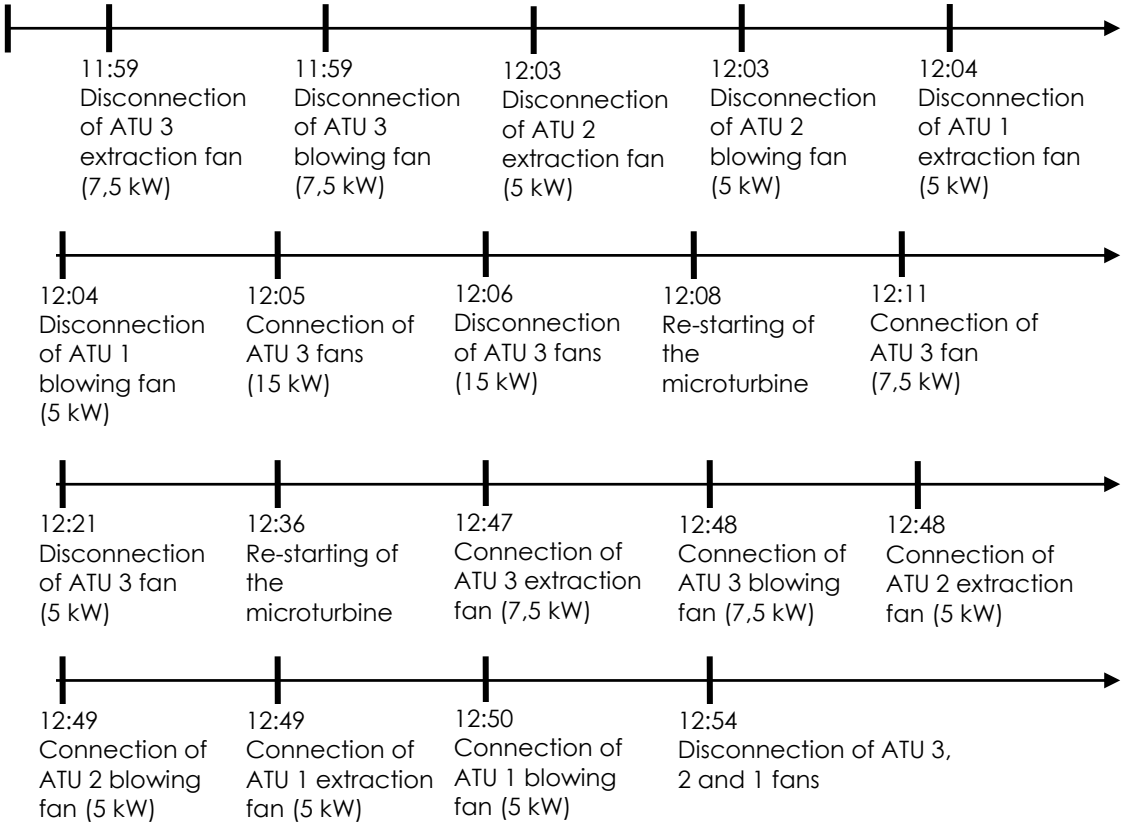

Figure 114 – Field tests time-line

6.2.1 Disconnection of load

To analyse the behaviour of the system in several load regimens, the test started with disconnection of the 2 fans of the ATU 3 (2 motors of 7,5 kW), followed by disconnection of some other loads.

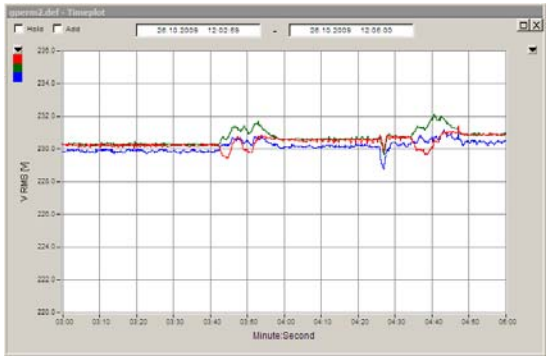

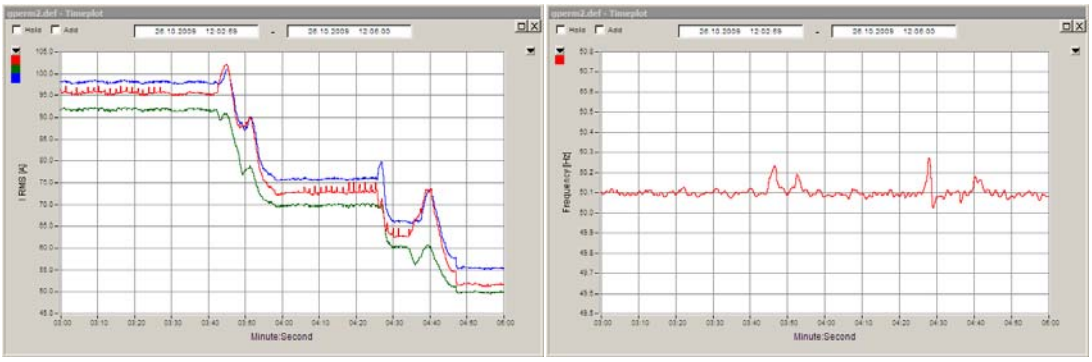

Figure 115 – Voltage, current and frequency at the generator output

Figure 116 – Voltage and current at the load panel

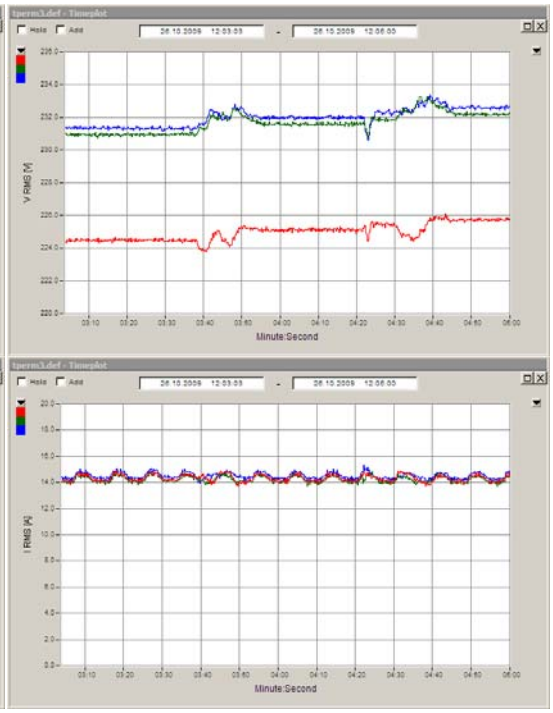

Figure 117 – Voltage and current at the microturbine in/output

As the Diesel gen-set operates as voltage source and the generation set-point of the microturbine was maintained constant, all load variations were answered by the Diesel gen-set, without expressive voltage and frequency variations.

6.2.2 Connection of heavy load

During this phase, in order to analyse the response of the system to heavy load variations, a load of 15 kW (2 fans of 7.5kW) was connected.

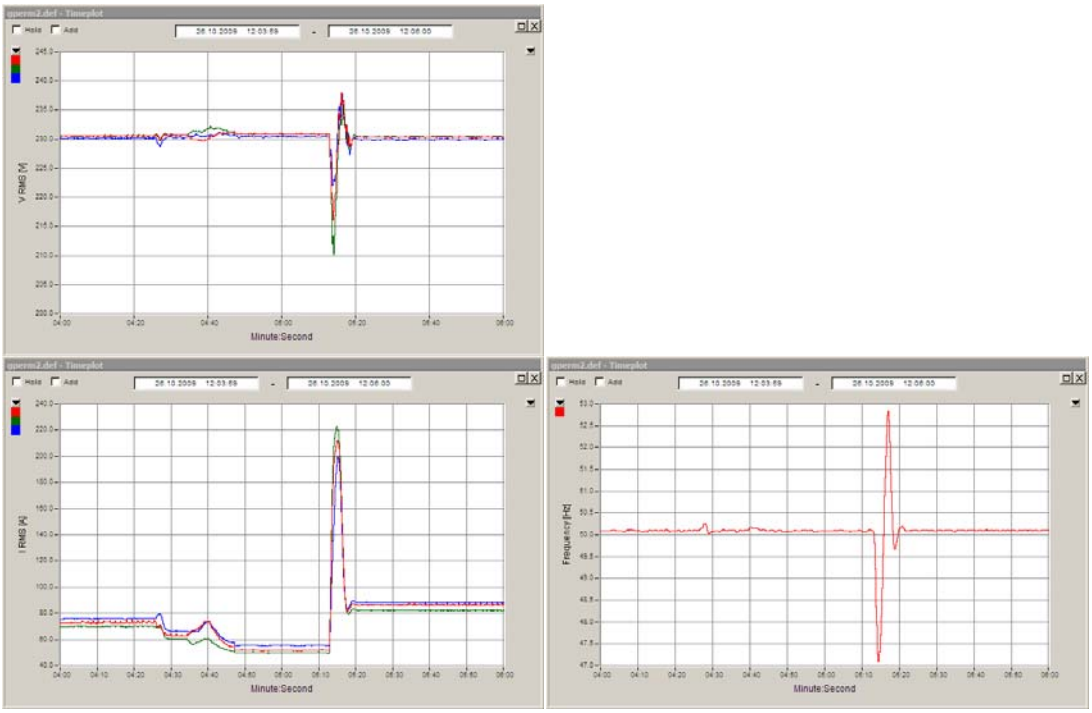

Figure 118 – Voltage, current and frequency at the generator output

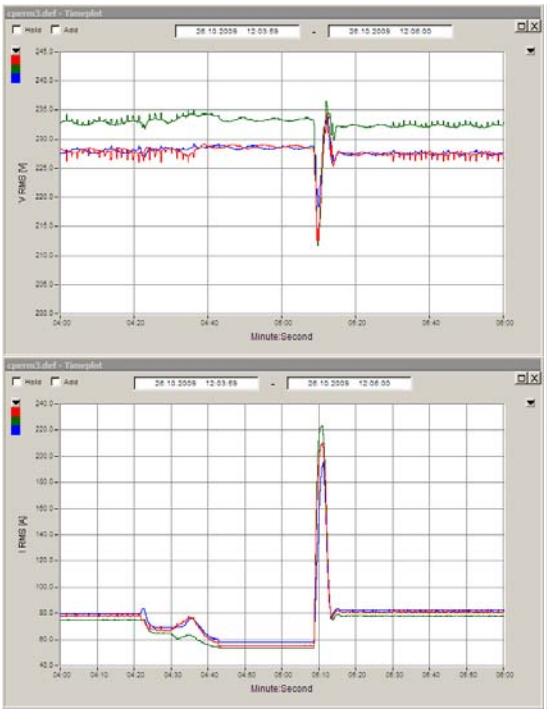

Figure 119 – Voltage and current at the load panel

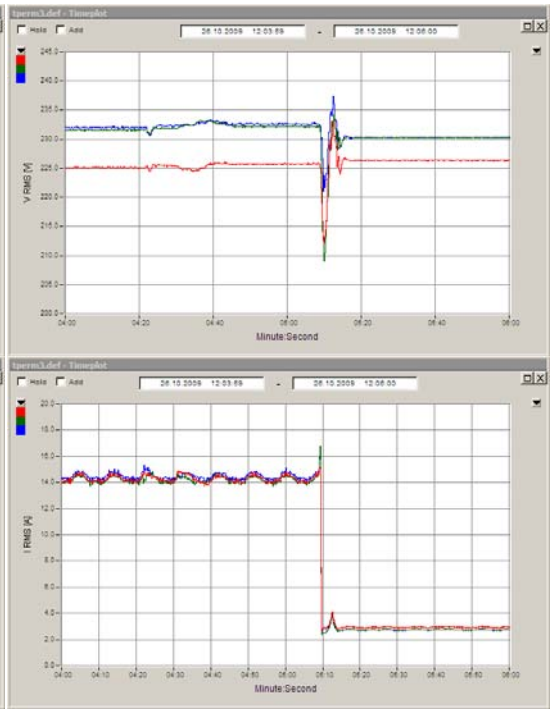

Figure 120 – Voltage and current at the microturbine in/output

Based on the previous graphs, the connection of this heavy load on the system caused significant voltage and frequency variations. The voltage dipped to 210 V (about 9%) and the frequency dropped to 47 Hz (about 6%).

Considering the under frequency settings of the microturbine´s protections, these frequency variations were enough to trip and shut-down of the microturbine. After this event, only the ancillary systems of the microturbine have remained in operation.

6.2.3 Connection and disconnection of several loads

After the microturbine shut-down during the previous test, the settings of the under frequency protections were changed from 49.3 Hz to 48 Hz.

With this new settings, several loads were connected and disconnected, as shown in the following graphs.

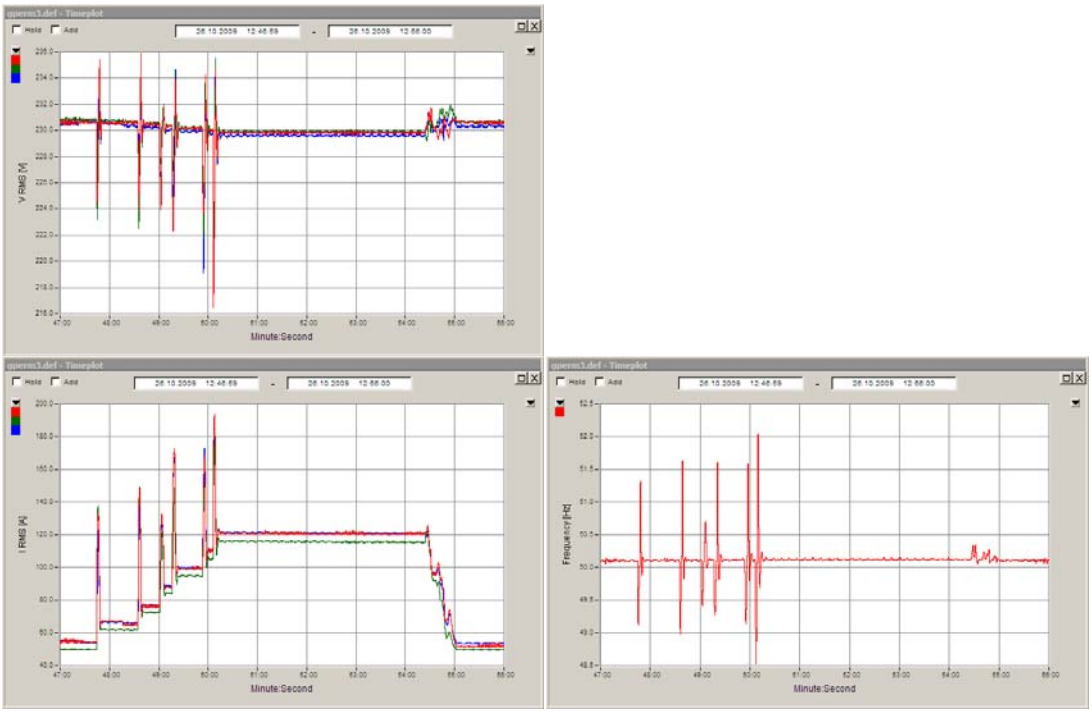

Figure 121 – Voltage, current and frequency at the generator output

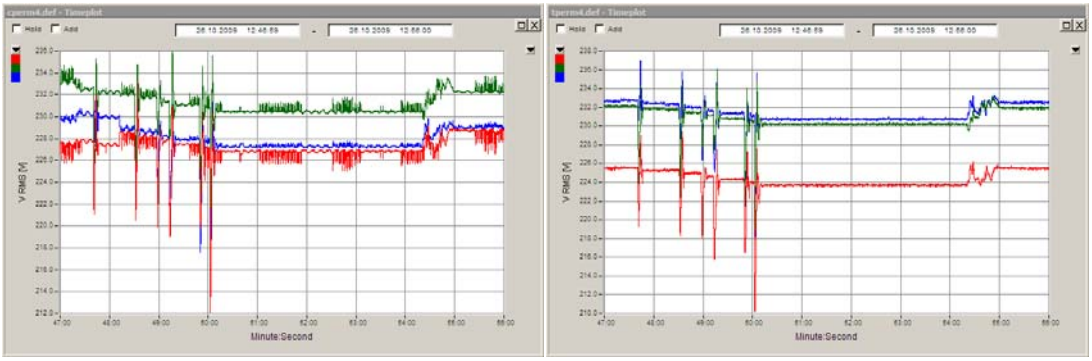

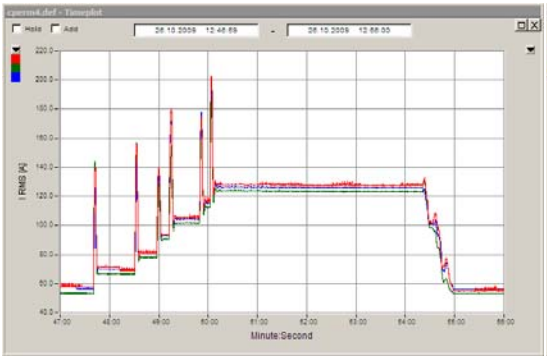

Figure 122 – Voltage and current at the load panel

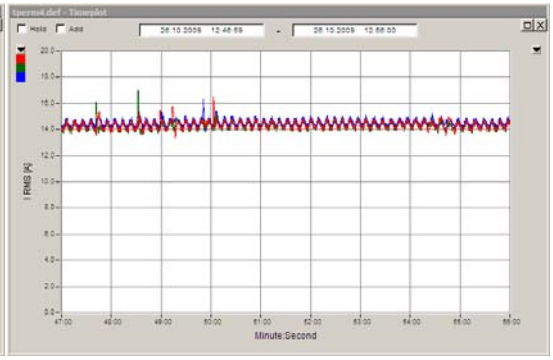

Figure 123 – Voltage and current at the microturbine in/output

The new under frequency settings allowed the desired test, as the frequency variations did not reach the new threshold value. The microturbine remained in parallel with the Diesel gen-set, without any tripping, injecting permanently 10 kW.

6.3 Gen-set operation on voltage control and reactive power injection

This field test was developed in order to analyse the behaviour of the system in several microturbine set-points, with the gen-set only providing reactive power and control of voltage and frequency.

The following time-line shows the development of this field test.

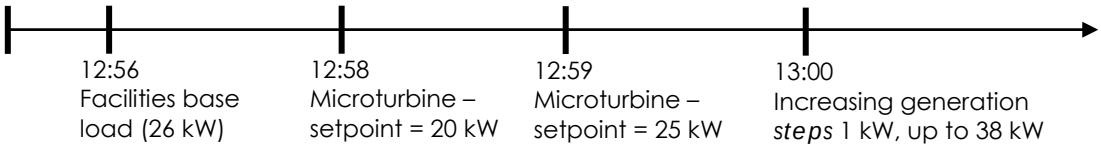

Figure 124 – Field tests time-line

6.3.1 Microturbine in several generation regimens

With a facilities base load about 26 kW, the microturbine was submitted to several generation regimens, increasing gradually the generation power in steps of 1 kW, from 25 kW up to 38 kW.

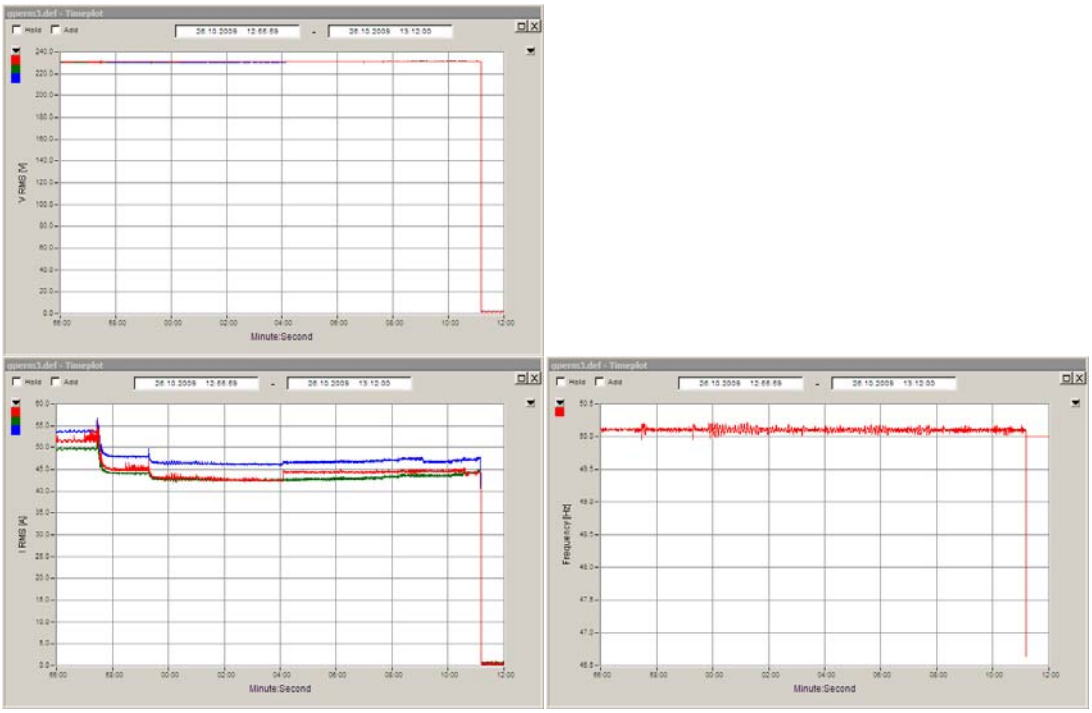

Figure 125 – Voltage, current and frequency at the generator output

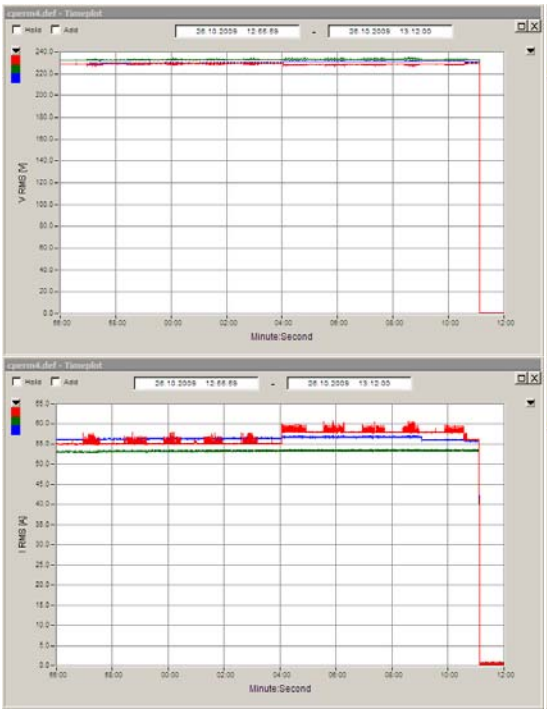

Figure 126 – Voltage and current at the load panel

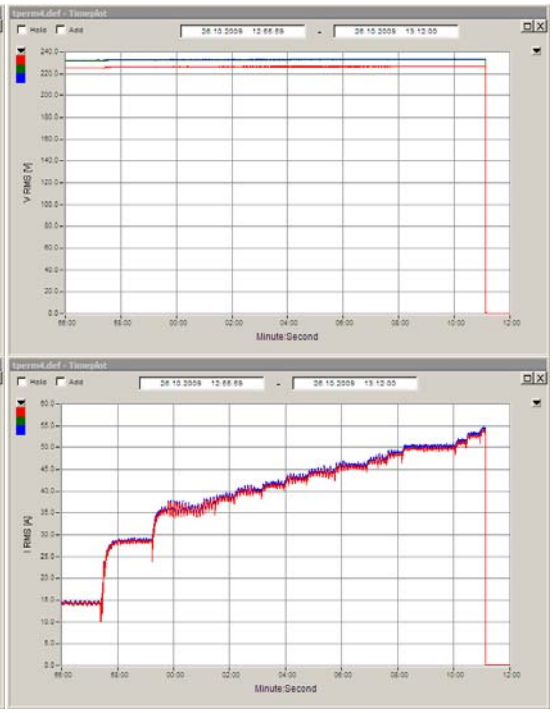

Figure 127 – Voltage and current at the microturbine in/output

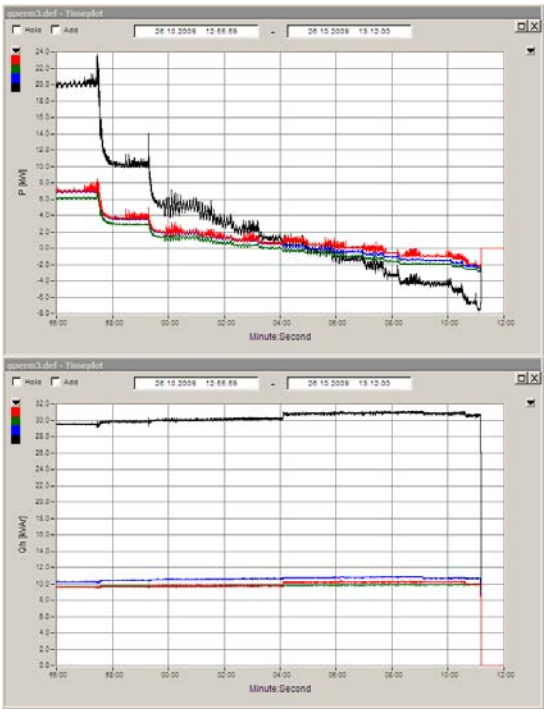

Figure 128 – Active and reactive power at the generator output

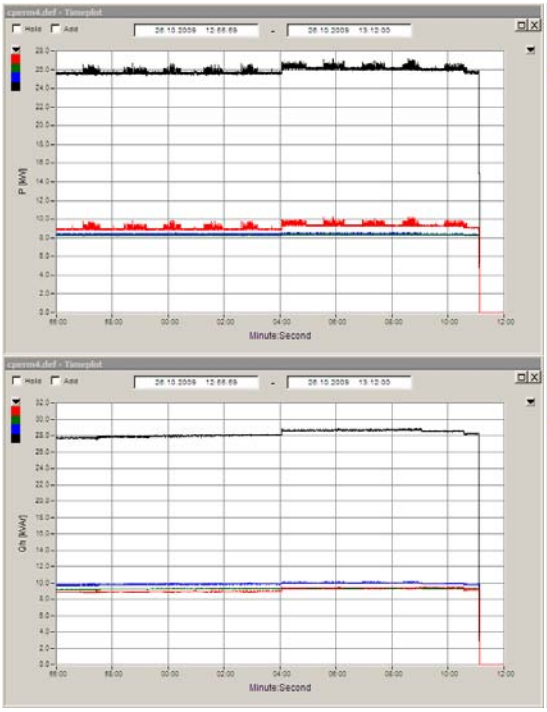

Figure 129 – Active and reactive power at the load panel

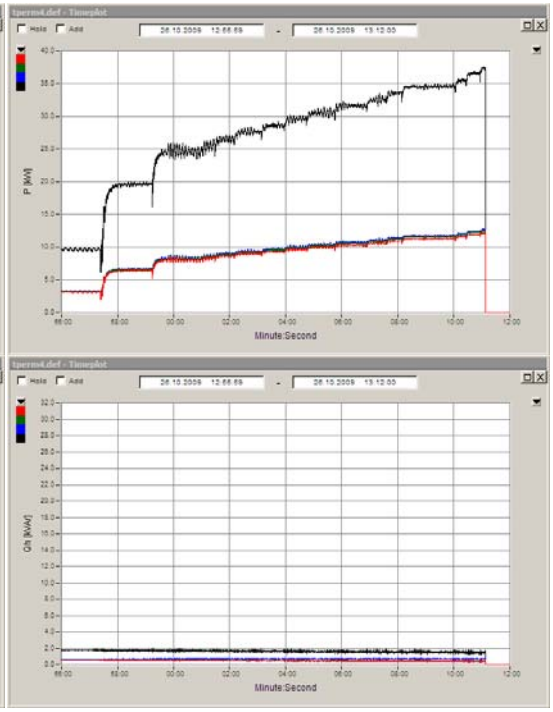

Figure 130 – Active and reactive power at the microturbine in/output

7 Parameter identification of the theoretical models and their control systems used to represent the microturbine dynamic behaviour

In this section, the results of the field tests carried out with the Capstone 60 Microturbine installed in the Ílhavo MSP are used for parameter identification of the theoretical models and corresponding control systems used to represent the microturbine dynamic behaviour with impact on the LV grids in dynamic simulations. Based on the structure of these models and with a given data set, the parameter identification procedure main task is to find good values for the parameters of the microturbine overall model in the sense of the identification criterion.

Thus, some considerations of the Capstone 60 Microturbine system concerning the parameter estimation procedure are presented in subsection 7.1. The mathematical models for the main components of the microturbine system and the issues related with their parameterization are presented in subsection 7.2. The parameter identification methodology is briefly described in subsection 7.3 and the results obtained are presented in subsection 7.4. Finally, the main conclusions are presented in subsection 7.5.

7.1 Some considerations of the Capstone 60 Microturbine system

The Capstone 60 Microturbine installed in the Ílhavo MSP is a 60 kW Single Shaft Microturbine (SSMT) type composed by the microturbine engine, the Permanent Magnet Generator (PMG), the power electronics interface to the LV grid and the recuperator. It also includes a control system that regulates the microturbine operation and all the power conversion functions. The schematic diagram of this SSMT is presented in figure 131.

The microturbine engine comprises the compressor, the combustor and the turbine. This high speed turbine and the PMG are mounted on the same shaft that rotates at up 96 000 RPM. Therefore, the power electronics interface converts the variable high frequency power from the generator into grid quality power at 400-480 V, three-phase AC 50 Hz. This power conditioning involves rectifying the high frequency AC voltage to DC and then inverting the DC to a 50 Hz AC voltage in order to allow grid interconnection, being the voltage at the DC-link of 760 V.

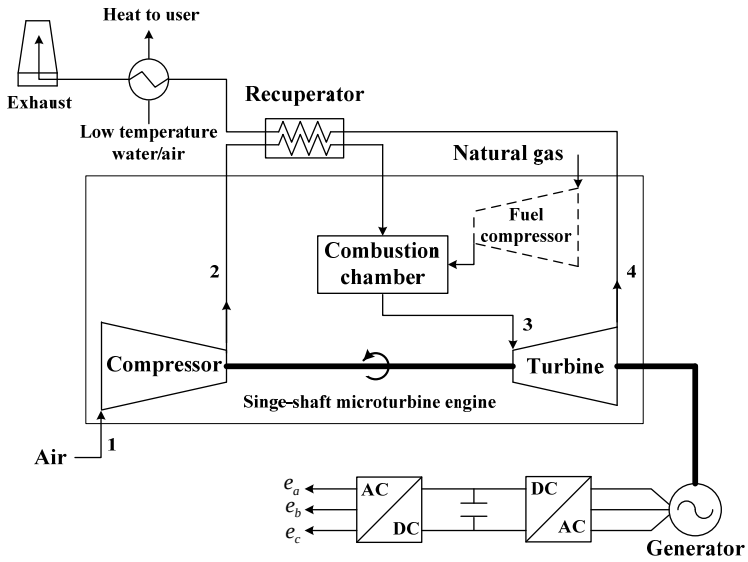

Figure 131 – The single-shaft microturbine generation system

The Capstone 60 Microturbine can be configured for either grid connected or stand alone operation modes. The automatic transition between grid connected and stand alone operational modes is supported by the dual mode controller, which allows the microturbine to maximize the power availability, providing power to the grid when it is available and feeding its protected load when it is operated in standing alone mode, during utility power outages. When the utility power is restored, the dual mode controller can be set to automatically return the microturbine and its protected loads to grid connected operation.

During stand alone operation the voltage and frequency of the microturbine are set to meet load requirements. So, the Capstone 60 Microturbine behaves as a voltage source that always follows the power requirements of the load, being the output power determined by the actual current draw demanded by the connected loads. A large on-board battery pack is used when no electric grid utility is available in order to provide energy for starting the microturbine and, once idle conditions are reached, to provide energy for supporting power draw while microturbine increases speed to provide the necessary load power. In addition, the battery absorbs energy during a loss of load while the microturbine decelerates to produce less power. Therefore, the battery pack provides an electrical buffer for sudden load increasing and decreasing, masking thus the microturbine system dynamics regarding mainly the load following response from the grid point of view.

In grid connected mode the Capstone 60 Microturbine system behaves like a current source only, being synchronized with the electric utility grid for both voltage and frequency references. Since this microturbine cannot vary the power factor while operated in grid connected mode, only active power is injected to the utility grid, which can be modified by changing the turbine speed. For this purpose, a given active power set point should be entered in the microturbine monitoring software, as it can be observed from figure 132, and the turbine generates only the selected amount of power regardless of the load on the system.

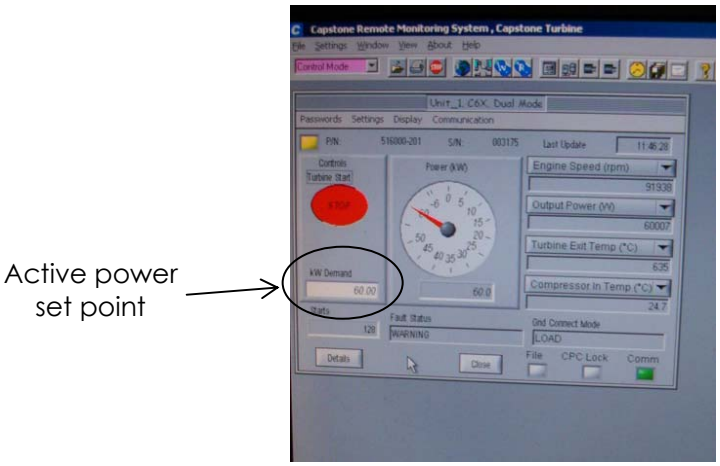

Figure 132 – Monitoring software of the electrical part of the Capstone 60 Microturbine

Based on these previous considerations and taking into account that it is not possible to collect experimental data inside the Capstone 60 Microturbine system, the procedure of the mathematical model parameters identification will be focused on the microturbine system operating in interconnected mode, regarding several different steps up and down in the microturbine output. The microturbine step change output is initiated by selecting the proper power level from the Capstone 60 Microturbine monitoring software.

7.2 Parameterization of the microturbine mathematical model

For parameter identification purposes, the mathematical model able to describe the Capstone 60 Microturbine dynamic behaviour while operated in grid connected mode has to be parameterized in terms of a finite number of parameters. Therefore, the subsection 7.2.1 is concerned to the mathematical model description and its parameterization is addressed in subsection 7.2.2.

7.2.1 The microturbine mathematical model

In order to describe the dynamic behaviour of the Capstone 60 Microturbine operated in interconnected mode, a suitable mathematical model was adopted. This model is based on the gas turbine model [1] which was successfully used for microturbine modelling purposes by several authors [2-9] and developed within the framework of the EU R&D MicroGrids Project [10].

Since the main objective of the mathematical model is to describe the SSMT dynamics with respect to the LV grid, only the microturbine electric-mechanical behaviour is focused assuming that the system is operated under normal conditions, neglecting thus the fast dynamics of the microturbine, such as start-up, shutdown and internal faults. In addition, the recuperator is not included in the model as it only serves to increase the system efficiency [2] and both the gas turbine temperature and acceleration control are omitted in the mathematical model, since they are of no impact under normal conditions and the governor model is not considered [10].

Therefore the SSMT model comprises three main parts: The power control, the SSMT engine and the PMG connected to the AC-DC bidirectional converter, as it can be observed from the simplified block diagram presented in figure 133.

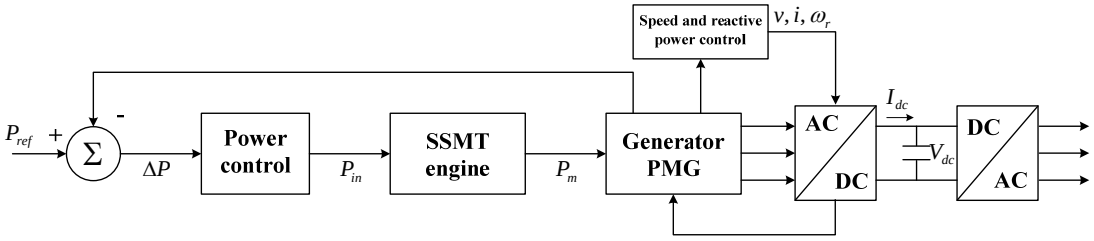

Figure 133 – Block diagram of the single-shaft microturbine model

The details of the mathematical model of the SSMT main parts are presented in the following subsections.

7.2.1.1 The active power control

In order to control de power output of the SSMT, a set point should be provided to the control system. A simple control of the turbine mechanical power can be performed through a Proportional-Integral (PI) control function [2]. The input of the controller is the error ΔP between the power set point, P_{ref}, and the effective power output, P.

The output of the controller is limited to the range of operation and then applied to the SSMT engine, as it can be observed from figure 134.

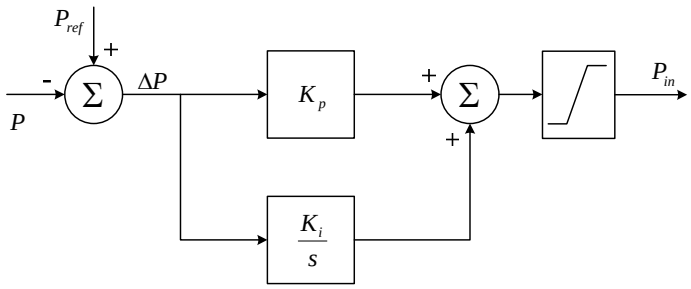

Figure 134 – SSMT active power control

7.2.1.2 The SSMT engine

As already mentioned previously, the SSMT engine comprises the air compressor, the combustion chamber, the recuperator and the power turbine driving the electrical generator, being this arrangement quite similar to combustion gas turbines [5]. Therefore, the SSMT engine is represented through the conventional model commonly used to represent the dynamics of simple cycle single shaft gas turbines, usually known as the GAST model, without the droop control [2], as depicted in figure 135.

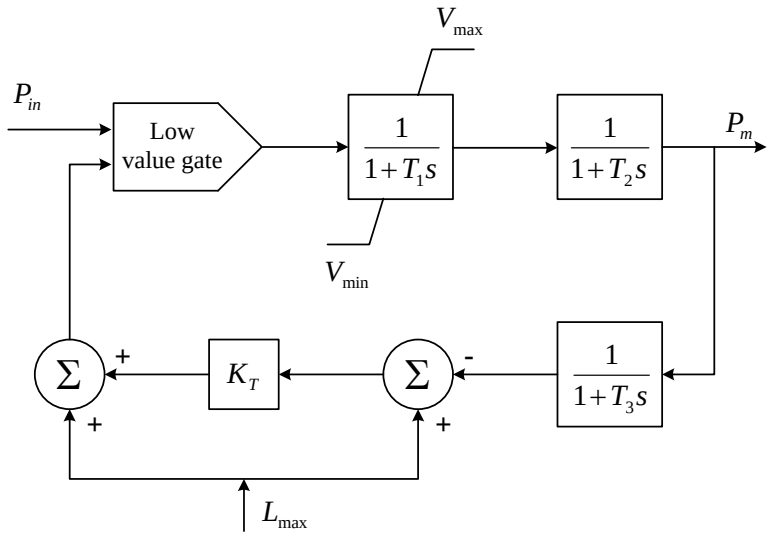

Figure 135 – Dynamic model of the SSMT engine

The parameters in the SSMT engine model are:

T_1, T_2 are the fuel system lag time constants;

T_3 is the load limit time constant;

L_{max} is the load limit;

V_{max}, V_{min} are the maximum and the minimum fuel valve positions;

K_T is the temperature control loop gain;

L_{max} is the load limit.

7.2.1.3 Permanent magnet synchronous generator model

The model adopted to represent the dynamic behaviour of the electrical generator is a two poles permanent magnet synchronous machine with a nonsalient rotor. The dynamics of this machine are described by the following equations written in the dq reference frame [9]:

$$v_d(t) = R_s i_d(t) - p\omega_r L_q i_q(t) + L_d \frac{di_d(t)}{dt} \quad (1)$$

$$v_q(t) = R_s i_q(t) + p\omega_r L_d i_d(t) + L_q \frac{di_q(t)}{dt} + p\omega_r \Phi_m \quad (2)$$

$$T_e = \frac{3}{2} p\left[\Phi_m i_q + (L_d - L_q) i_d i_q\right] \quad (3)$$

$$T_e = J\frac{d\omega_r}{dt} + F\omega_r + T_m; \quad (4)$$

where:

L_d, L_q are the d and q axis inductances in H;

R_s is the resistance of the stator windings in Ω;

i_d, i_q are the d and q axis currents in A;

v_d, v_q are the d and q axis voltages in V;

ω_r is the angular velocity of the rotor in $rad/\sec$;

Φ_m is the flux induced by the permanent magnets in the stator windings in Wb;

p is the number of pole pairs;

T_e is the electromagnetic torque;

J is the combined rotor and load inertia in $kg \cdot m^2$;

F is the combined rotor and load viscous friction;

T_m is the shaft mechanical torque.

7.2.1.4 Machine side converter

The machine-side converter in generating mode operates as a power source with controlled current [9] and controls both the generator speed and the power factor [11]. A block diagram of this machine-side converter controller is reported in [3] and its block diagram is illustrated in figure 136.

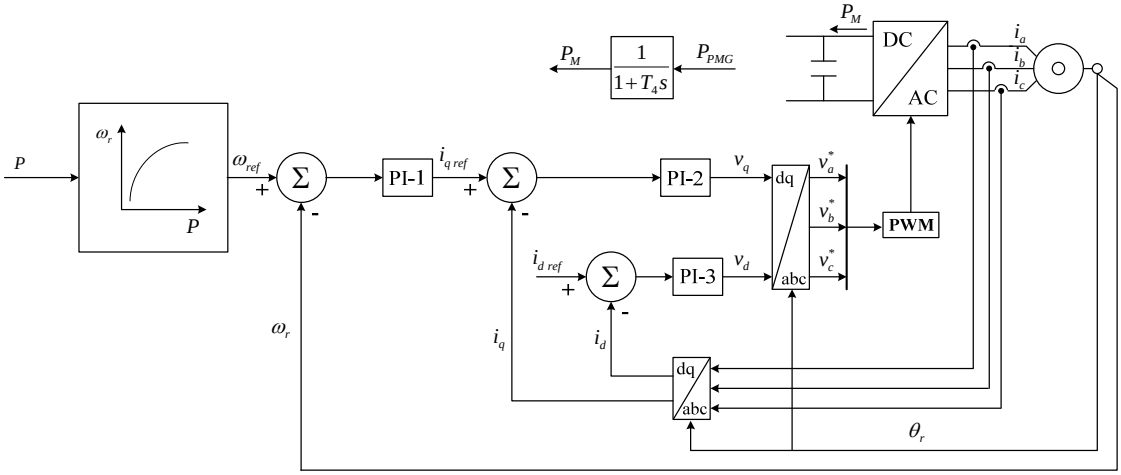

Figure 136 – Permanent magnet synchronous machine-side converter control

The microturbine shaft speed is controlled through a pre-defined characteristic curve (ω versus P) in order to operate the microturbine at optimal efficiency for each value of output power [3]. Concerning the Capstone 60 Microturbine, this characteristic was implemented based on the results obtained in a Capstone SSMT laboratorial test reported in [12]. The microturbine speed error is used to compute the i_q reference current, $i_{q\,ref}$, which is supplied to the PI-2 controller in order to regulate v_q and thus the microturbine angular velocity. The $i_{d\,ref}$ current component is previously calculated and regulated by the PI-3 regulator to ensure a unity power factor for the PMG.

Regarding the mathematical representation of the SSMT mechanical part, such as the dynamics of the fuel system and the dynamics of both compressor and turbine, the models reported in the literature present some differences when compared to the SSMT engine described in subsection 7.2.1.2. In addition they use very different

time constants, ranging from 30 milliseconds to 20 seconds [13] and typical values are not referred. Therefore, and taking into account that the Capstone 60 Microturbine technological characteristics are not well known, a first order transfer function with a lag time constant T_4 was included in the mathematical model, as it can be observed from figure 136, in order to account lag time constants related with the electro-mechanical conversion, increasing thus the model flexibility.

7.2.1.5 The grid side converter control

A three phase PQ inverter is employed to convert the DC output from the rectifier to 50 Hz AC, injecting the power available at its input into the grid. In addition to active and reactive power flow control, this inverter is also responsible for the control of the DC-link voltage of the AC/DC/AD system [14]. Therefore, the internal voltage of the inverter is controlled in order to maintain the DC-link voltage at a specified reference and the reactive power output at a desired set point.

Neglecting losses, the power balance at the capacitor of the DC-link, P_C, is the difference between the power received from the SSMT, P_M, and the inverter output power, P_{inv}, as it can be observed from figure 137 (a).

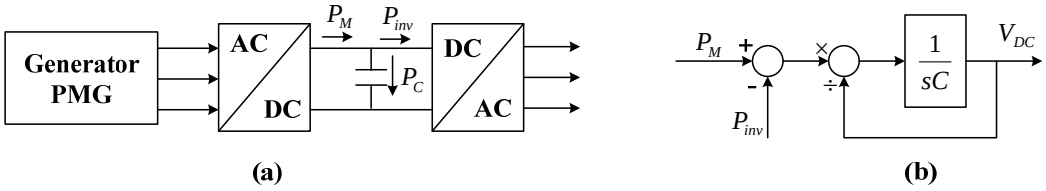

Figure 137 – (a) DC-link capacitor power balance and (b) DC-link dynamic model

The DC-link voltage, V_{DC}, can be computed as:

$$\begin{cases} P_C = P_M - P_{inv} = V_{DC} \times I_{DC} \\ V_{DC} = \dfrac{1}{C}\int I_{DC}\,dt \end{cases} \quad (6)$$

where C is the value of the DC-link capacitance. Therefore, taking the Laplace transform, the DC-link dynamics is modelled as it can be observed from figure 137 (b).

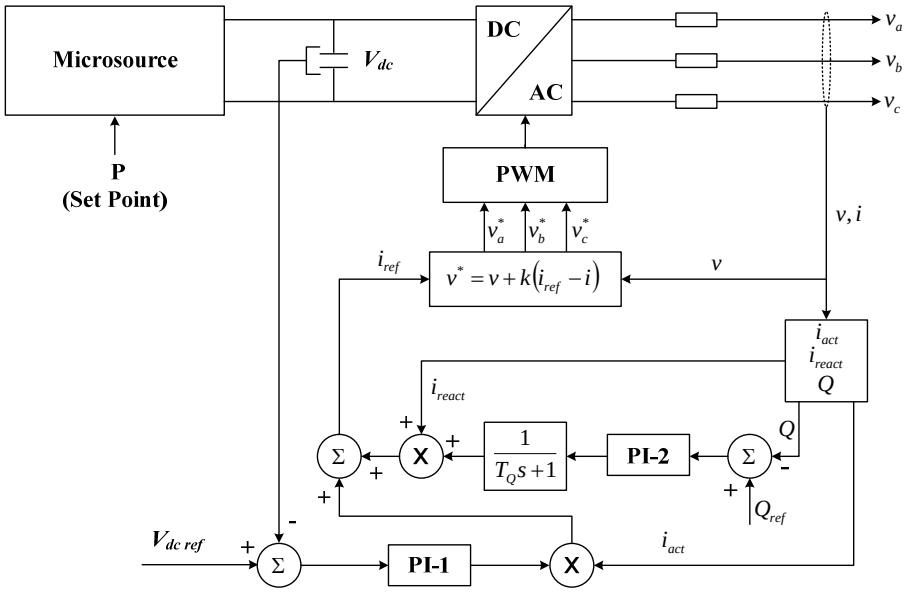

Figure 138 – PQ inverter control system

The control scheme of PQ inverter was implemented as a current controlled voltage source [14]. The block diagram of this power electronic interface along with its controller blocks is presented in figure 138.

Current components in phase, i_{act}, and in quadrature, i_{react}, with the inverter terminal voltage are computed based on a method presented in [15] for power calculation in single-phase inverters. Power variations in the microturbine induce a DC-link voltage error, which is corrected through the PI-1 regulator by adjusting the magnitude of the active current output delivered to the grid. The reactive power output is controlled via the PI-2 regulator by adjusting the magnitude of the inverter reactive current output.

As it can be observed from figure 138, the PQ inverter control system is formed by two cascaded loops. The inner most control loop regulates the inverter internal voltage, v^*, to meet a desired reference current, i_{ref}. The outer most control loop consists on active and reactive power regulators. This inverter can be operated with a unit power factor or receive a set-point for the output reactive power.

Although there are more advanced inverter control architectures, this model was adopted due to its simplicity.

7.2.2 Parameterization of the microturbine mathematical model

For parameter identification purposes, the mathematical model of the microturbine described through the block diagrams presented along the subsection 7.2.1 has to be parameterized in terms of a set of parameters. Regarding each part of the SSMT mathematical model, this set of parameters comprises:

- **The active power control:** Both proportional and integral gains of the proportional integral controller;
- **The microturbine engine:** The two fuel system lag time constants, the load limit time constant and the temperature control loop gain;

- **Machine side converter control system:** Both the proportional and integral gains of the three proportional integral controllers and the output power lag time constant;
- **PQ inverter control:** Both proportional and integral gains of the two proportional integral controllers and the reactive lag time constant.

These parameters represent unknown values of the microturbine mathematical model and, therefore, are gathered into the vector of parameters given by (7) in order to be considered as variables into the resulting model structure.

$$\theta = \left[\theta_1 \quad \cdots \quad \theta_{18}\right] \tag{7}$$

A detailed description of this set of parameters is presented in table 4.

Table 4: Parameters to be identified in the microturbine model

θ	Model parameter	Description
θ_1	*P_KP*	Active power control proportional gain
θ_2	*P_KI*	Active power control integral gain
θ_3	*MTE_T1*	Fuel system lag time constant 1
θ_4	*MTE_T2*	Fuel system lag time constant 2
θ_5	*MTE_T3*	Load limit time constant
θ_6	*MTE_KT*	Temperature control loop gain
θ_7	*PM_KP1*	Machine side inverter control proportional gain 1
θ_8	*PM_KI1*	Machine side inverter control integral gain 1
θ_9	*PM_KP2*	Machine side inverter control proportional gain 2
θ_{10}	*PM_KI2*	Machine side inverter control integral gain 2
θ_{11}	*PM_KP3*	Machine side inverter control proportional gain 3
θ_{12}	*PM_KI3*	Machine side inverter control integral gain 3
θ_{13}	*MT_T4*	Microturbine output lag time constant
θ_{14}	*PQ_KPa*	PQ inverter control active current proportional gain
θ_{15}	*PQ_KIa*	PQ inverter control active current integral gain
θ_{16}	*PQ_KPr*	PQ inverter control reactive current proportional gain
θ_{17}	*PQ_KIr*	PQ inverter control reactive current integral gain
θ_{18}	*PQ_TQ*	PQ inverter control reactive current time constant

The methodology used for identification of this set of parameters is presented on the following section.

7.3 Parameter identification methodology

In order to determine the set of parameters given by (7) suitable parameter identification techniques are adopted. The problem is twofold, comprising mainly:

- The definition of the identification experiment in order to collect an informative enough data set;
- The estimation of the model parameters in the sense of the identification criterion.

The issues related with these two subjects are addressed in the following two subsections.

7.3.1 The identification experiment and data collection

Based on the microturbine model structure, resulting from the model parameterization presented in subsection 7.2.2, an informative enough data set will be used in order to fit the mathematical model properties to those of the Capstone 60 Microturbine system. In order to collect a data set that describes how this system behaves over its entire range of operation, the design of appropriate excitation signals is an important task, since the quality of the observed data will determine an upper bound on the accuracy that can be achieved by the corresponding mathematical model.

Taking into account the Capstone 60 Microturbine system considerations described previously, in subsection 7.1, the identification experiment comprises the Capstone 60 Microturbine being operated in grid connected mode according to the PTD ILH0074/Ílhavo MSP system depicted in figure 140 through its simplified single-line diagram.

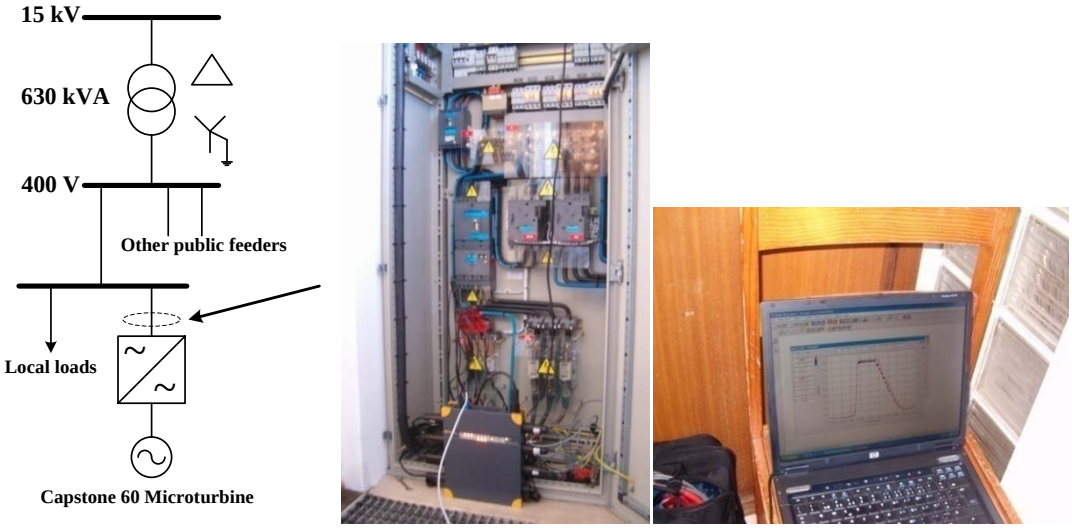

Figure 139 – Single line diagram of the Capstone 60 Microturbine experimental setup

Following the microturbine system inputs, the corresponding impact on the microturbine system output is observed and measured with a sample time of 200 ms using the PQA FLUKE 1760, which was installed in the circuit that connects the microturbine output to the switch board of the Ílhavo MSP, as it can also be observed from figure 140.

Since the Capstone 60 Microturbine does not perform load following functionalities while operated in grid connected mode, the system is excited through variations of the active power references, which are entered manually on the microturbine monitoring software, in order to change the output power delivered to the grid.

Thus, after the microturbine start-up in grid connected mode the power reference is modified from no load to its rated power (60 kW). After a given time period tests were conducted with several 5 kW steps down from 60 kW to 0 kW and afterwards with several 5 kW steps up from 0 kW to 60 kW. After a given time period, the active power reference is set to zero again. The step changes in the Capstone 60 Microturbine output power were initiated by selecting the proper power level on the microturbine monitoring software and after each step change was entered, time was allowed for microturbine output power levels to stabilise before the next step change was initiated. Therefore, the data set is given by these Capstone 60 Microturbine active power references and the time sequences corresponding to the subsequent microturbine system outputs, measured in terms of RMS values, per phase, of both injected current and terminal bus voltage, as it can be observed from figure 140.

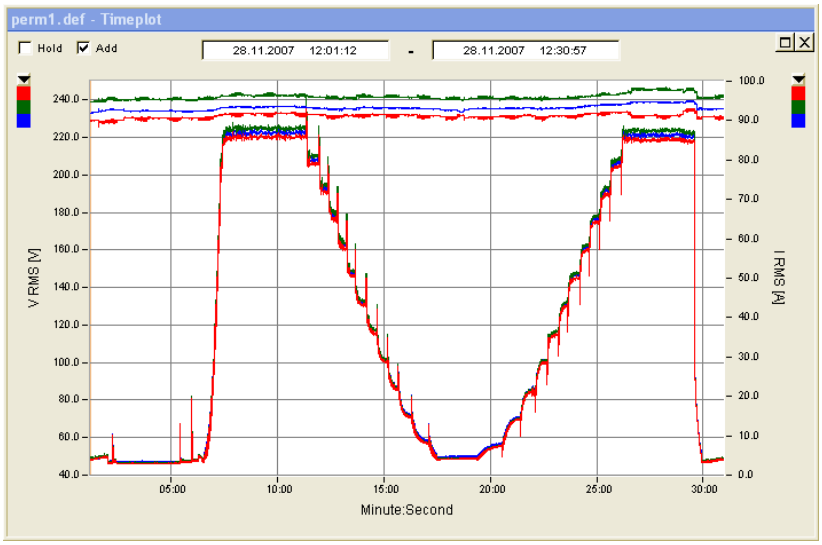

Figure 140 – Capstone 60 Microturbine injected current and terminal bus voltage

As the Capstone 60 Microturbine operated with a unitary power factor during grid connected mode, the field tests do not allow obtaining an informative enough data set in order to identify all the model parameters gathered into the parameter vector given by (7), namely these ones related with the reactive power output of the PQ inverter control (θ_{16}, θ_{17} and θ_{18}). However, although these parameters do not influence the model response, they are also included on the parameter identification procedure, in order to find suitable values that ensure numerical stability during dynamic simulations.

7.3.2 The identification method

With the observed data set, the parameter identification procedure relies on the estimation procedure of the microturbine mathematical model parameters, given by (7), in the sense of the identification criterion. Thus, during the parameter identification procedure, this set of model parameters will be adjusted in an attempt to minimize the performance function, quantified by an error criterion. For this purpose both the Capstone 60 Microturbine system and the corresponding

parametric model are fed with the same inputs, $\varphi(t)$, and the corresponding outputs, $y(t)$ and $\hat{y}(t/\theta)$, respectively, are compared for $t = 1, ..., N$, where N is the number of collected data samples, yielding an error signal,

$$\varepsilon(t/\theta) = y(t) - \hat{y}(t/\theta) \tag{8}$$

which is used, in some sense, for adapting the model parameters, as depicted in figure 141.

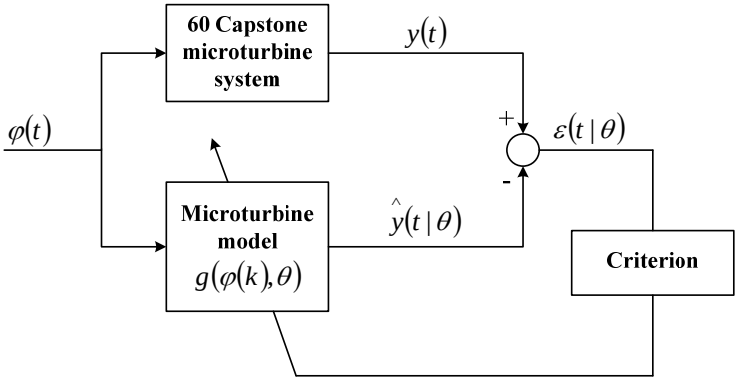

Figure 141 – The basic search concept used for parameters estimation

As it can be observed from figure 141, the parametric model of the microturbine is augmented with a suitable identification criterion that measures how well it fits the Capstone 60 Microturbine system output and with an optimization algorithm that will adapt the model parameters in order to minimize the identification criterion, which is taken as the square function of the error given by equation (9).

$$V_N = \frac{1}{N}\sum_{t=1}^{N}\left\|\varepsilon(t/\theta)\right\|^2 \tag{9}$$

Thus, the parameters of the microturbine system model are derived as in (10) exploiting the Evolutionary Particle Swarm Optimization (EPSO) as the optimization tool.

$$\hat{\theta}_N = \arg\min_{\theta} V_N \tag{10}$$

EPSO was built over the concepts of self-adaptive evolution strategies and particle swarm optimization, combining thus the best of both techniques [16]. Applications of EPSO have already been reported in many power systems problems [16-18], where superiority was confirmed, giving a faster convergence and better solutions when compared with other meta-heuristics. More recently, the EPSO robustness was exploited as a global parameter optimization tool to build dynamic equivalents for MicroGrids using system identification theory [19-20].

From an evolutionary point of view, the set of potential solutions for the microturbine model parameters is called a set of particles. Each particle comprises a set of object parameters and a set of strategy parameters, corresponding to the particle position

into the parameter space and to the weights that govern the movement rule, θ_i and w_i, respectively. The general algorithm of EPSO can be described as follows:

1. Choose an initial swarm of *S* particles;
2. Iterate for $k = 1, 2, \ldots$;
3. Replicate each particle;
4. Perform mutation of the weights of each particle;
5. Each mutated particle generates an offspring according to the movement rule;
6. Evaluate the fitness of each particle;
7. Perform selection;
8. Test for the termination criterion and either go to step 3 or stop.

In order to find the values of the microturbine mathematical model parameters, which minimize the error criterion given by (9), a suitable evaluation function was developed. The performance of each particle, measured in terms of the mean square error, is evaluated through the numerical simulation of the microturbine model. Therefore, the microturbine parameterized model was implemented under *MatLab®/Simulink®* environment exploiting the "mask" functionalities provided by this simulation tool in order to aggregate the whole microturbine parametric model in a single block and to exchange parameters between the EPSO algorithm and the microturbine parameterized model. Figure 142 shows the microturbine model connected to the LV grid and the dialog box for the SSMT parametric model can be observed from figure 143.

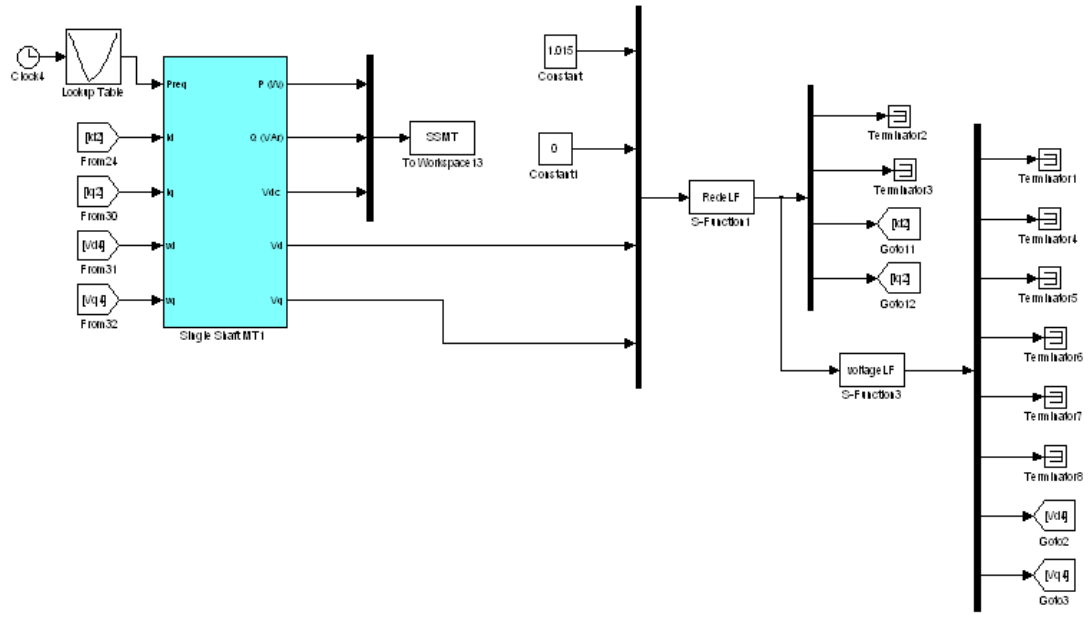

Figure 142 – The microturbine parametric model in MatLab®/Simulink® environment

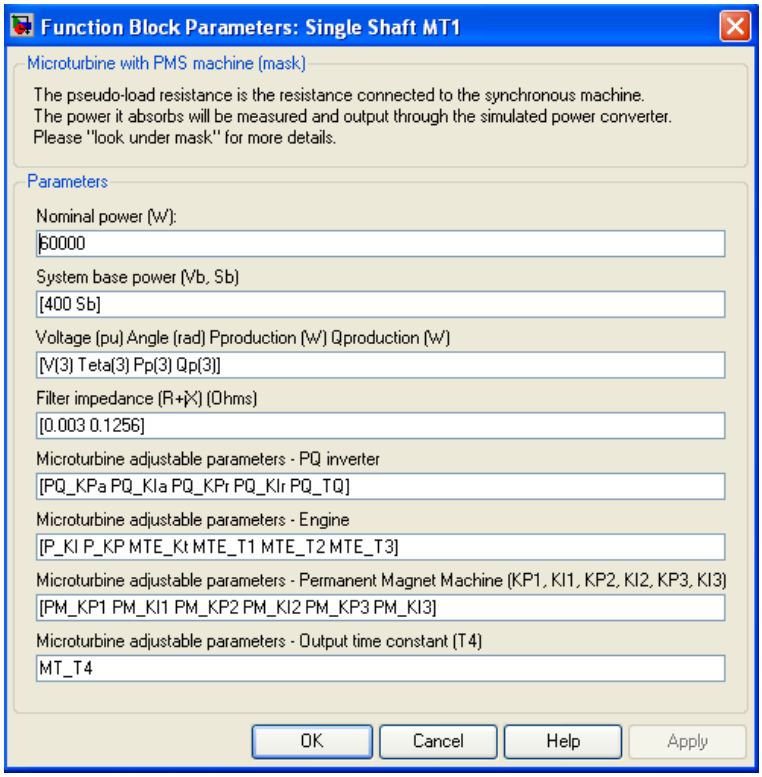

Figure 143 – The microturbine parametric model mask subsystem

The interaction between the EPSO algorithm and the dynamic simulation model as well as the global algorithm for microturbine parameters estimation purposes can be observed from the diagram depicted in figure 144.

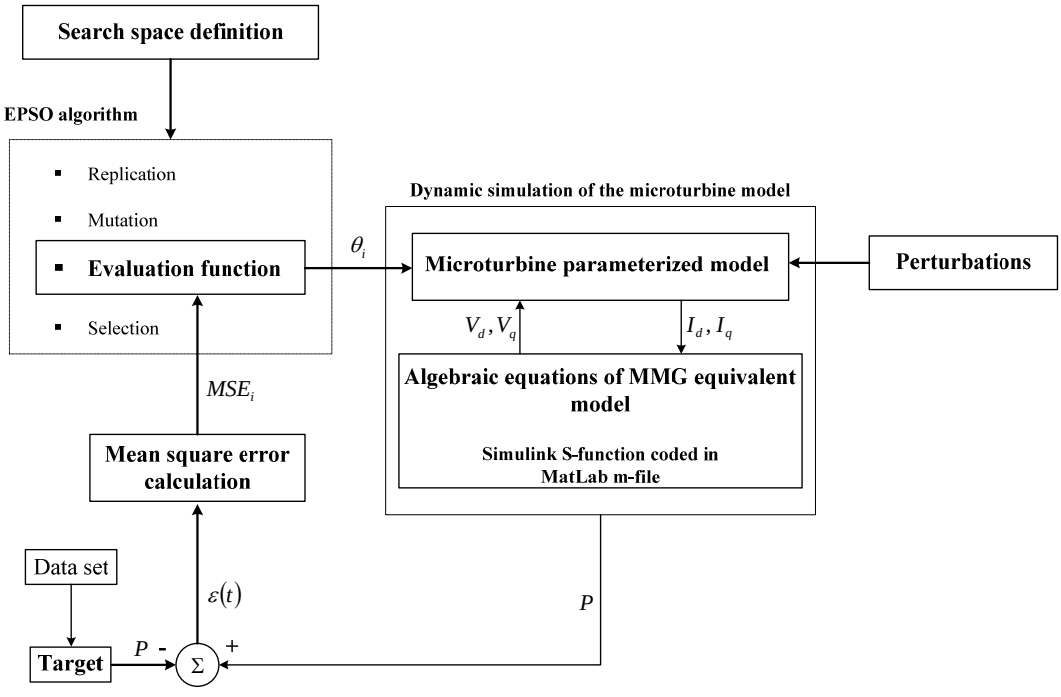

Figure 144 – Flow-chart of microturbine model parameters estimation

After defining the search space through both the minimum and maximum values of each parameter into the parameter vector, it is expected that the EPSO algorithm will perform the search to the global optimum or, at least, to a good local optimum under the sense of the error criterion. For this purpose, after mutation has been performed by the EPSO algorithm, the following sequence of steps will be carried out for each particle in the swarm.

- The evaluation function sends the particle object parameters to the parametric microturbine model;
- A pre-specified set of disturbances occurring at defined time instants are simulated during a certain time period;
- The response of the microturbine model is compared with the target response, which was derived from the 60 Capstone microturbine field tests, yielding an error sequence;
- The mean square error of the error sequence is then calculated and sent back to the evaluation function;
- Based on the mean square error information, EPSO algorithm performs selection in order to build the swarm corresponding to the next generation.

The above procedure is repeated while the EPSO algorithm termination condition is not verified.

7.4 Results

The methodology described previously, in subsection 7.3, is applied to find the parameters of the mathematical model that has been used to describe the microturbine dynamic behaviour with respect to the LV grid.

As already mentioned previously, time sequences corresponding to the current and voltage measurements following the gradually decreasing and subsequent increasing of the microturbine generating power in steps of 5 kW are used to build the data set. As the Capstone 60 Microturbine runs at unity power factor, the active power output is calculated as the product of currents and voltages. After some pre-processing, these power sequences are stored in a *file.mat* in order to be used directly in the developed approach as the training data set or target output, as it can be observed from figure 144. The data set thus obtained is illustrated in figure 145.

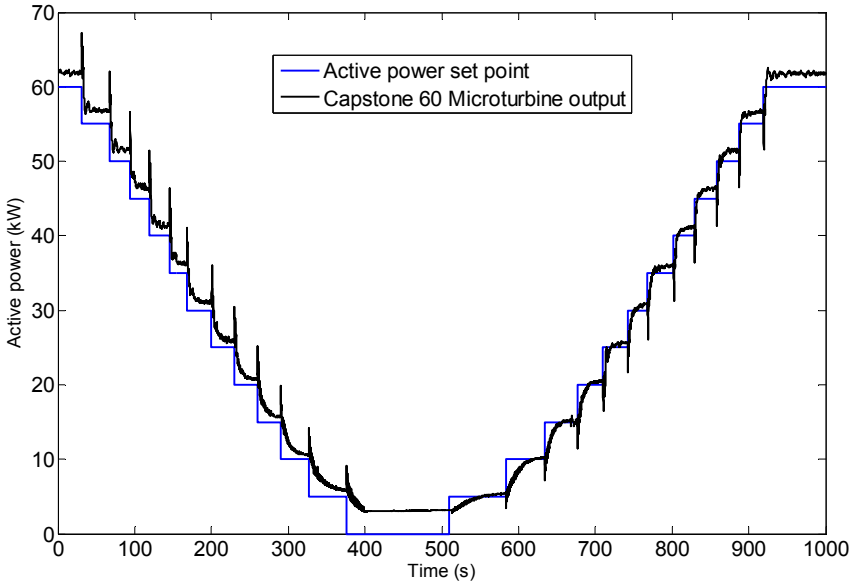

Figure 145 – The Capstone 60 Microturbine active power output following power set points

From the qualitative analysis of the Capstone 60 Microturbine response, presented in figure 145, the following assumptions should be highlighted:

- The minimum output power is limited to a value around 3 kW;
- The microturbine response presents a lag time constant whose value is not constant during the entire range of operation;
- Following the different microturbine generation levels, a nonlinear relationship is suggested between the lag time constant value and the microturbine generation level.

Based on the first assumption the lower limit of the SSMT input power, in the microturbine active power model depicted in figure 134 of the subsection 7.2.1.1, is defined. Following the last two assumptions, it should be verified that the time delay experimented by the microturbine output can be represented through the microturbine output power transfer function of the mathematical model, presented in subsection 7.2.1.4. Therefore, two identification procedures are carried out in order to find "optimal parameters" for the mathematical model considering the lag time constant T_4, as a constant parameter and as an adaptive one. The results obtained are presented in the following two subsections.

7.4.1 Model parameters considering a constant value for T4

In order to find suitable parameters for the microturbine mathematical model, the EPSO algorithm with 20 particles, replication factor $r = 1$ (each parent gives birth to one descendant) and Gaussian mutation with learning rate $\tau = 0{,}5$ was used. The stopping criterion involves 10 consecutive generations without finding a better global fitness. The founded parameter vector, θ, which provides the best performance in the sense of the MSE is presented as follows:

$$\theta = \left[\theta_{MTE} \quad \theta_{PMG} \quad \theta_{T4} \quad \theta_{PQ}\right] \tag{11}$$

$$\theta_{MTE} = [0.018 \quad 29.985 \quad 0.8194 \quad 1 \quad 0.05 \quad 3.892]$$
$$\theta_{PMG} = [1 \quad 35.52 \quad 96.89 \quad 102.77 \quad 57.63 \quad 19.68]$$
$$\theta_{T4} = [3.75] \qquad (12)$$
$$\theta_{PQ} = [-0.6985 \quad -0.5462 \quad 531 \quad 795 \quad 0.0225]$$

where:

- θ_{MTE} is the subset of the microturbine engine parameters;
- θ_{PMG} is the subset of the permanent magnet generator control parameters;
- θ_{T4} is the subset of the microturbine output time constant;
- θ_{PQ} is the subset of the PQ inverter parameters.

Based on this vector of parameters, the microturbine mathematical model performance is evaluated by comparing the time domain response obtained from dynamic simulations with the measurements carried out during the Capstone 60 Microturbine system experiment. For this purpose, the complete sequence of disturbances, based on variations of the microturbine active power references in steps of 5 kW, was simulated and the results obtained are presented in the following figures.

Figure 146 shows the active power outputs of both microturbine mathematical model and Capstone 60 Microturbine for the power settings referred previously. As it can be observed, the dynamic behaviour of the microturbine mathematical model is in an acceptable agreement with this one of the Capstone 60 Microturbine over the considered entire range of operation. However, a small loss of accuracy is verified during the transients following the microturbine active power reference variations, namely when it is operated near its rated power and under low generation levels.

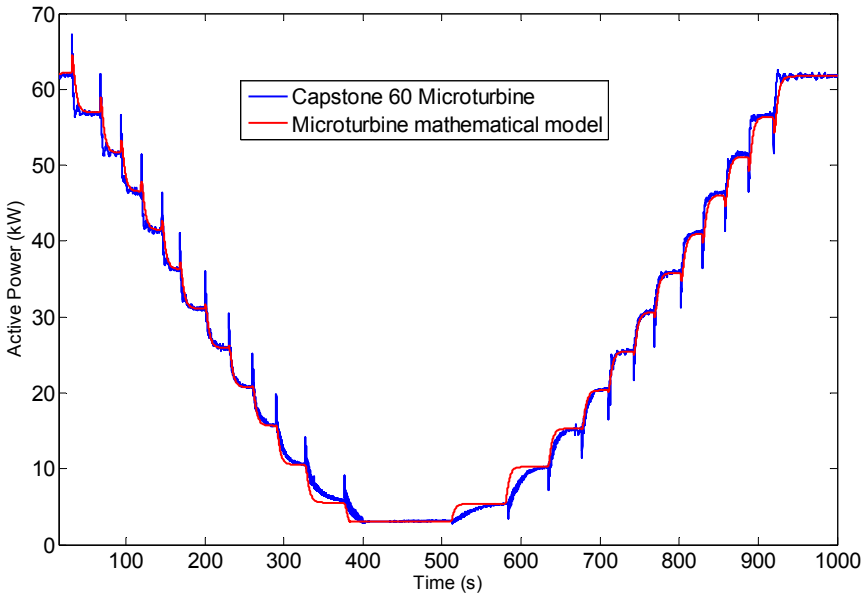

Figure 146 – Microturbine active power output

The active power variations presented in figure 146 are accomplished by microturbine injected current and terminal bus voltage variations, as illustrated in figures 147 and 148.

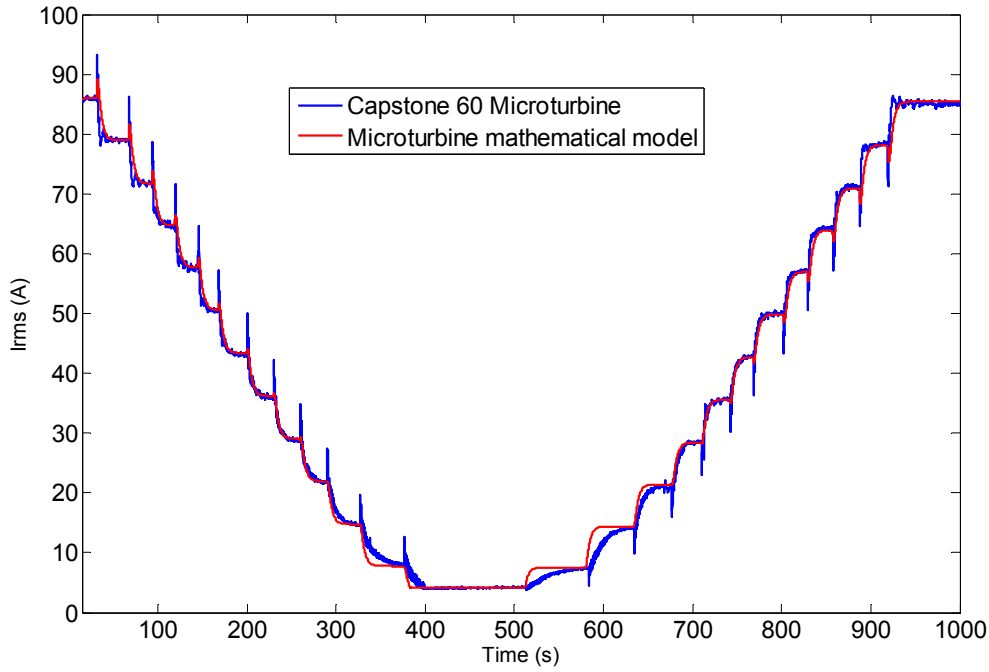

Figure 147 – Microturbine injected current

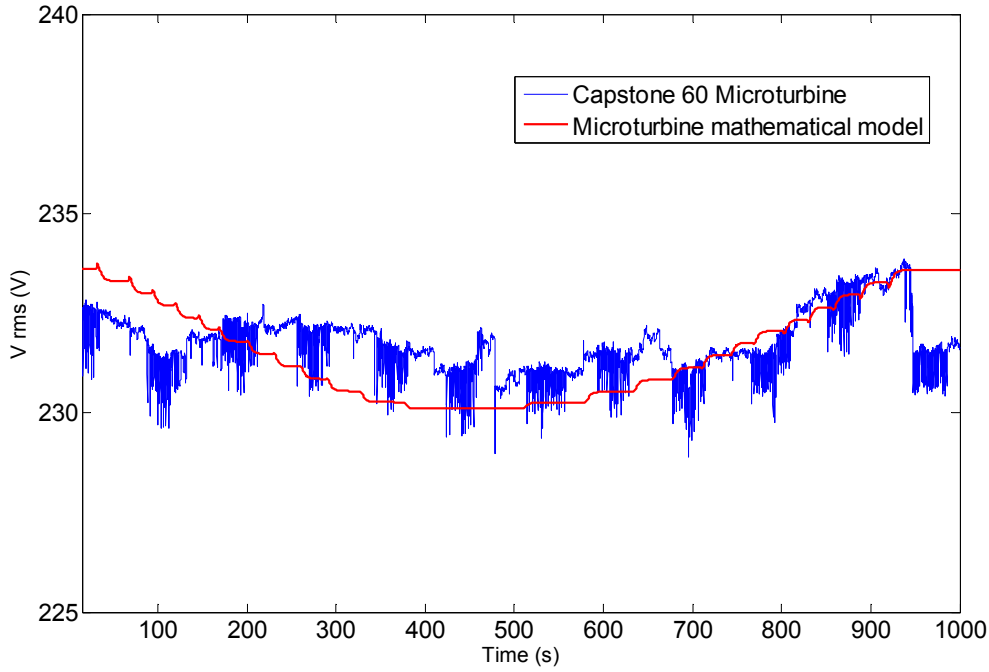

Figure 148 – Microturbine terminal bus voltage

As it can be observed from figures 146, 147 and 148, the microturbine mathematical model with the set of parameters whose values are given by (12) represents the

Capstone 60 Microturbine dynamic behaviour following the simulated sequence of disturbances with an acceptable level of accuracy. The small loss of accuracy, already referred previously, is verified during transients, since the Capstone 60 Microturbine output presents a time delay whose value in not constant during the entire range of operation, as it can be observed from the output power and injected current illustrated in figures 146 and 147, respectively.

In fact, this time delay can be represented in microturbine mathematical model through the constant parameter, $\theta_{T4} = T_4$, whose value was identified taking into account the model performance over the Capstone 60 Microturbine entire range of operation. Therefore the mathematical model response is too fast during variations in the active power reference for low generation levels and too slow for generation levels near the microturbine rated power, as it can be observed from figures 146 and 147.

7.4.2 Model parameters considering T4 as an adaptive parameter

In order to increase the microturbine mathematical model accuracy, the parameter corresponding to the active power output lag time delay was considered as an adaptive parameter, whose value is given by a nonlinear function of the microturbine generation conditions, as already mentioned previously. Therefore, for identification purposes, the subset of vector parameters corresponding to the microturbine output time constant, θ_{T4}, in (11), includes several parameters corresponding to several values of T_4, as given by (12). Based on the Capstone 60 Microturbine output power presented in figure 146, it was considered the same time constants for decreasing and increasing steps from the same generating conditions. Therefore, the subset of these time constants is given by:

$$\theta_{T4} = [T_{4i}] \tag{12}$$

where T_{4i}, for $i = 1, \ldots, 12$, represents the time constants for each power step corresponding to the several decreasing active power settings.

The nonlinearity between the microturbine output time constants and its generation conditions is represented through a look up table in which the time constants are considered as variables whose values have to be identified. These variables are used on the corresponding transfer function, which is implemented through a *Simulink s-function* coded in a *MatLab m-file*.

In order to find suitable values for the subset of parameters given by (12), a new identification procedure was carried out, as already mentioned previously, considering the remaining parameters of the microturbine mathematical model as constants whose values were identified previously and given by (11). The founded subset of microturbine time constants that presents the best performance in the sense of the MSE criterion is as follows:

$$\theta_{T4} = [0.99 \quad 1.2 \quad 1.5 \quad 1.6 \quad 1.75 \quad 2 \quad 3.36 \quad 5.5 \quad 6.8 \quad 9.23 \quad 13.37 \quad 16.73] \tag{13}$$

Based on the set of model parameters given by (11) and replacing the subset θ_{T4} by the values given by (13), the performance of the microturbine mathematical model is illustrated on the following figures.

In order to evaluate the generalization capability of the microturbine mathematical model, disturbances not used during the parameter estimation procedure are also simulated. These disturbances comprise active power references to increase the microturbine power output from the minimum to the maximum value and to decrease the microturbine power output from the maximum to the minimum value. These set points are entered on the microturbine monitoring software at t=340 s and t=1702 s, respectively.

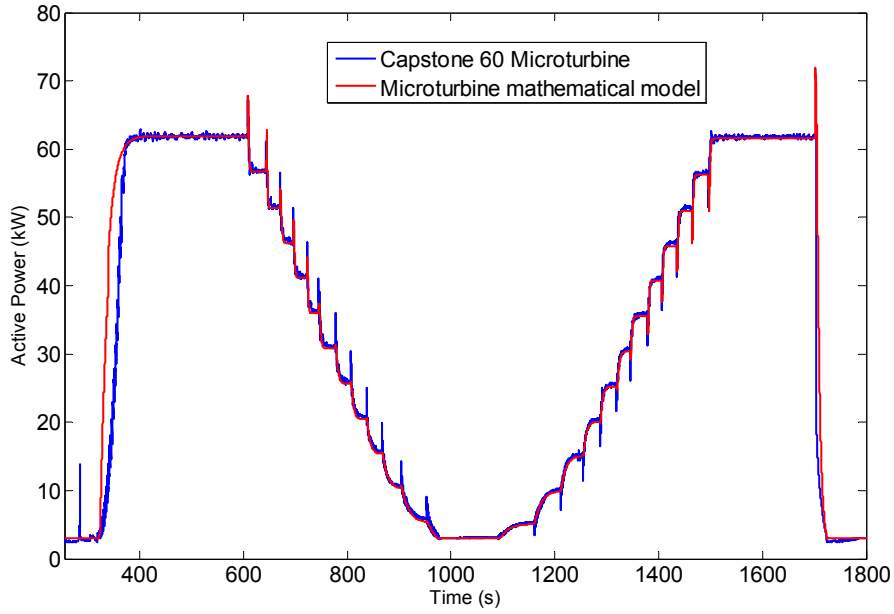

Figure 149 – Microturbine active power output for adaptive output power time delay

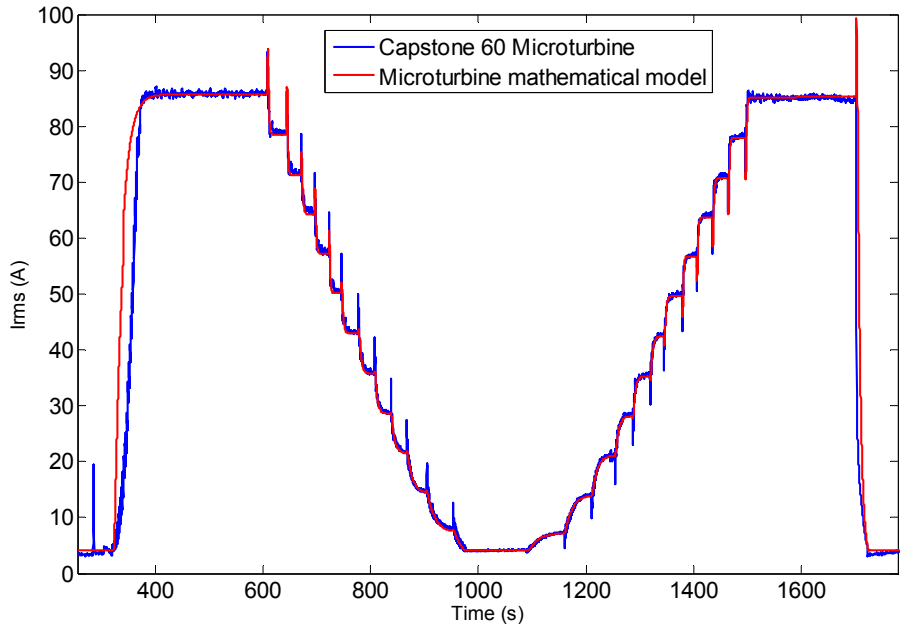

Figure 150 – Microturbine injected current per phase for adaptive power output time delay

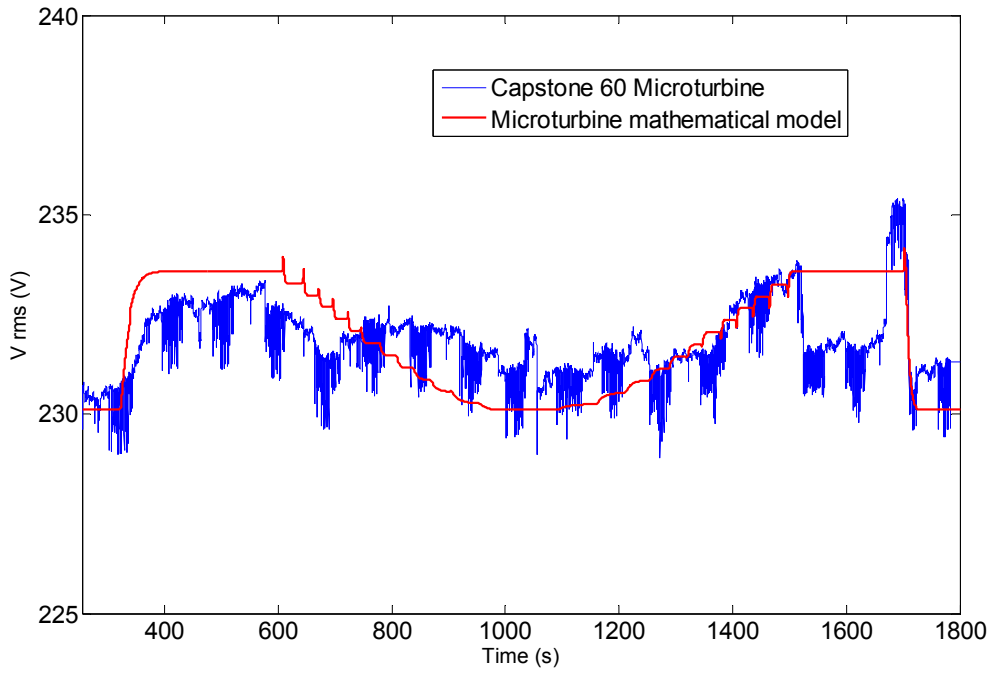

Figure 151 – Microturbine terminal bus voltage per phase for adaptive output power time delay

As it can be observed from figures 149 and 150, the microturbine mathematical model dynamic behaviour is in a good agreement with this one of the Capstone 60 Microturbine over the entire range of operation, ensuring thus a good performance of the microturbine mathematical model for the set of parameters given by (12) being the subset θ_{T4} given by (13).

In addition, the microturbine mathematical model presents a good generalization capability, since a good agreement is verified between the Capstone 60 Microturbine and the mathematical model responses following active power variations not used during the parameter estimation procedure.

7.5 Conclusions

The results presented in the previous section allow concluding that the microturbine mathematical model can be used to represent the Capstone 60 Microturbine dynamic behaviour during output power variations following set points of active power generation, over its entire range of operation. In addition, in order to increase the model performance the lag time parameter corresponding to the microturbine output should be considered as an adaptive one.

8 Final Conclusions

The main purpose of these field tests was to demonstrate the feasibility of transferring the microgrid between grid connected and islanding modes under several operating conditions.

Before the field tests, it was performed a detailed characterization of this Portuguese study case, including description and PQ analysis of the MV and LV distribution grids, where the Ílhavo MSP is integrated.

Concerning to voltage quality, several parameters were analysed, like voltage variations, harmonics, unbalance, flicker and fundamental frequency. The results allow to conclude that measured voltage in the LV busbar of the ILH0074 was in accordance to the NP EN 50160 standard before the installation of the microturbine and after its connection to the LV public grid.

During the first field tests phase, it was studied the behaviour of the system. In grid connected mode, the microturbine behaviour was as expected, without any significant RMS voltage variations, during the microturbine starting, shutdown and on several generation regimens. Regarding the good level of short-circuit power and the reduced length between the distribution transformer and the microturbine, the impact of the microturbine on the grid power quality was not significant. With the microturbine operating at the maximum generation power, the voltage RMS values and the THDv increase slightly.

In case of power outage in grid connected mode, the dual-mode controller forces the microturbine to a shutdown followed by restarting in islanding mode, remaining the protected load without supplying during a period of about 4 minutes.

After the microturbine black-starting, voltage takes about 500 ms to 1 s to stabilize, oscillating between +4 % and -6 % around the reference voltage. The frequency decreases slightly, to about 0,2 % of the 50 Hz, and then it recovers slowly to stabilize around the reference. The operation of the microturbine in islanding mode was possible without significant voltage and frequency variation for moderate load variations.

Regarding to the second field tests phase, the following conclusions can be highlighted:

- A stable operation of the 2 micro-sources (microturbine and Diesel gen-set) in islanding mode was possible with slacken of the frequency protections. Due to tripping of the frequency relay, the first 2 attempts to parallel the microturbine with the Diesel gen-set were not successful, but it was possible with the following frequency settings: under-frequency = 49,3 Hz; over-frequency = 51,5 Hz.
- With a constant load, the generation regimens of the microturbine did not impact significantly the island voltage and frequency stability. The Diesel gen-set followed, without any problem, the generation variations imposed by the microturbine.
- As expected, the Diesel gen-set followed all load variations and the microturbine remained on its generation set-point in a slightly oscillating regimen.

- The connection of heavy loads to the island system, like 2 induction motors of 7,5 kW caused strong voltage and frequency variations, leading to the microturbine shutdown.
- The voltage stability in islanding operation mode can be improved with control of the micro-sources and loads.
- The results achieved allow to conclude that transitions between grid connected and islanding modes, and vice-versa, can be easily performed with reduced power flow between the grid and the islanding system.

References

[1] A. Malmquist, O. Aglen, E. Keller, M. Suter, J. Wickstrom, "*Microturbines: Speeding the shift to distributed heat and power*", ABB review, nº.3, March, 2000.

[2] Y. Zhu, K. Tomsovic, "*Development of models for analysing the load following performance of microturbines and fuel cells*", Electric Power System, Research, vol. 62, 2002.

[3] O. Fethi, L. A. Dessaint, K. Al-Haddad, "*Modelling and simulation of the electrical part of a grid grid connected microturbine*", IEEE Power Engineering Society General Meeting, Denver, Colorado, USA, 2004.

[4] F. Jurado, J. Ramon Saenz, "*Adaptive control of a fuel cell-microturbine hybrid power plant*", IEEE Transactions on Energy Conversion, vol. 18, nº. 2, June, 2003.

[5] A. Al-Hinai, A. Feliachi, "*Dynamic model of a microturbine used as distributed generator*", Proceedings of the 34th Southeastern Symposium on Systems Theory, Hunstsville, Alabama, March, 2002.

[6] Working Group of Prime Mover and Energy Supply Models for System Dynamic Performance Studies, "*Dynamic models for combined cycle plants in power system studies*", IEEE Transactions on Power Systems, vol. 9, nº. 3, August, 2004.

[7] L. N. Hannet, A. Khan, "*Combustion turbine dynamic model validation from tests*", IEEE Transactions on Power Systems, vol. 8, nº. 1, February, 1993.

[8] S. R. Guda, C. Wang, M. H. Nehrir, "*Modelling of microturbine power generation systems*", Electrical Power Components and Systems, August, 2007.

[9] M. Napgal, A. Moshref, G. K. Morison, P. Kundur, "*Experience with testing and modelling of gas turbines*", IEEE/PES 2001 Winter Meeting, Columbus, Ohio, USA, 2001.

[10] Deliverable do MG sobre modelos. MICROGRIDS project deliverable DA 1, "Digital models for microsources." [Online.] Available: http://microgrids.power.ece.ntua.gr/micro/micro2000/delivarables/Deliverable_DA1.pdf

[11] B. K. Bose, "*Power electronics and AC drives*", New Jersey, 1986.

[12] R. J. Yinger, "Behavior of Capstone and Honeywell microturbine generators during load changes." [Online.] Available: http://certs.lbl.gov/certs-pubs.html.

[13] C. L. Moreira, "*Identification and Development of MicroGrids Emergency Control Procedures*", Ph. D. Thesis, FEUP, Porto, 2008.

[14] J. A. Peças Lopes, C. L. Moreira, A. G. Madureira, "Defining *control strategies for microgrids islanded operation*", IEEE Transactions on Power Systems, vol. 21, 2006.

[15] L. Goldstein, B. Hedman, D. Knowles, S. I. Freedman, R. Woods, T. Schweizer, "*Gas-fired distributed energy resource technology characterization*", National Renewable Energy Laboratory, NREL/TP-620-34783, November, 2003.

[16] V. Miranda, N. Fonseca, "*EPSO – Best of two worlds meta-heuristic applied to power system problems*", Proceedings of the World Congress of Computation Intelligence Conference of Evolutionary Computing, Hawaii, USA, 2002.

[17] A. Mendonça, J. A. Peças Lopes, "*Robust tuning of PSS in power systems with different operating conditions*", Proceedings of the IEEE Bologna PowerTech2003, Bologna, Italy, 2003.

[18] V. Miranda, N. Fonseca, "*Reactive power dispatch with EPSO – Evolutionary Particle Swarm Optimization*", Proceedings of the International Conference of Probabilistic Methods Applied to Power Systems, Naples, Italy, 2002.

[19] F. O. Resende, J. A. Peças Lopes, "*Development of dynamic equivalents for microgrids using system identification theory*", Proceedings of the IEEE Lausanne PowerTech2007, Lausanne, Switzerland, 2007.

[20] F. O. Resende, "*Contributions for MicroGrids Dynamic Modelling and Operation*", Ph. D. Thesis, FEUP, Porto, 2007.